



UNIVERSITY OF
BIRMINGHAM

Multivariate Statistical Modelling of the Meteorological Extremes that
Drive Soil Moisture Drought

by

Colin Manning

A thesis submitted to the University of Birmingham for the degree of
DOCTOR OF PHILOSOPHY

School of Geography, Earth and Environmental Sciences

College of Life Sciences

University of Birmingham

December 2018

UNIVERSITY OF
BIRMINGHAM

University of Birmingham Research Archive

e-theses repository

This unpublished thesis/dissertation is copyright of the author and/or third parties. The intellectual property rights of the author or third parties in respect of this work are as defined by The Copyright Designs and Patents Act 1988 or as modified by any successor legislation.

Any use made of information contained in this thesis/dissertation must be in accordance with that legislation and must be properly acknowledged. Further distribution or reproduction in any format is prohibited without the permission of the copyright holder.

Abstract

A compound event is an extreme impact that arises from the joint occurrence of the underlying contributing events. In this thesis, soil moisture drought is analysed as a compound event of meteorological drought and extremely high temperatures. A conceptual framework is developed to (1) disentangle contributions of the meteorological hazards to soil moisture drought, (2) quantify the probability of long-duration meteorological drought events that coincide with extreme temperatures, and (3) assess the representation of such events in climate models. The conceptual framework is implemented using copula-based statistical models.

Using the models, it is found that: (1) precipitation is the main driver of soil moisture drought. In wet climates, PET is additionally required to explain the onset, severity and persistence of soil moisture drought over different time scales. At dry sites, where evapotranspiration (ET) is moisture limited in summer, PET does not improve the estimation of soil moisture. Thus, drought indices that incorporate PET should be interpreted carefully and within the context of climate in which they are applied. (2) the probability of long-duration dry and hot (*DH*) events has increased throughout Europe over the period (1950-2013), with largest increases found in Southeast Europe. We also highlight the need to account for the dependence between these hazards to avoid an underestimation in the probability of *DH* events. (3) it is found that the probability of long-duration *DH* events is largely underestimated throughout Europe in a set of CMIP5 climate models, we highlight that more research is needed to understand the physical sources of this underestimation.

The frameworks here have been developed to study concurrences of meteorological drought and extremely high temperatures in Europe, though the conceptual frameworks may be readily applied in other locations and to different types of extreme events such as heat waves.

Acknowledgements

First and foremost, I would like to express my sincere gratitude to my supervisors Dr. Martin Widmann and Dr. Anne Van Loon. Throughout the Ph.D they have always maintained an open door policy, provided me the support when needed and the trust to make my own decisions. I have thoroughly enjoyed our many lengthy scientific discussions that have shaped my way of thinking and given me a more in depth knowledge and appreciation for topics such as drought and climate. In particular, I would like to thank Martin for the numerous discussions or even lessons on statistics, and to Anne for the team environment she has created in our Drought research group, which has provided an enormous support, both academically and personally. I hope our working relationship will continue to grow in the future.

Further thanks go to everyone involved in the CE:LLO project, I have been lucky to be involved in this international collaboration which has afforded me the opportunity to spend time at other research centres including the LSCE in Paris and the Wegener Centre in Graz. These experiences have allowed me to broaden my knowledge and perspective, as well as meet many great people along the way. I would like to thank Prof. Douglas Maraun who, along with Martin, gave me the opportunity to pursue this Ph.D and provided much support and direction at important times during the project. I have learned a lot from the insight he has offered, my time spent in Graz was very fruitful experience. I would also like to thank Dr. Mathieu Vrac who welcomed me into his research group during my time in Paris and has been a support throughout the project in providing his invaluable knowledge of statistics. Lastly, I have been fortunate to share my Ph.D experience in the CE:LLO project with (the now) Dr. (compa) Emanuele Bevacqua. Throughout the Ph.D I have shared many experiences in sharing apartments, travelling to nice places and working with Emanuele. I am grateful for the sup-

port he has given throughout the project and for all the discussions and ideas he has shared.

As much as I enjoy research, these past few years could not have been as fruitful an experience without the people I have met along the way and worked alongside on a day to day basis. I want to thank everyone at the Wegener Centre and at the LSCE who welcomed me there. Particularly, I want to thank everyone in Birmingham in our drought research group: Sally, Mel, Danny, Doris and Lucy and those who I have shared an office and few beers with along the way these past few years: Michael, Simon, Vasileios, Jenny, Vicki, Clemens, Daniel, Gregor, Michael A. and Kelvin. Most of all, I want to thank my family and Sally for their constant support.

Finally, I am grateful to my examiners Dr. Gregor Leckebusch and Dr. Florian Pappenberger for the valuable time they have taken to read this thesis and for the insightful feedback they offered during the viva which was altogether a very enjoyable experience.

Author Contributions

This thesis is based on one published work and two that are in preparation for submission, one of which will be submitted in January 2019. These works are laid out below along with information of my individual contributions.

1. **Chapter 2 contributions:** The idea for the study has been developed by CM with contributions from MW, AVL, EB and DM. The conceptual model design for the soil moisture model was developed by CM, EB, MW and AVL while the statistical model was developed by EB and MV. CM carried out the analysis, interpreted results and wrote the paper with contributions from all co-authors at different stages. The results of this chapter are published in the Journal of Hydrometeorology as:

Manning, C., Widmann, M., Bevacqua, E., Van Loon, A.F., Maraun, D. and Vrac, M., 2018. Soil Moisture Drought in Europe: A Compound Event of Precipitation and Potential Evapotranspiration on Multiple Time Scales. Journal of Hydrometeorology, 19(8), pp.1255-1271.

2. **Chapter 3 contributions:** The initial idea was formulated by DM and developed by CM, MW, EB and AVL. The experimental design was developed by CM and EB, while the statistical approach was developed by EB, DM and MV. CM carried out the analysis, interpreted the results and wrote the paper with contributions from all co-authors. The results of this chapter have been accepted for publication in Environmental Research Letters as:

Manning, C., Widmann, M., Bevacqua, E., Van Loon, A.F., Maraun, D. and Vrac, M., 2018. Increased Probability of Compound, Long-Duration, Dry and Hot Events in Europe. Accepted.

3. **Chapter 4 contributions:** The initial idea was formulated by DM and developed by CM, MW, and AVL. The experimental design was developed by CM. CM carried out the analysis, interpreted the results and wrote the results with contributions from MW and AVL. Analysis will be ongoing after this thesis is submitted. *Representation of Long-Duration Dry and Hot Events in CMIP5 models. In preparation.*

Contents

List of Figures	ix
List of Tables	xii
1 Introduction	1
1.1 Soil Moisture: Its Relevance, Quantification and Relationship with a Changing Climate	4
1.1.1 Quantification of Soil Moisture	7
1.1.2 Relationship with Climate Change	13
1.2 Soil Moisture Drought as a Compound Extreme Event:	21
1.3 Research Gaps	25
1.3.1 Objectives of the Thesis	28
2 Soil Moisture Drought in Europe: A Compound Event of Precipitation and Potential Evapotranspiration on Multiple Time Scales	31
2.1 Introduction	32
2.2 Data and Methods	33
2.2.1 Dataset	33
2.2.2 Conceptual Model	35
2.2.3 Copula	36

2.2.4	Pair Copula Constructions (PCCs)	37
2.2.5	Model Construction	42
2.2.6	Model Evaluation Metrics	47
2.3	Results	48
2.3.1	Model Performance	48
2.3.2	Assessment of Contributing Variables to Soil Moisture	49
2.3.3	Assessing the Relevance of Y Dependence Structure	54
2.3.4	Relevance of PET over Short and Long Integration Periods	58
2.4	Summary and Conclusions	59
3	Long-Duration, Dry and Hot Events in Europe	64
3.1	Introduction	65
3.2	Methods	66
3.2.1	Data	66
3.2.2	Event Definition	67
3.2.3	Estimation of Univariate and Bivariate Return Periods	68
3.2.4	Estimation of Annual Trends and Return Period Variation	71
3.2.5	Contributions to Return Period Variation	72
3.3	Results	73
3.3.1	Return Periods for Long Duration and Bivariate Extreme Events	77
3.3.2	Variations in Duration and Magnitude	81
3.3.3	Variations in Bivariate Return Periods	82
3.4	Summary and Conclusions	85
3.5	Supplementary Information	88
4	Long Duration, Dry and Hot Events in CMIP5	92

4.1	Introduction	93
4.2	Data	96
4.2.1	Observed Data	96
4.2.2	Global Climate Models	96
4.3	Methods	98
4.3.1	Event Definition	98
4.3.2	Estimation of Duration Return Levels	99
4.3.3	Estimation of Bivariate Return Periods	99
4.4	Results	100
4.4.1	Representation of Long Duration Events in CMIP5 Models . . .	101
4.4.2	Representation of Bivariate Return Periods in CMIP5	107
4.5	Summary and Conclusions	113
4.6	Supplementary Information	118
5	Synthesis	120
5.1	Summary and Discussion	121
5.1.1	Limitations of Findings	128
5.2	Outlook	130
	Bibliography	134
6	Appendix: Published Article	161

List of Figures

2.1	Locations of Fluxnet sites employed for this study	34
2.2	Schematic of the variables used in this study to construct the soil moisture model	36
2.3	Comparison of observed and modelled soil moisture time series	50
2.4	Contributions of meteorological variables to soil moisture drought estimation	51
2.5	Contributions of meteorological variables to soil moisture drought estimation in 2003 and 2006 events	54
2.6	Contributions of dependencies arising through land-atmosphere interactions to the estimation of low soil moisture values	56
2.7	Relevance of short- and long-term integrations of PET for soil moisture drought estimation	59
3.1	Summary of DH event characteristics	76
3.1	Summary of DH event characteristics	77
3.2	Return periods ($T(d)$) of dry events from $pref$ with durations (d) exceeding (a) 15; (b) 20; (c) 30; and (d) 40 days.	78
3.3	Absolute values at the 95 th and 99 th percentiles throughout Europe for D (a and c) and M (b and d).	79

3.4	Bivariate return periods for events in which both D and M are extreme	80
3.5	Trends in annual maxima as well as changes in frequency of extremes in D and M over historical period (1950-2013)	82
3.6	Changes in bivariate return periods of DH events over historical period (1950-2013)	83
3.7	Contributions to the variations in bivariate return periods from changes in the marginals D and M as well as the (D, M) dependence	85
3.8	Changes in bivariate return periods of DH events over historical period (1950-2013) for $IE=1, 2$, and 3	90
3.9	Same as Figure 3.7 but with the year 2010 removed from the analysis. Contributions to the variations in bivariate return periods from changes in the marginals D and M as well as the (D, M) dependence	91
4.1	Comparison of duration return levels between observations and CMIP5 models	102
4.2	Kernel density estimates of the pdf of duration return levels from all grid points across Europe for each ensemble member within a model's ensemble	105
4.3	Comparison of duration return levels between observations and each member of the HadCM3 ensemble	107
4.4	Comparison of bivariate return periods for joint extremes of D and M between observations and CMIP5 models	109
4.5	Kernel density estimates of the pdf of bivariate return periods ($T(D_{95}, M_{95})$) from all grid points across Europe for each ensemble member within a model's ensemble	111

4.6	Comparison of bivariate return periods for joint extremes of D and M between observations and each of the HadCM3 ensemble members . .	113
4.7	Comparison of duration return levels between observations and CMIP5 models obtained using the pdf mapped dry day threshold	118
4.8	Comparison of bivariate return periods for joint extremes of D and M between observations and CMIP5 models obtained using the pdf mapped dry day threshold	119

List of Tables

2.1	Summary of FLUXNET sites used in this study	35
2.2	Skill scores for sensitivity simulations	53
3.1	Top 5 Events from Stockholm grid cell.	88
3.2	Top 5 Events from Paris grid cell. Events ranked as described in the caption of Table 3.1.	89
3.3	Top 5 Events from Belgrade grid cell. Events ranked as described in the caption of Table 3.1.	89
3.4	Top 5 Events from Moscow grid cell. Events ranked as described in the caption of Table 3.1.	89
3.5	Top 5 Events from Madrid grid cell. Events ranked as described in the caption of Table 3.1.	89
4.1	Summary of CMIP5 Models Employed in this Study	97

Acronyms

ET Evapotranspiration

PET Potential Evapotranspiration

CE Compound Event

SPEI Standardised Precipitation Evapotranspiration Index

PDSI Palmer Drought Severity Index

RDI Reconnaissance Drought Index

DH Long-duration, dry and hot event

D Duration of event

M Magnitude of Event

PCC Pair Copula Constructions

CMIP5 Coupled Model Intercomparison Project Phase 5

JJA June, July, and August

$Y_{1_{PS}}$ Short-term integrated precipitation variable

$Y_{2_{PL}}$ Long-term integrated precipitation variable

$Y_{3_{PET}}$ Integrated PET variable

L_1 Short-term integration length for $Y_{1_{PS}}$

L_2 Long-term integration length for $Y_{2_{PL}}$

L_3 Integration length for $Y_{3_{PET}}$

CDF Cumulative Distribution Function

PDF Probability Distribution Function

S1 Set of Y variables with short-term integration of PET

S2 Set of Y variables with long-term integration of PET

LG Set of L for grassland sites

LF Set of L for forest sites

BS Brier Score

BSS Brier Skill Score

PP Persistence Probability

ACF Autocorrelation function

PACF Partial Autocorrelation function

CTRL Control Simulation

SENS- $Y_{1_{PS}}$ Sensitivity Simulation for contribution of $Y_{1_{PS}}$

SENS- $Y_{2_{PL}}$ Sensitivity Simulation for contribution of $Y_{2_{PL}}$

SENS- $Y_{3_{PET}}$ Sensitivity Simulation for contribution of $Y_{3_{PET}}$

IND- $Y_{2_{PL}}$ Sensitivity Simulation for contribution of $(Y_{2_{PL}}, Y_{3_{PET}})$ dependence

d_{sel}^{uni} Exceedance threshold for selection of values for fitting univariate model of D

m_{sel}^{uni} Exceedance threshold for selection of values for fitting univariate model of M

d_{sel}^{bi} Exceedance threshold for selection of D values for bivariate model

m_{sel}^{bi} Exceedance threshold for selection of M values for bivariate model

RP Return Period

RL Return Level

AIC Akaike Information Criterion

CvM Cramer von Mises criterion

ref Reference period (1950-1979)

pref Post-reference period (1984-2013)

Chapter 1

Introduction

Drought is an anomalous lack of water at the land-atmosphere interface (Berg and Sheffield, 2018). Two types of drought include meteorological drought and soil moisture drought. Meteorological drought is defined here as a persistent period in which daily precipitation is consistently below 1mm, while soil moisture drought is defined as a negative moisture anomaly in the upper layers of soil known as the root zone. The persistence of meteorological drought leads to the propagation of drought into soil moisture resulting in a negative moisture anomaly. Although soil moisture drought is primarily driven by a lack of precipitation, high levels of evapotranspiration (ET), related to high temperatures, can accelerate the propagation of drought from meteorological drought to soil moisture drought, and are required for the development of extremely negative soil moisture anomalies (Teuling et al., 2013; Seneviratne et al., 2012a).

The occurrence of soil moisture drought, resulting from the combination of meteorological drought and extremely high temperatures, can cause a diverse range of impacts. For instance, the recent 2014 drought in California that was characterised by low precipitation and high temperatures (AghaKouchak et al., 2014), led to a soil moisture drought that contributed to crop revenue losses of \$810 million and a total economic loss of \$2.2 billion arising from livestock losses, additional pumping costs and the loss of 17,100 seasonal and part-time jobs (Howitt et al., 2014). In 2003, the combination of soil moisture drought and extremely high temperatures led to the failure of the Wilnis Dike in the Netherlands (Van Baars, 2005). This displaced approximately 2,000 residents and left around 600 houses under a half meter of water (Van Baars, 2004). During that same summer, heavy reductions were seen in crop yields in large parts of Europe (van der Velde et al., 2012). Most recently, according to the European Drought Observatory, the 2018 European meteorological drought

and heat wave caused damages to crops and the livestock sector, interruptions to transportation due to low river levels, increased electricity costs in hydro-power dependent countries as well as wildfires in much of Northern Europe. The co-occurrence of soil moisture drought and extremely high temperatures also enhances the probability of wildfires as reduced moisture levels in soil and vegetation leads to heightened ignition conditions (Gudmundsson et al., 2014; Ruffault et al., 2016).

The co-occurrence of extreme events, such as meteorological drought with high temperatures, is termed a compound event (CE). CEs "*refer to the combination of multiple meteorological/climatic drivers and/or hazards that contribute to societal or environmental risk*" (Zscheischler et al., 2018). These events have received an increased amount of attention in recent years due to the growing awareness of the severity of their impacts which can be far greater than those arising from one extreme alone (Hegerl et al., 2011; Zscheischler et al., 2014).

Traditionally, climatological studies have approached extreme events from a univariate perspective (Zscheischler et al., 2018). Such an approach ignores the possibility of concurrent extremes, and thus underestimates the risk posed to society from meteorological extreme events. Furthermore, where impacts are identified as compound, ignoring the dependence between contributing meteorological hazards can result in an underestimation of the probability of a given impact (Bevacqua et al., 2017; Zscheischler et al., 2017).

The main aim of this thesis is to increase our understanding of the meteorological hazards that influence soil moisture drought, namely meteorological drought and extremely high temperatures. In particular, we develop frameworks to firstly quantify their contributions to the onset, persistence, and severity of soil moisture drought throughout Europe and secondly to quantify the probability of long-duration meteo-

rological droughts that co-occur with extremely high temperatures. The latter framework is applied in Europe to investigate changes in the frequency of such events over a 60 year time period (1950-2013) as well as to assess the representation of such events in global climate models (GCMs). Although this framework is developed to quantify the probability of long-duration meteorological droughts that co-occur with extreme temperatures in Europe, the framework may be readily applied to other locations and will have applications for other types of extreme events such as heat waves.

Within the following sections of this chapter, I will outline the current knowledge of soil moisture drought in terms of its relevance to society and the climate, how it is quantified and the current thinking on its relationship with climate change. Its quantification and relationship with climate change are important to consider in tandem as the method used to quantify soil moisture has a large influence on its response to increasing temperatures, and has been the subject of much discussion. Each of the above mentioned points will be important in gaining perspective on the relevance of the results presented throughout this thesis.

1.1 Soil Moisture: Its Relevance, Quantification and Relationship with a Changing Climate

Soil moisture is generally defined as the water contained in soil above the water table, otherwise called the unsaturated or vadose zone (Seneviratne et al., 2010). This definition can vary depending on the study as often only a certain portion is even measurable (Seneviratne et al., 2010) or indeed relevant, such as the root zone where vegetation can extract water from (Berg and Sheffield, 2018). As plants' transpiration is the largest contributor to total land evapotranspiration (ET) (Dirmeyer et al., 2006),

soil moisture is generally defined as water within the root zone, while soil moisture drought is a deficit of moisture within the root zone. These definitions will be used throughout this thesis.

Moisture availability in soil is of course important for vegetative growth and crop yields. The occurrence of severe soil moisture drought has led to large agricultural economic losses in the past. For instance, drought events in 2000 and 2012 in Serbia contributed to estimated losses of USD 500 million (Sepulcre-Canto et al., 2012) and USD 2 billion (Zurovec et al., 2015) respectively. Furthermore, the recent 2015 drought in California contributed to crop revenue losses of USD 810 million and a total economic loss of USD 2.2 billion arising from livestock losses, additional pumping costs and the loss of 17,100 seasonal and part-time jobs (Howitt et al., 2014).

Soil moisture also has an important influence on the climate system, and particularly on the variability of temperature. Soil moisture partitions incoming solar radiation into latent heat fluxes arising from ET and sensible heat fluxes that directly heat surface air temperatures. The influence of soil moisture on the climate system primarily arises through the moisture available in soil for ET to take place (Seneviratne et al., 2010). When soil moisture is low, there is a reduced availability of moisture for ET to take place leading to a reduced latent heat flux and an enhanced sensible heat flux. The presence of this interaction between the land-surface and atmosphere has a large impact on temperature variability, mostly in transitional climate zones between a drier climate to the south and a wetter climate to the north (Seneviratne et al., 2006; Schwingshackl et al., 2017). Indeed, much research in recent years has revealed the importance of land-atmosphere interactions in the development of extremes in temperature. For example, Hirschi et al. (2011) found that the number of hot days with temperature above a specified high threshold during summer months, is suppressed in

wet conditions but enhanced in dry conditions. From this study, we see also see that dry soil conditions are a necessary, though not sufficient, condition for the development of hot temperature extremes. Similar results were later found in Oklahoma, USA (Ford and Quiring, 2014), across Europe (Whan et al., 2015), and globally (Mueller and Seneviratne, 2012) using the same or similar methods.

Dry soils also have non-local effect on the development of temperature extremes. Vautard et al. (2007) found that the 10 hottest summers in Europe were preceded by a precipitation deficit in Southern Europe that propagated northwards in summer leading to the development of dry soil conditions and amplification of temperature extremes in Central and Eastern Europe through land-atmosphere interactions. They proposed a mechanism for this northward propagation which was verified using simulations from a limited area model (Zampieri et al., 2009). This was further complimented by Stefanon et al. (2012) who identified six European heat wave clusters in space and found that heat waves in Western and Eastern European clusters are generally preceded by spring precipitation deficits in the Mediterranean.

Many studies have since highlighted the contribution of land-atmosphere interactions in the development of temperature extremes during extreme heat waves. For example, by comparing four extremely hot summers taken from two regional climate simulations where the influence of land-atmosphere interactions is included in one simulation and not in the other, Fischer et al. (2007a) estimated the contribution of land-atmosphere interactions to the exceedance frequency of the 90th percentile of temperature. They found a 50-80% decrease in the frequency of exceedances throughout Europe when removing the influence of soil moisture. In similar experiments using regional climate models, other studies have shown a significant contribution to the severity of the extreme heat waves in 2003 and 2010 (e.g. Fischer et al. (2007b);

Miralles et al. (2014); Hauser et al. (2016)). These events were devastating in their impacts where they contributed to tens of thousands of excess deaths in France (Fouillet et al., 2006) and Russia (Shaposhnikov et al., 2014) as well as extreme impacts to vegetation (Ciais et al., 2005), further highlighting the important influence of soil moisture on temperature extremes.

1.1.1 Quantification of Soil Moisture

Despite the highlighted importance of soil moisture to agriculture, its influence on climate variability and extremes, in-situ soil moisture observations remain sparse in comparison to variables such as precipitation and temperature. Relatively few point measurements are available and only cover very short time periods (Robock et al., 2000; Dorigo et al., 2011). And even where point measurements exist, they are generally highly localised values as differences in soil properties can cause important differences in the mean and variance of soil moisture (Koster et al., 2009). Albeit, it should be noted that point measurements in space, although different from one location to the next, can show a temporal correspondence as seen by Mittelbach and Seneviratne (2012) who investigated 14 sites throughout Switzerland. These results suggested that point locations may be different in their climatology due to variations in soil characteristics, but the meteorological conditions driving soil moisture anomalies at each site will be similar.

Besides point measurements, remote sensing offers an alternative method for measuring soil moisture but suffers from its own limitations. Microwave remote sensing only characterises surface soil moisture and the retrievals are difficult to interpret in highly vegetated regions (Robock et al., 2000). As a result, soil moisture must be estimated via indirect methods using physically based land-surface models and drought indices.

It is important to understand the advantages and limitations of these methods when applying them in present and future climates, and so below I give a brief introduction into land-surface models and drought indices.

Land-Surface Models: land-surface models provide a physically-based representation of soil moisture. A large advantage is that they can provide spatially and temporally continuous fields of soil moisture at large scales (Sheffield and Wood, 2012). These models provide reasonably realistic representations of soil moisture and thus provide a valuable resource for drought monitoring (e.g. Mitchell et al. (2004); Sheffield et al. (2014)), soil moisture drought forecasting (Wanders and Wood, 2017; Thober et al., 2015) which also lends to improvements in sub-seasonal and seasonal forecasts of temperature (Orth and Seneviratne, 2014; Weisheimer et al., 2011), and climatic studies of soil moisture (e.g Sheffield and Wood (2008); Berg et al. (2017); Samaniego et al. (2018)).

However, as with all models, land-surface models are imperfect and subject to biases. Such biases can arise from the calibration of model parameters which is complicated by the scarcity of observations of land surface hydrology as well as the large spatial heterogeneity of soil characteristics (Orth et al., 2016). Improving these models is not a trivial task and efforts to do so do not always pay off, as found by (Orth et al., 2015). They compared three models of differing complexity in their ability to forecast soil moisture drought, with the most complex model seen as an improvement from the intermediate model, which is also an improvement from the simplest model. They found no improvement with increasing complexity, and actually found that the simplest model performed best. Such a finding highlights a reality faced by model developers who have too few observations to constrain model parameterisations of more complex processes in soil hydrology. In a attempt to overcome this problem, Orth et al.

(2016) incorporated parameter uncertainty into forecasts and found improvements in their ability to forecast soil moisture by doing so. Their method involved searching the parameter space for combinations of six parameter values that yield the best results, and although this method is more adhoc than an improvement gained via process-based understanding, it nonetheless signifies the difficulty in improving such models while also providing an alternative means for a step forward.

The large uncertainties associated with parameterisations can also produce large differences in output produced by a variety land-surface models, even when driven by the same meteorological information (Koster et al., 2009). These differences arise from a diverse range of parameterisation schemes used to represent soil, vegetation and land hydrology in various models which furthermore produces difficulties in the interpretation of output from these models (Koster et al., 2009). The biggest differences between models lie in the prescribed soil depth in models that varies between 3 to 14m, the number of soil layers which can vary between 3 and 23, and the different hydraulic parameters (Berg et al., 2017). It is worth noting that alongside the large differences in soil depths between models, Orth et al. (2016) found soil moisture forecasts from a single model to be most sensitive to changes in soil depth than a number of other parameters. Results from Koster et al. (2009) and Orth et al. (2016) are obtained using the the total column integral of soil moisture over all layers, and so will include moisture from varying depths. This is a somewhat arbitrary variable and care is needed in its interpretation, particularly when comparing output across models as it is a model specific quantity that is largely sensitive to the choice of parameterisations (Koster et al., 2009). Although large quantitative differences will exist in this variable between models, Koster et al. (2009) show that when driven by the same meteorological input, the models show a temporal correspondence in this quantity. In

terms of differences seen in future projections of total column soil moisture, Berg et al. (2017) find large quantitative differences between model projections but do show a qualitative agreement in the sign of change. Berg et al. (2017) also argue the point for assessing soil moisture layers relevant for vegetation such as in root zone which can be compared between models in absolute terms, while also offering more impact relevant information. In doing so they were able to disentangle changes at various depths which will be discussed further on in this chapter. Overall, the temporal correspondence and qualitative agreement between models highlights the importance of the meteorological input which largely governs the general state of soil moisture in models (i.e. dry or wet), while the quantitative differences between model output will be influenced by variations in the individual model formulations.

Drought Indices: Drought indices incorporating precipitation and temperature are often used as proxies of soil moisture (Dai et al., 2004; Hirschi et al., 2011; Törnros and Menzel, 2014) for drought monitoring (Vogt et al., 2011) and in analyses of soil moisture drought response to increasing temperatures as a result of climate change (Dai et al., 2004; Dai, 2011; Sheffield et al., 2012; Dai, 2013; Trenberth et al., 2014; Törnros and Menzel, 2014; Vicente-Serrano et al., 2014; Zarch et al., 2015; Stagge et al., 2017). An advantage of these indices lies in their simplicity and their use of widely available meteorological variables such as precipitation and temperature. They thus provide an invaluable tool where soil moisture data and resources for land-surface modelling are not available. However, the inclusion of temperature in commonly used indices such as the Standardised Precipitation Evapotranspiration Index (SPEI) (Vicente-Serrano et al., 2009) and the Palmer Drought Severity Index (PDSI) (Palmer, 1965) has drawn criticism when using such indices to infer information of the response of soil moisture drought to climate change (Sheffield et al., 2012;

Seneviratne, 2012).

Soil moisture is a slowly varying quantity that shows temporal persistence and holds memory of the meteorological conditions in preceding months. Thus, describing soil moisture with drought indices requires one to account for antecedent meteorological conditions that soil moisture holds memory of. This is done using integrations of a climatic water balance (precipitation-PET) varying in length from 1 to 24 months for the SPEI. The SPEI is calculated through fitting a parametric distribution to the climatic water balance variable. The cumulative probabilities are obtained using the CDF of this distribution and are then transformed to a normal distribution with a mean of zero and a standard deviation of 1. Values below indicate drier than normal conditions while values greater than 1 indicate wetter than normal conditions. The selection of this integration length for indices such as the SPEI is important; a length that is too short will not capture drought persistence while longer periods can include redundant information (Törnros and Menzel, 2014). Studies using the SPEI to represent soil moisture generally use integration periods between 3 and 6 months (Hirschi et al., 2011; Törnros and Menzel, 2014). The PDSI is a recursive model that is calculated using monthly integrations of the climatic water balance and it can hold memory of the previous winter and spring in summer months (Dai et al., 2004). It is a type of bucket model and so it is quite similar to many land-surface models which are also generally bucket models that will fill the surface layer with moisture before allowing moisture to move to lower layers. Although the PDSI is similar to land-surface models, a key difference is in its output. Land-surface models output soil moisture in units of % saturation with upper and lower bounds, while the PDSI is unit-less with no upper or lower bounds. Hence it can thus only be considered an index of soil moisture rather than a model producing soil moisture output.

Temperature is incorporated into drought indices through potential evapotranspiration (PET). This measures the evaporative demand of the atmosphere and indicates the amount of ET that would occur given an unlimited water supply. The influence of PET on soil moisture thus depends on the availability of moisture in the soil for ET to take place (Seneviratne et al., 2010). Under moisture-limited conditions, values of PET and ET can diverge where ET may verge to zero while PET can continue to rise with an increase in temperature (Seneviratne et al., 2010). In such dry conditions, PET and temperature can have little contribution to the estimation of soil moisture (Luo et al., 2017) and lead to drying biases in terms of moisture levels in soil when incorporated into drought indices (Sheffield et al., 2012; Seneviratne, 2012; Milly and Dunne, 2016), and greatly overestimate drying in comparison to land-surface models (Burke, 2011; Hoerling et al., 2012).

However, the use of a climatic water balance implies that PET influences soil moisture over the same time-scale as precipitation. Drying of soil occurs on a daily time-scale where excesses in ET can be driven by days and periods of extreme temperature that are filtered out through the use of longer integration periods. The long integration period also hides explicit information of singular or even sequences of meteorological drought events and temperature extremes during such events. In a drought monitoring context, such a caveat of long integrations of the climatic water balance may not have any large implications as their output will be supplemented with the users interpretation. However, in a climatic context, the use of such integrations can lead to an inability to identify the most relevant changes in the meteorological hazards, namely the duration of meteorological droughts and the temperature during those events.

1.1.2 Relationship with Climate Change

It is important to distinguish between changes in soil moisture and changes in soil moisture drought events with climate change. The former refers to changes in the background state and climatology of soil moisture, while the latter refers to changes in drought events which are generally defined as transient departures from the local climatological norm that have a duration, area and magnitude (e.g. maximum deficit). Although they are intrinsically linked to one another, their drivers are not the same and so I will provide separate discussions of the two below and link them together to give a more rounded perspective.

Soil Moisture and Climate Change: There have been many studies looking to gauge the response of soil moisture to increasing global temperatures. These studies have employed both drought indices and land-surface models. Through the analysis of indices such as the SPI and SPEI in Europe, potential changes in drought risk have been assessed in Europe. (Gudmundsson and Seneviratne, 2016) employ both observations and two sets of simulations from climate models where the anthropogenic forcing on climate is included and excluded. They find an increase in drought risk in Southern Europe, a decrease in Northern Europe and inconclusive results in Central Europe. This found in observations and climate model simulations that incorporate the anthropogenic climate forcing, but not in simulations that exclude this forcing. They conclude that anthropogenic climate change has already increased the risk of drought in Southern Europe. These results are complimented by (Stagge et al., 2017) who analysed changes in both the SPI and the SPEI which includes the influence of temperature through PET. They again found increased risk in Southern Europe in both indices but a divergence between them in Northern Europe where both show decreased

drought risk but much less so in the SPEI. They concluded that increased temperatures and PET are compounding reduced precipitation in Southern Europe while actually counteracting the increased precipitation in Northern Europe.

In global analyses of the PDSI, conflicting results have arisen from the choice of method used to compute PET as well as in the observation datasets employed in the given study. For instance, using the temperature only based Thornthwaite equation to estimate PET for inclusion in the PDSI, both Dai et al. (2004) and (Dai, 2011) found a significant increase in the global area that could be defined as "very dry" according to the PDSI. In contrast, using the physically based Penman-Monteith equation to estimate PET for its inclusion in the PDSI, Sheffield et al. (2012) found little or no change to global drought area. The latter method used to estimate PET incorporates relative humidity, incoming solar radiation and wind speed and is thus considered a more reliable method of computing PET than the Thornthwaite method which relies solely on temperature. In a later publication, the authors of the above studies joined forces to assess alternative sources for their discrepancies. They highlighted that results derived from the PDSI were sensitive to time period used to calibrate the model, the method used to estimate PET, as well as the choice of precipitation dataset (Trenberth et al., 2014). Taking such uncertainties into account, they concluded that increased temperatures due to global warming may not cause drought but when drought events occur, it is expected they will set in quicker and become more severe.

Further to the uncertainties outlined above, changes in soil moisture are closely linked to the response of vegetation. For instance, an increase in atmospheric CO₂ concentration stimulates carbon assimilation in plants while also reducing stomatal conductance (the rate of water vapour loss through stomata in plant leaves) which leads to a general increase in water use efficiency in vegetation (Field et al., 1995; Hungate

et al., 2002; Long et al., 2006). Although bulk stomatal conductance is included in the Penman-Monteith formulation of PET, it assumes that stomatal conductance will remain unchanged in a future climate (Scheff and Frierson, 2014). Using simulations of future climate in which stomatal conductance alters with increases in CO₂ concentrations, Milly and Dunne (2016) showed in non-water stressed areas, where PET should equal ET in theory, that PET derived using the Penman-Monteith method actually largely overestimates ET simulated by the climate models. They attributed this overestimation to the assumption made when using PET that stomatal conductance remains unchanged. Thus, accounting for changes in this quantity is quite important as a reducing stomatal conductance can act to conserve soil moisture in climate models (Berg et al., 2016a; Swann et al., 2016; Burke, 2011).

The findings of Milly and Dunne (2016) are pertinent for studies employing drought indices. Disagreements have been found between soil moisture simulated within a coupled climate model and offline drought indices that incorporate PET. For example, Burke (2011) show that the PDSI exhibits a much higher drought frequency in a climate where CO₂ is doubled than a precipitation based metric alone or indeed soil moisture simulated from the model. Similarly, Hoerling et al. (2012) find that the PDSI grossly overstates future changes in soil moisture in comparison to simulated soil moisture. Generally, the only agreement found between these two quantities are when considering only regions of strong precipitation changes (Zhao and Dai, 2015a), which is actually quite an imposed measure of agreement. In summary, drought indices that incorporate PET overestimate the sensitivity of soil moisture changes to changes in temperature. The use of drought indices over land-surface models is often justified using the uncertainties associated with land-surface models that may be 'bypassed' in using drought indices. However the structural and physical model uncer-

tainties discussed above in previous paragraphs and sections reflect a reality and the deep uncertainties in our understanding changes in soil moisture (Berg and Sheffield, 2018). Incorporating such uncertainty in the assessment of drought risk both in future climate and seasonal forecasting is highly necessary to gain a full appreciation of the potential risk posed by soil moisture drought in the future.

As highlighted above, the main drivers of changes in the climatology of soil moisture arise from changes in precipitation, temperature and CO₂ concentrations that influence stomatal conductance. The relative importance of these drivers remains unclear. For instance, the response of temperature in future simulations of climate models is related to the level of drying in soil in each model. Models that become drier show higher projected increases in temperature which is largely attributed to land-surface interactions (Berg et al., 2015; Vogel et al., 2017, 2018). It should also be noted that the drier/wetter models also have lower/higher mean precipitation (Vogel et al., 2018) which would suggest that the response of precipitation to climate change will firstly determine the response of soil moisture that then modulates/amplifies temperature through land-atmosphere interactions. However, this causal chain is perhaps over-simplified as it could also be related to the choice of land-surface model within the coupled model which may determine how soil moisture responds and represents different feedbacks such as soil moisture-temperature, soil moisture-precipitation and soil moisture-radiation (Vogel et al., 2018). Similarly Berg et al. (2016b) demonstrate that land-atmosphere interactions increase atmospheric aridity through amplifying the higher warming over land compared to oceans. This land-ocean contrast has been demonstrated as a driver soil moisture drying as the relative humidity of the air advected from oceans contains insufficient water vapour to keep pace with the greater increase in the saturation vapour pressure deficit over land (Rowell and Jones, 2006;

Byrne and O’Gorman, 2013; Sherwood and Fu, 2014), resulting in decreasing relative humidity.

Soil Moisture Drought and Climate Change: It is important to distinguish between changes in soil moisture (as described previously) and changes in soil moisture drought events with climate change. The former refers to changes in the background state and climatology of soil moisture, while the latter refers to changes in drought events which are generally defined as transient departures from the local climatological norm that have a duration, area and magnitude (e.g. maximum deficit). To what extent soil moisture should "depart" from its climatology before a drought event is declared varies from study to study and can depend on the aim of the given study.

Although it is important to distinguish between changes in soil moisture and changes in soil moisture drought, they are of course intrinsically linked. For instance, by assessing changes in soil moisture across layers in the top 3m in soil moisture as depicted by an ensemble of 25 CMIP5 models, Berg et al. (2017) show a gradient in changes in soil moisture where the top layer of soil moisture changes are much greater than those at lower layers. They point out that assessing top layers only will overestimate the impact of such changes to vegetation which will still have ample water resources within lower layers on top of their hypothesised future increase in water use efficiency. However, if we superimpose meteorological drought events which may be warmer in a future climate, soil moisture at lower layers may be left more exposed from a reduced buffering effect due to less moisture in the top layers, thus leading to larger soil moisture deficits and an increased exposure of vegetation and vulnerability to drought conditions if the background state has become drier.

Very few studies have focussed on changes in soil moisture drought event characteristics. Those that have done so have investigated changes in the duration and area of

such events. For example, Sheffield and Wood (2008) analyse changes in the duration of drought events globally. Of interest to Europe, the frequency of long duration soil moisture events was found only to have a significant increase (and difference) in the Mediterranean region in future projections. In a more recent study, changes in the duration and area of such events was examined using an ensemble of CMIP5 simulations (Samaniego et al., 2018). They found significant increases in duration and area affected throughout Europe with higher increases found for larger increases in global mean temperature.

Rather surprisingly, and to the best of my knowledge, there has been no studies analysing the drivers of soil moisture drought events, namely the frequency and duration of meteorological droughts and the level temperature during those events that will modulate the amount of ET. Thus, such events have not been validated in climate models. Given that soil moisture drought events are driven by meteorological conditions (Teuling et al., 2013; Seneviratne et al., 2012a), the confidence we can have in projections of soil moisture drought events, and perhaps soil moisture itself, is limited by the representation of the meteorological drought events and their response to climate change.

Of course, in an implicit way, there have been validation studies on events related to meteorological drought in the form of studies on atmospheric blocking events and heat waves. In terms of blocking, the majority of this literature has focussed on the representation of winter blocking in climate models where the persistence of blocking is systematically underestimated (Lucarini et al., 2007; Scaife et al., 2011; Anstey et al., 2013; Berckmans et al., 2013; Hoskins and Woollings, 2015; Woollings et al., 2018), although improvements are found with increasing model resolution (Scaife et al., 2011). Those that have studied the representation of blocking frequency dur-

ing summer in CMIP5 models have found mixed results but no systematic bias. For example, Masato et al. (2013) find a varied performance between CMIP5 models with underestimations and overestimations of blocking frequency found in different models, while other models show good agreement with the observed blocking frequency. In general though, they see an underestimation of blocking frequency over Eurasia where the Russian heat wave took place. However, in this study, the blocking frequency is estimated with respect events lasting longer than 5 days which sheds little light on the representation of the extreme duration events in climate models. Similarly, Dunn-Sigouin and Son (2013) compare the multi-model mean of blocking frequency in CMIP5 models where the blocking frequency refers to events lasting at least 5 days. They found a slight underestimation over the East Atlantic and over Europe. However this analysis considers annual blocking frequency and so no specific information of summer may be extracted. However, they do compare the pdf of the duration of events lasting longer than 5 days, but only for the East Atlantic sector finding a tendency in CMIP5 models to underestimate the frequency of events less than 7 days but a good comparison for events up to at least 15 days in duration. It should be noted that this comparison was made for the multi-model mean in the frequency of events for given durations and so we are given no information of the performance of individual models. Also, the east Atlantic sector obviously does not lie over land and so there is no specific information of how long duration events are represented over Europe. Scaife et al. (2010) also investigates summer blocking frequency with respect to events lasting longer than 5 days, and find an underestimation over Europe and Asia. Also related are studies investigating the representation of heat waves in climate models. In general, the representation of heat waves is quite variable across models in terms of characteristics such as duration and area (Schoetter et al., 2015) as well as

the large-scale drivers of heat waves (Lhotka et al., 2018). (Schoetter et al., 2015) studied changes in the representation of characteristics such as duration, area and severity of heat waves in an ensemble of CMIP5 models. They found the ensemble median of the characteristics to be in line with the mean of observed characteristics, although no model was able to produce an event with a duration or spatial extent as the 2003 heat wave. This is somewhat unsurprising however given the extremity and rarity of the event that may not be seen in 30 year time periods analysed in the models. However, the strength of their conclusions are somewhat hampered by the time period chosen which yielded 7 heat wave events. Lhotka et al. (2018) analysed the driving processes behind three major central European heat waves and looked at similar heat waves in a set of EURO-CORDEX regional climate models driven by differing GCMs. The analysis again is limited to three observed events and so information of good performance or systematic biases in event characteristics is difficult to obtain. However, in models that generally seemed to produce events with characteristics similar to those observed, the drivers behind the events were suspect and could be found to compensate one another. For instance, in some models the south-easterly flow leading to a heat wave was too strong and overly persistent but was compensated by the soil moisture which was too wet, and vice-versa. Although such conditions are not impossible, the models may be producing heat waves through driving mechanisms that are uncommon in observations leading to questions of whether heat waves occur for the right reason in climate models. This persistence of the flow was also shown to be overestimated in other studies of EURO-CORDEX models (Vautard et al., 2013; Plavcová and Kyselý, 2012). Besides circulation biases, land-atmosphere interactions have also been found to be a driver of temperature biases during heat waves as soil moisture can dry out too quickly in summer leading to the onset of a moisture limiting ET

regime and the amplification of temperatures (Stegehuis et al., 2012) and overestimation of temperature variability during summer (Fischer et al., 2012a). It has later been shown that such biases in temperature can be reduced through improvements in the land-surface models in their partitioning of latent and sensible heat fluxes (Fischer et al., 2012a; Stegehuis et al., 2013; Lorenz et al., 2012; Davin et al., 2016).

1.2 Soil Moisture Drought as a Compound Extreme Event:

A compound event "refers to the combination of multiple meteorological/climatic drivers and/or hazards that contribute to societal or environmental risk" (Zscheischler et al., 2018). The topic of compound events and considering extreme impacts from a multivariate perspective is a relatively new area of research that has previously been highlighted by (Hegerl et al., 2011) and Leonard et al. (2014) as well in the most recent report from the Intergovernmental Panel on Climate Change (IPCC) (Stocker et al., 2014) as an important area for future research. The notion that impacts are driven by multiple variables not a new concept. It is more a recognition of the importance in approaching extreme events from a multivariate perspective as the co-occurrence of extremes can lead to impacts that are far greater than those arising from one extreme occurring alone. As a consequence, it is vital to understand which drivers of extreme impacts are dependent in their extremes and which are independent, such that a co-occurrence may be random bad luck. However, cases that may at first been seen as random co-occurrences, may in fact have arisen from a complex chain of events that when viewed in hindsight, could be disentangled to reveal a causal mechanism for their co-occurrence making it more likely than random chance. Although not the focus of this thesis, it worth noting the work on storyline methods

currently being developed to help shed light on such extreme impacts and unforeseen events in order to view them with foresight and reduce the potential risk of extreme impacts (Hazeleger et al., 2015; Shepherd et al., 2018).

As mentioned already, the focus of this thesis will be on soil moisture drought and its meteorological hazards. Soil moisture drought arises from the interplay of reduced precipitation, high temperatures, and land-atmosphere interactions that combine and feed off one another to further reduce a soil moisture deficit. The onset of drought events arises from the persistence of meteorological drought that is driven by large-scale processes such as blocking events and sub-tropical ridges that are themselves embedded within planetary-scale Rossby waves. The persistence of meteorological drought leads to the propagation of drought into soil moisture resulting in a negative moisture anomaly in the upper layers of soil known as the root zone. This propagation depends on both the duration of the meteorological drought and the temperature during the event. Longer dry periods allow for more drying of soil than shorter intermittent dry periods separated by wet days providing recharge, while high temperatures that increase evapotranspiration (ET) can accelerate this propagation of drought (Seneviratne et al., 2012a; Orlowsky and Seneviratne, 2012; Teuling et al., 2013). The joint occurrence of extremely long-duration and high magnitude events may thus lead to higher soil moisture deficits than events where only one characteristic is extreme. Larger deficits can then produce longer lasting soil moisture droughts as higher amounts of precipitation are then required for drought recovery (Seneviratne et al., 2012a).

The above paragraph highlights the compound nature of soil moisture drought, and throughout this thesis the aim is to develop a framework in order to disentangle the meteorological drivers of soil moisture drought, namely precipitation and PET, over

relevant time-scales and provide a framework to quantify the probability of meteorological drought events that coincide with extreme temperatures. For the latter case, accounting for the dependence between drivers will be important. Neglecting the dependence between extremes in a statistical model can lead to the underestimation of the probability of the two drivers to exceed a specified extreme threshold at the same time. This has been demonstrated by (Zscheischler and Seneviratne, 2017) who showed the probability of dry and hot summers were underestimated when considering accumulated summer precipitation and mean summer temperature independent of one another. Similarly AghaKouchak et al. (2014) have shown that the probability of co-occurrences of extremely low monthly accumulated precipitation with extremely high temperatures is underestimated when not accounting for their dependence. The underestimation of such probabilities have a knock on effect in the estimation of the likelihood of extreme impacts. For instance, Zscheischler et al. (2017) have shown that ignoring the dependence between precipitation and temperature at specified times leads to an underestimation in the probability of low crop yields estimated via a statistical model. Each of these studies have employed a copula based approach to quantify these joint probabilities.

A copula is a bivariate distribution function that models the dependence between the marginal variables (e.g. precipitation and temperature) independent of the marginal distributions, which creates much flexibility when modelling bivariate pdfs. Throughout this thesis, copula-based methods are employed in fitting bivariate and multivariate pdfs. More details are given within the results chapters that are each accompanied by their own methods section. The use of a parametric approach allows one to extrapolate outside the observed distribution to gain an estimate of the probability of an unforeseen event, albeit such estimates may be accompanied by large uncertainties.

The use of parametric statistical models also allows one to perform sensitivity analysis in which contributions from different variables to the estimation of an impact may be quantified. Furthermore, when assessing changes in probabilities from one period to another (e.g. changes between 1950-1979 and 1983-2013), contributions to the change in bivariate probabilities arising from changes in either of the marginal distributions and indeed their dependence, may be quantified.

Alternative methods to study compound extremes include non-parametric approaches, although a caveat of this is that they cannot extrapolate outside of the observed distribution. Nonetheless, many studies have availed of non-parametric approaches in studying multivariate extremes. For example, Beniston (2009) assessed the change in joint dry and hot extremes on monthly time-scales by basically counting the number of joint exceedances above specified thresholds finding an increase joint occurrences of dry and hot extremes. Other studies have assessed the influence of co-occurring extremes on different impacts. For example, (von Buttlar et al., 2018) studied the joint effect of the duration drought events and temperature on different measures of ecosystem productivity by comparing conditional distributions of these measures, where the conditional distributions are extracted for events in which the duration and temperature exceeds specified thresholds. They found that duration is more important than temperature but importantly they also find that the most extreme impacts arose during long duration events in which temperature was most extreme. Similarly, using accumulated precipitation over three months alongside the mean temperature of the most recent month, (Zscheischler et al., 2014) assess the influence of dry and hot extremes on carbon fluxes. They find that the impacts arising from joint dry and hot extremes are far greater than the impacts arising from individual extremes alone.

1.3 Research Gaps

Land-surface models provide a physical representation of soil moisture, but with large uncertainties in their resulting output (Koster et al., 2009), it remains necessary to use drought indices and widely available meteorological information to approach soil moisture drought from multiple lines of enquiry. The simplicity of drought indices is advantageous but it also leaves their output open to interpretation (Sheffield et al., 2012; Seneviratne, 2012). Such features of drought indices has led to conflicting results with regards to historical changes in soil moisture drought and its relationship with climate change (e.g. (Sheffield et al., 2012) and (Dai, 2011)). With increasing temperatures, soil moisture drought events are expected to set in quicker and become more severe (Trenberth et al., 2014). However, due to the divergence between PET and ET when soil is dry, it is difficult to put these changes in drought indices incorporating PET into context for soil moisture in dry climates. To address this issue, we disentangle the information withheld by the integration periods used by drought indices and analyse the contributions of precipitation and PET to soil moisture drought over different integration periods. In doing so, we look to gain information of the contributions of PET and precipitation to soil moisture drought in wet, transitional and dry climates in Europe during the summer months June, July and August (JJA), and examine the credibility of the assumed relationships between soil moisture, precipitation and PET in drought indices.

Changes in soil moisture drought are driven by changes in meteorological hazards, namely the duration of meteorological droughts and the temperatures during those events. Within this thesis, we term these events as long-duration, dry and hot (*DH*) events. *DH* events are characterised by their duration (*D*) and magnitude (*M*). *D* is defined as the consecutive number of days where precipitation is below 1mm, and

long duration events are combined if separated by 2 days or less. M is then defined as the maximum temperature reached during an event. Longer durations allow for more drying of soil than shorter intermittent dry periods separated by wet days providing recharge, while extremely high temperatures can lead to high levels of ET. Thus, changes in the probability of their co-occurrence of extremes of D and M will have direct implications for soil moisture drought.

With regards to D , an increasing frequency of long-duration events has been seen in the Netherlands (Zolina et al., 2013), while only small changes were found in the annual maximum duration over Europe (Donat et al., 2013). Ye (2018) showed increases in the seasonal mean duration across Russia and demonstrated that locations with largest increases exhibit a higher rise in seasonal mean temperature. However, although we expect to see high temperatures during dry periods due to the anti-cyclonic systems such as blockings and sub-tropical ridges that underlie dry periods in Europe (Pfahl and Wernli, 2012; Sousa et al., 2018), there are currently no studies which quantify the probability of long duration meteorological droughts that co-occur with extremely hot temperatures. Previous studies have estimated the probability of co-occurring dry and hot conditions (e.g. AghaKouchak et al. (2014); Zscheischler and Seneviratne (2017); Zscheischler et al. (2017)), though these studies investigate precipitation accumulations over specified periods of time (e.g. monthly, seasonal etc.), and not the duration of events which has an important influence on ecosystem impacts (von Buttlar et al., 2018). Furthermore, drought analysis based on meteorological variables has for the most part focussed on trends in drought indices such as the SPI (Gudmundsson and Seneviratne, 2016), SPEI (Stagge et al., 2017) and PDSI (Dai et al., 2004; Sheffield et al., 2012; Dai, 2013; Trenberth et al., 2014). These indices are calculated by integrating variables such as precipitation and potential ET over time, and so bear

no explicit information of individual *DH* events. We therefore look to add further insight to changes in the meteorological hazards that influence soil moisture drought through analysing *DH* events. Within this analysis and following recommendations of Zscheischler et al. (2018), we propose a framework to that can be used to characterise compound *DH* events and quantify their probability through the application of a copula-based approach introduced in Bevacqua et al. (2018). This framework can be applied in other regions and in the assessment of climate model output, and to other types of events such as heat waves.

Climate models are central to our understanding of how climate change will influence *DH* events. As the planning of adaptation and mitigation measures for a future climate are mostly based on their projections, it is important to assess their skill in representing these extreme events (Hoskins and Woollings, 2015). Although the limitations of climate models in representing single variables has been widely investigated, it is not clear how well climate models can capture the multivariate nature of CEs (Fischer and Knutti, 2013; Collins et al., 2013). The representation of the duration of events, defined in this manner, has not been studied in climate models in depth. Donat et al. (2013) have compared the maximum duration event between observations and models, but little has been done in terms of their frequency of relationship with extreme temperatures.

The characteristics of *DH* events are representative of anti-cyclonic systems such as blockings and sub-tropical ridges. Results from previous studies assessing blocking in climate models are therefore relevant here. The majority of this literature has focussed on the representation of winter blocking in climate models where the persistence of blocking is systematically underestimated (Lucarini et al., 2007; Scaife et al., 2011; Anstey et al., 2013; Berckmans et al., 2013; Hoskins and Woollings, 2015;

Woollings et al., 2018), although improvements are found with increasing model resolution (Scaife et al., 2011). Those that have studied the representation of blocking frequency during summer in CMIP5 models have found mixed results but no systematic bias. For example, Masato et al. (2013) find a varied performance between CMIP5 models with underestimations and overestimations of blocking frequency found in different models, while other models show good agreement with the observed blocking frequency. While Dunn-Sigouin and Son (2013) find a good agreement between the multi-model mean and observed summer blocking frequency, though information of individual models is not given. Overall, little attention has been given to the representation of *DH* events, and so we assess their performance in this regard.

The importance of meteorological input into land-surface models has been highlighted throughout this chapter. Large quantitative differences can exist between models owing to a diversity of model formulations, but their output will show temporal correspondence (Koster et al., 2009) and qualitative agreement (Berg et al., 2017) owing to the strong influence of the meteorological input. Our confidence in future projections of soil moisture drought events such those provided by (Samaniego et al., 2018) are therefore ultimately limited by the representation of meteorological drought events in climate models. And so to gain knowledge of the full uncertainties around future projections of soil moisture drought, we must understand their limitations in representing the meteorological drought events.

1.3.1 Objectives of the Thesis

Again, the main aim of this thesis is to increase our understanding of the influence that meteorological hazards have on soil moisture drought, namely meteorological drought and extremely high temperatures. In particular, this research focuses on their

contributions to soil moisture over varying time-scales and the co-occurrence of their extremes. To address these research gaps and fulfil the aim outlined above, we look to complete the following objectives:

Chapter 2: Develop a Framework That Will Provide a Method to Assess the Contributions of Precipitation and PET to Soil Moisture Drought at local scales in Wet, Transitional and Dry Climates Throughout Europe Over Multiple Time-Scales

In this chapter we analyse soil moisture drought as a compound event of meteorological drought and extreme temperatures in Europe. We use a conceptual framework developed in Bevacqua et al. (2017) and apply it to a system in which we describe soil moisture as a function of precipitation integrated over preceding months, and PET integrated over recent days. This conceptual framework allows us to capture days of extreme temperature within the PET variable and its dependence on antecedent conditions. The framework is implemented via a multivariate statistical model based on Pair Copula Constructions (PCCs) (Aas et al., 2009). Using the statistical model, we perform sensitivity simulations to test the contributions of precipitation and PET as well as the contribution of their dependence to the estimation of soil moisture.

Chapter 3: Develop a Framework to Characterise and Quantify the Probability of Compound Long Duration, Dry and Hot (DH) Events Across the European Continent and Estimate Changes in their Probability over the Period 1950-2013

In this chapter, we quantify the probability of DH events in which both the duration D and magnitude M exceed their respective 95th percentiles. We assess changes in this probability throughout Europe and identify the main drivers behind these changes. We employ an approach developed for compound flooding in Bevacqua et al. (2018) and estimate joint probabilities through the application of a parametric copula-based

probability distribution.

Chapter 4: Assess the Representation of Compound Long Duration, Dry and Hot Events in Global Climate Models We apply the same approach as applied in Chapter 3 to a set of CMIP5 models. We assess their ability in representing *DH* events, both in terms of the duration of these events as well as the probability of *DH* events in which *D* and *M* jointly exceed their 95th percentiles.

How to Read Thesis: The thesis is structured according to the objectives outlined above, I present the results in three chapters. Each chapter includes its own short introduction and conclusion such that they may be read independently of one another. The methods and data used in each chapter are described within the given chapter. The same methods are used for Chapters 3 and 4, therefore these methods are only described in full within Chapter 3 but are briefly repeated in Chapter 4. Finally a synthesis of the results along with an outlook on possible future research is given in Chapter 5.

Chapter 2

Soil Moisture Drought in Europe: A Compound Event of Precipitation and Potential Evapotranspiration on Multiple Time Scales

2.1 Introduction

Drought indices incorporating precipitation and potential evapotranspiration (PET) to account for the effect of temperature on drought conditions, are often employed as proxies for soil moisture (Dai et al., 2004; Törnros and Menzel, 2014). Drought indices that incorporate PET to account for the effect of temperature on drought conditions are sensitive to global warming and thus are often used in studies of soil moisture drought response to increasing temperatures as a result of climate change (Dai et al., 2004; Dai, 2011; Sheffield et al., 2012; Dai, 2013; Trenberth et al., 2014; Törnros and Menzel, 2014; Vicente-Serrano et al., 2014; Zarch et al., 2015; Stagge et al., 2017). Soil moisture drought refers to moisture deficits in the upper layer of soil known as the root zone. Soil moisture in the root zone is primarily controlled by antecedent precipitation while excesses in evapotranspiration (ET), related to high temperatures, are required to explain the severity of a negative soil moisture anomaly (Teuling et al., 2013; Seneviratne et al., 2012a). High temperatures driving excesses in ET can be partly attributed to land-atmosphere interactions induced by deficits in precipitation. By leading to dry soil conditions, low antecedent precipitation is associated with an increased probability of hot days (Hirschi et al., 2011; Mueller and Seneviratne, 2012; Whan et al., 2015; Ford and Quiring, 2014), amplified extreme temperatures and the persistence of heat waves (Miralles et al., 2014; Lorenz et al., 2010) that, in turn, can further deplete soil moisture where moisture is available. The individual roles of precipitation, temperature (that drives excesses in ET), and that of their dependence driven through land-atmosphere interactions, highlights the compound nature of soil moisture drought.

However, the contribution of ET to soil moisture drought depends on the availability of moisture in the soil for ET to take place (Seneviratne et al., 2010). PET measures

the evaporative demand of the atmosphere and indicates the amount of ET that would occur given an unlimited water supply. Under moisture-limited conditions, values of PET and ET can diverge where ET may verge to zero while PET can continue to rise with an increase in temperature (Seneviratne et al., 2010).

The use of drought indices incorporating PET has often been criticised (Sheffield et al., 2012; Seneviratne, 2012). We therefore assess the relevance of the contributions of precipitation, PET, and their dependence to the estimation of soil moisture drought in Europe during the summer months June, July and August (JJA) at locations in wet, transitional, and dry climates. This chapter aims to demonstrate the individual contributions of precipitation and PET to the estimation of soil moisture drought and highlight where, when and over what integration period lengths PET and its dependence with precipitation are important for the estimation of soil moisture in a statistical setting. In doing so we aim to characterise the compound nature of soil moisture drought in differing climates during summer to provide information that may aid with the interpretation of drought indices incorporating PET and allow further insight to be gained from such indices.

This chapter is organised as follows: the data employed in this study as well as the statistical methods involved are described in section 2.2, the main results are presented in Section 2.3 and a summary and conclusion are provided in Section 2.4.

2.2 Data and Methods

2.2.1 Dataset

We employed the Fluxnet dataset (Baldocchi et al., 2001) for this study using 11 stations situated across Europe. The selection of sites was based both on an initial review

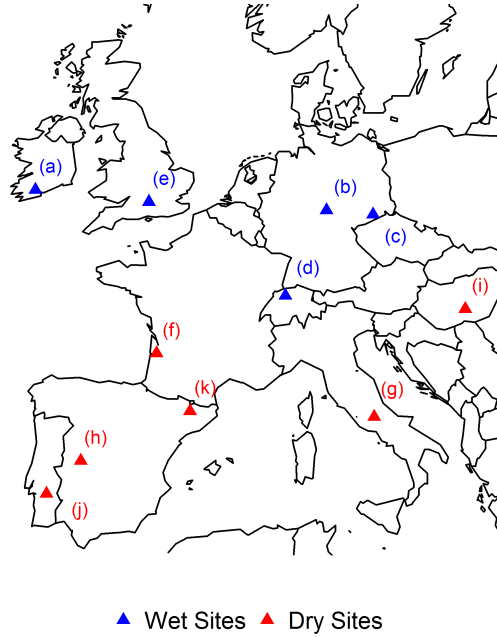


Figure 2.1: Locations of Fluxnet sites employed for this study

of data quality and length across many sites as well as the recommendations of Rebel et al. (2012). Table 2.1 provides a summary of the site characteristics. To aid the interpretation of the results, we classify the sites as wet or dry based on values of soil moisture. Locations are provided in Figure 2.1. At each site, soil moisture measurements are provided for 3 layers in the top 30cm of soil (Rebel et al., 2012) along with precipitation data as well as the variables required for the calculation of PET via the reference crop Penman-Monteith equation, as described in Zotarelli et al. (2010). These variables include incoming solar radiation, temperature, wind speed and relative humidity. Among the selected sites, two general land cover types are available; grassland and forest. The data used here are at a daily resolution. We use soil moisture values for the summer months of June, July and August (JJA). For the contributing meteorological variables, we used observations that extend back into previous months in order to calculate integration periods prior to a given soil moisture observation.

Table 2.1: Summary of FLUXNET sites used in this study

Site	Site Name	Lat.	Long.	Site Type
(a)	Dripsey, Ireland	51.99° N	8.75° W	Grassland
(b)	Hainich, Germany	51.08° N	10.45° E	Forest
(c)	Klingenberg, Germany	50.89° N	13.52° E	Grassland
(d)	Oensingen, Switzerland	47.28° N	7.73° E	Grassland
(e)	Pang/Lambourne, UK	51.45° N	1.27° W	Forest
(f)	Le Bray, France	44.72° N	0.77° W	Forest
(g)	Amplero, Italy	41.9° N	13.6° W	Grassland
(h)	Las Majadas del Tietar, Spain	39.94° N	5.77° W	Savanna/Grassland
(i)	Bugacpuszta, Hungary	46.69° N	19.6° E	Grassland
(j)	Mitra IV Tojal, Portugal	38.48° N	8.02° W	Grassland
(k)	Vall d'Alinya, Spain	42.15° N	1.45° E	Grassland

2.2.2 Conceptual Model

We design a conceptual model, based on a framework developed by Bevacqua et al. (2017), in which we describe soil moisture h as an impact of contributing meteorological variables Y . The contributing meteorological variables include a short-term precipitation variable ($Y_{1_{ps}}$), a long-term precipitation variable ($Y_{2_{pl}}$) and a PET variable ($Y_{3_{pet}}$) that are integrated over periods L_1 , L_2 and L_3 respectively. A schematic representation of the variables modelled is given in Figure 2.2.

$Y_{1_{ps}}$ and $Y_{2_{pl}}$ respectively represent the most recent and antecedent precipitation that influence the short and long-term variability of soil moisture. Their respective integration periods L_1 and L_2 are non-overlapping. Two precipitation variables are required to better capture the temporal distribution of precipitation that would otherwise be lost using one long-term integration only.

$Y_{3_{pet}}$ represents PET integrated over the period L_3 . PET is often employed as an estimate of ET in drought indices given the lack of ET data. We calculate PET using the reference crop Penman-Monteith equation as defined in Zotarelli et al. (2010) where

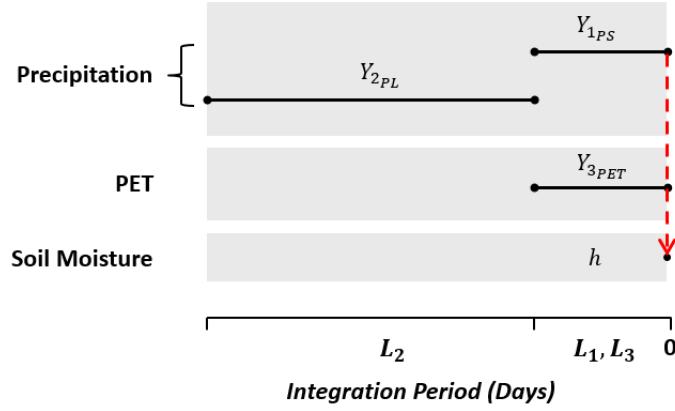


Figure 2.2: Schematic of the variables used in this study to construct the soil moisture model

it is derived from incoming solar radiation, temperature, wind and the actual and saturation vapour pressures. $Y_{3_{PET}}$ includes temperature within its calculation and so can capture heat waves that influence the drying of soil moisture. Depending on the question at hand, the integration length L_3 is varied, more details of this are given in the Model Development section.

2.2.3 Copula

A copula is a multivariate distribution function that describes the dependence structure between random variables independent of their marginal behaviour. The selection of structure of dependence, defined by the given copula family, is hence not constrained by the choice of the marginal distribution functions. This feature provides much flexibility in modelling multivariate distributions as it allows for the application of complex marginal distributions (Salvadori et al., 2007). According to Sklaar's theorem (Sklar, 1959), the joint cumulative distribution function (CDF) F of an n -dimensional random

vector $Y = (Y_1, \dots, Y_n)$ with marginal CDFs F_1, \dots, F_n can be written as

$$F(y_1, \dots, y_n) = C(u_1, \dots, u_n), \quad (2.2.1)$$

where C is an n -dimensional copula and $u_i = F_i(y_i)$ are uniformly distributed variables in the domain $[0,1]$. Provided the marginal distributions F_i are continuous, the multivariate probability density function (PDF) may be decomposed as:

$$f(y_1, \dots, y_n) = f_1(y_1) \cdot \dots \cdot f_n(y_n) \cdot c(F_1(y_1), \dots, F_n(y_n)), \quad (2.2.2)$$

where c is the copula density and f_i are marginal PDFs.

There exists a large number of bivariate copula families that each provide an explicit formulation for a given structure of dependence. However, the number of copula families applicable to a dimension of three or higher is quite limited (Aas et al., 2009) and in contrast to reality, where heterogeneous dependence structures often exist, each copula will usually assume the same structure of dependence between all marginals (Aas et al., 2009; Acar et al., 2012; Noh et al., 2013; Bevacqua et al., 2017). We therefore employ pair copula constructions (PCCs) which provide higher flexibility than multivariate copulas and more simplicity in terms of the selection of dependence structure (Aas et al., 2009; Noh et al., 2013).

2.2.4 Pair Copula Constructions (PCCs)

PCCs, initially proposed by Joe (1997), allow us to mathematically decompose an n -dimensional copula density into a product of $n(n-1)/2$ bivariate copulas, of which some are conditional. They allow much flexibility in modelling multi-dimensional distributions (Aas et al., 2009; Bevacqua et al., 2017) and provide a means to easily

calculate quantiles of the multivariate conditional distribution of an impact h given values of Y (Noh et al., 2013; Bernard and Czado, 2015; Kraus and Czado, 2017; Fischer et al., 2017).

For a high-dimensional distribution, there exists a significant number of decompositions of a multivariate PDF into a PCC that are each mathematically equivalent to one another (Aas et al., 2009). Two special types of decompositions called vines exist for PCCs, the Canonical Vine (C-Vine) and the D-Vine (Kurowicka and Cooke, 2005). Throughout this study we employ a D-Vine decomposition. For the four-dimensional distribution under study here, there are twelve possible D-Vine decompositions. For convenience we select one decomposition to be applied throughout the study at all sites, the procedure we follow for this selection is outlined in the Model Development section. The selected D-vine decomposition for the conditional model is given as:

$$\begin{aligned}
 f_{3,2,1,h}(y_3, y_2, y_1, h) = & f_3(y_3) \cdot f_2(y_2) \cdot f_1(y_1) \cdot f_h(h) \\
 & \cdot c_{32}(u_3, u_2) \cdot c_{21}(u_2, u_1) \cdot c_{1h}(u_1, u_h) \\
 & \cdot c_{31|2}(u_{3|2}, u_{1|2}) \cdot c_{2h|1}(u_{2|1}, u_{h|1}) \\
 & \cdot c_{3h|21}(u_{3|21}, u_{h|21}).
 \end{aligned} \tag{2.2.3}$$

The difference between each of the 12 possible decompositions are in the ordering of variables within the PCC which determines the bivariate dependencies that are modelled. As can be seen in equation (3), the ordering of variables in the selected decomposition are (Y_3, Y_2, Y_1, h) . To sample h conditioning on the Y we employ a sampling algorithm provided by the CDVineCopulaConditional R package (Bevacqua, 2017), this uses a modified version of the algorithm presented in Aas et al. (2009). This algorithm requires that h is positioned last (or equivalently first) in the order of variables

as shown above. This constraint reduces the number of possible decompositions to six. And although each of these possibilities are mathematically equivalent, the explanatory power of h from the resulting conditional model varies depending on the order of the contributing variables Y within the decomposition as each Y can have differing levels of influence over h (Kraus and Czado, 2017).

Estimation of PCC

The estimation of the PCC given in equation (2.2.3) is obtained through a sequential approach. Firstly, the unconditional bivariate copulas c_{32} , c_{21} and c_{1h} are fitted to capture the respective pairwise dependencies of the variables u_3 , u_2 , u_1 and u_h . Secondly, the conditional bivariate copulas $c_{31|2}$ and $c_{2h|1}$ are then fitted to the respective conditional probabilities $u_{3|2}$, $u_{1|2}$, $u_{2|1}$ and $u_{h|1}$. These variables are obtained from the conditional distributions given by the partial differentiation of the respective unconditional bivariate copula with respect to the conditioning variable:

$$\begin{aligned} u_{3|2} &= F_{3|2}(u_3|u_2) = \frac{\partial}{\partial u_2} C_{32}(u_3, u_2) \\ u_{1|2} &= F_{1|2}(u_1|u_2) = \frac{\partial}{\partial u_2} C_{21}(u_2, u_1) \\ u_{2|1} &= F_{2|1}(u_2|u_1) = \frac{\partial}{\partial u_1} C_{21}(u_2, u_1) \\ u_{h|1} &= F_{h|1}(u_h|u_1) = \frac{\partial}{\partial u_1} C_{1h}(u_1, u_h). \end{aligned} \tag{2.2.4}$$

In the final step of the estimation procedure, a copula $c_{3h|21}$ is fitted to the conditional probabilities $u_{3|21}$ and $u_{h|21}$. These conditional probabilities are obtained from the conditional distributions given from the partial differentiation of the respective conditional bivariate copula with respect to the conditioning variable:

$$\begin{aligned}
 u_{3|21} &= F_{3|21}(u_3|u_2, u_1) \\
 &= \frac{\partial C_{31|2}(F_{3|2}(u_3|u_2), F_{1|2}(u_1|u_2))}{\partial F_{1|2}(u_1|u_2)} \\
 u_{h|21} &= F_{h|21}(u_h|u_2, u_1) \\
 &= \frac{\partial C_{2h|1}(F_{2|1}(u_2|u_1), F_{h|1}(u_h|u_1))}{\partial F_{2|1}(u_2|u_1)}.
 \end{aligned} \tag{2.2.5}$$

From the conditional copula $c_{3h|21}$, the conditional CDF $F_{h|321}$ can be obtained through partial differentiation of $C_{3h|21}$ with respect to $F_{3|21}$:

$$F_{h|321}(u_h|u_3, u_2, u_1) = \frac{\partial C_{3h|21}(F_{3|21}(u_3|u_2, u_1), F_{h|21}(u_h|u_2, u_1))}{\partial F_{3|21}(u_3|u_2, u_1)}. \tag{2.2.6}$$

As will be shown, all unconditional and conditional bivariate CDFs described above are required when sampling from the PCC.

Sampling from PCC

Sampling variables u_3 , u_2 , u_1 and u_h from the four-dimensional D-Vine PCC repeatedly, results in four uniformly distributed variables that exhibit a dependence structure specified by the given PCC. Algorithms proposed by Aas et al. (2009) provide a convenient means of sampling variables u_3 , u_2 , u_1 and u_h . Within these algorithms, variables w_3 , w_2 , w_1 and w_h are firstly drawn independently from a random uniform distribution on $[0,1]$. Then, u_3 , u_2 , u_1 and u_h are determined as:

$$\begin{aligned}
 u_3 &= w_3 \\
 u_2 &= F_{2|3}^{-1}(w_2|u_3) \\
 u_1 &= F_{1|2}^{-1}(F_{1|23}^{-1}(w_1|u_2, u_3)) \\
 u_h &= F_{h|1}^{-1}(F_{h|21}^{-1}(F_{h|321}^{-1}(w_h|u_3, u_2, u_1))).
 \end{aligned} \tag{2.2.7}$$

Given specified values of Y , the model may be used to sample $h = F_h^{-1}(u_h)$ from a conditional distribution defined by the given Y values. In this case, the variables u_3 , u_2 , u_1 and u_h are obtained as:

$$\begin{aligned}
 u_3 &= F_3(y_3) \\
 u_2 &= F_2(y_2) \\
 u_1 &= F_1(y_1) \\
 u_h &= F_{h|1}^{-1}(F_{h|21}^{-1}(F_{h|321}^{-1}(w_h|u_3, u_2, u_1))).
 \end{aligned} \tag{2.2.8}$$

Throughout this study, we use an algorithm proposed by Bevacqua et al. (2017) to sample from equation (2.2.8) and carry out all simulations using the CDVineCopula-Conditional R package (Bevacqua, 2017).

When sampling from equation (2.2.8) given observed Y , we produce a stochastic time series of h . Repeated simulations conditioning on observed Y will produce multiple time series with varying statistics and agreement with observed h values (Pham et al., 2016). Throughout this study, given an observed time series of Y , we produce an ensemble consisting of 1000 members of h time series and obtain a probabilistic forecast

of h at each time step.

2.2.5 Model Construction

In this section we lay out the procedure taken for selecting integration period lengths L_i for the contributing meteorological variables Y_i (Figure 2.2). We also provide details of the selection procedure for the D-Vine decomposition of the PCC and the selection of copula families within the PCC.

Meteorological Predictor Selection

We describe soil moisture h as a function of two precipitation variables, $Y_{1_{PS}}$ and $Y_{2_{PL}}$, integrated over periods L_1 and L_2 , and a PET variable, $Y_{3_{PET}}$ integrated over the period L_3 . By developing a statistical model with these variables and soil moisture, we look to answer the following three questions:

1. What are the individual contributions of the meteorological variables Y_i to the estimation of soil moisture h on timescales related to meteorological drought and heat waves?
2. What relevance does the dependence between antecedent precipitation ($Y_{2_{PL}}$) and recent PET ($Y_{3_{PET}}$) have for the estimation of low soil moisture values?
3. What relevance does PET have for the estimation of soil moisture over varying integration lengths L_3 ?

To answer these questions, we propose two sets of Y variables, $S1$ and $S2$. Questions 1 and 2 are then approached using variable set $S1$ while Question 3 is approached using variable set $S2$. The difference between $S1$ and $S2$ is the integration L_3 chosen

at each site. A short integration period is considered for PET in S1, while a long integration period is considered for PET in S2. For each value of L_i used, the contributing meteorological variable Y_i may be defined as:

$$\begin{aligned} Y_{1_{PS}}(t) &= \sum_{t-L_1+1}^t p(t) \\ Y_{2_{PL}}(t) &= \sum_{t-(L_1+L_2)+1}^{t-L_1} p(t) \\ y_{3_{PET}}(t) &= \sum_{t-L_3+1}^t \text{pet}(t), \end{aligned} \tag{2.2.9}$$

where $p(t)$ and $\text{pet}(t)$ are respectively daily precipitation and PET.

We address the first two questions with variable set S1. The selected L_i for S1 must result in Y variables that provide satisfactory estimates of soil moisture h , hold physically meaningful dependencies and capture timescales relevant for both meteorological drought and heat waves. By physically meaningful dependencies, we mean that the dependence between the predictors are physically consistent in that the short-term variables are always integrated over the same time period and the long-term variable does not overlap them on a given time-step. Physically meaningful dependencies are obtained by constraining L_i such that $L_1 = L_3$ and through ensuring that there is no overlap between L_2 and the short-term integrations.

Based on the analysis described below, we find a difference between grassland sites and forest sites. Forest sites require a longer integration L_1 . This is possibly explained by the deeper root systems at forest sites which filter the influence of short-term variability in rainfall on the integrated soil column. We therefore choose two sets of L ; LG and LF for grassland and forest sites respectively. At all grassland (forest) sites, the same LG (LF) are used.

We choose integrations of $LG_1 = LG_3 = 7$ and $LG_2 = 63$ for grassland sites. For forest sites, we choose integrations of $LF_1 = LF_3 = 30$ and $LF_2 = 60$. We thus use information of precipitation over the previous 70 and 90 days for each daily soil moisture observation at grassland and forest sites respectively.

To select LG_i (LF_i) in S1, we firstly calculate the Spearman correlation between $Y_i(t)$ and $h(t)$ for multiple integrations within a window of 120 days prior to day t . We then choose the integration length that maximises the Spearman correlation for each Y_i . Integration periods are then constrained such that $LG_1 = LG_3$ ($LF_1 = LF_3$). This ensures physically meaningful dependencies and avoids arbitrary dependencies that would otherwise arise between differing LG_1 (LF_1) and LG_3 (LF_3).

The sensitivity of the conditional model's performance, in representing h conditioning on Y , to changes in LF (LG) is tested by varying the short-term LG (LF) by $+/-4$ days while the long-term integration LG (LF) is varied by $+/-10$ days. Changes in performance are found to be minimal (not shown). Assuming the same LG (LF) at all grassland (forest sites) and constraining the integration periods is therefore expected to have little weight in the outcome of this analysis.

We acknowledge in S1 that the influence of most recent daily temperature extremes on soil moisture is potentially filtered out at forest sites by setting $LF_3 = 30$. This is addressed in variable set S2 where we assess the relevance of the selection of L_3 to the estimation of h (Question 3). In S2, two models are constructed using a short and long-term integration of L_3 . The same LG_1 , LF_1 , LG_2 , and LF_2 as S1 are used while LG_3 and LF_3 are set to 7 and 70 days, and 7 and 90 days respectively.

As the variables are all calculated on a daily resolution, from day t to day $t + 1$, there will be an overlap of $LG_i - 1$ or $LF_i - 1$ mutual days used in the integration periods associated with two consecutive days. We thus violate the assumption that data are

independent and identically distributed (i.i.d.), which the statistical methods used here are based upon. It should therefore be noted that the performance of the model as well as any estimated dependence between variables may be overestimated.

Statistical Inference of the Multivariate pdf

The parameters of each bivariate copula in equation (2.2.3) are estimated based on the marginal variables u_i drawn from the marginal CDFs F_i . We use a kernel density estimate for all marginal distributions. All marginal densities are estimated using the *ks* R package (Duong, 2017) which employs the bandwidth selector of Wand and Jones (1994).

The estimation of copula parameters requires that no equal ranks are present in u_i . We follow the approach used in (Pham et al., 2016) to remove ties from the data. In this approach, a small random noise is drawn from a uniform distribution on $[-0.001, 0.001]$ and added to $Y_{1_{PS}}$ and $Y_{2_{PL}}$ values greater than zero. For values equal to zero, we add a random noise drawn from the uniform distribution on $[0, 0.001]$.

The use of kernel density estimates provides a convenient way of estimating the marginal distribution of h . Soil moisture has natural upper and lower bounds, according to its wilting and saturation points respectively, and can also exhibit a bimodal distribution (Porporato and D'Odorico, 2004; D'Andrea et al., 2006).

The selection of the D-vine decomposition in equation (2.2.3) is based on an initial test in which we assess the performance of each of the six possible decompositions in their ability to represent h when conditioning on observed Y . At all sites we fit a PCC for each of the six decompositions and use the AIC criterion when selecting the type of copulas to be used. The selection of copula families and the estimation of their parameters is carried out at each site separately. Each copula is chosen from a

range of copulas provided by the VineCopula R package (Schepsmeier et al., 2017). To assess each of the six possible decompositions, a probabilistic forecast of h consisting of 1000 members is produced at all sites. These are compared with observed soil moisture using the root mean squared error. We then select the decomposition that generally shows the highest explanatory power of h at all sites.

After selecting the decomposition to apply, the goodness of fit (GoF) of the selected copulas is tested. Copulas initially selected according to the AIC did not always provide a satisfactory fit. For this reason we use two criteria in the selection of a copula for each pair in the PCC. This procedure is carried out sequentially as outlined in the Estimation of PCC section where unconditional copulas are first selected followed by the conditional copulas. For each pair, we firstly select the top three copulas according to the AIC and secondly test the GoF of each using K-plots (Genest and Favre, 2007; Bevacqua et al., 2017). We then select the highest ranked copula according to the AIC that shows satisfactory compliance in the K-plots.

K-plots plot the Kendall function $K(w) = P(C_{i,j}(U_i, U_j) \leq w)$ obtained from the fitted copula against $K(w)$ computed with the empirical copula obtained using the observed data. Similarly to a qq-plot for univariate distributions, the K-plot indicates good quality of fit when points follow the diagonal. These plots provide uncertainties around the empirical copula as well as a qualitative idea of the quality of fit of each copula (Bevacqua et al., 2017). Most selected copulas show good agreement according to the K-plots (not shown) where parametric $K(w)$ values generally follow the mean of the empirical values and mostly remain within the uncertainty intervals calculated from 1000 simulations. Some small problems are found with the copulas at sites (e) and (f) which may limit the strength of conclusions drawn from these sites.

2.2.6 Model Evaluation Metrics

The model simulations are evaluated overall and in their ability to represent low values of soil moisture h . Using the Brier score (BS), we evaluate the accuracy of probabilistic predictions of low h values defined as those below the 15th percentile of observed soil moisture. The closer BS is to zero, the better the predictions. BS is defined as:

$$BS = \frac{1}{N} \sum_{t=1}^N (p_t - o_t)^2, \quad (2.2.10)$$

where p_t is the probability of getting a simulated value of h below the observed 15th percentile from the model at time t , while o_t is 1 if observed soil moisture $h^{\text{obs}}(t)$ is below the 15th percentile and 0 otherwise. Along with BS we calculate the associated Brier skill score (BSS) that evaluates the model relative to a reference model BS_{ref} :

$$BSS = 1 - \frac{BS}{BS_{\text{ref}}}, \quad (2.2.11)$$

We consider the climatology as the reference model in which the probability of a value occurring below the 15th percentile is always 0.15.

The model is also evaluated in its ability to capture the persistence of drought conditions by comparing the autocorrelation function (ACF) and using an empirical order 1 persistence probability (PP). Both are derived from the observed values and the mean of the simulated values. We choose an order 1 persistence after assessing partial autocorrelation function (PACF) at each site which only showed significant correlations for order 1. PP is defined as:

$$PP = Pr(h_{t+1} < F_h^{-1}(0.15) \mid h_t < F_h^{-1}(0.15)). \quad (2.2.12)$$

PP may be interpreted as the probability that h_{t+1} will be below the 15th percentile

given that h_t is below the 15th percentile.

2.3 Results

The set of variables S1, described in the Meteorological Predictor Selection section, are employed to evaluate the contributions of the individual Y variables and that of their dependence structure to soil moisture. To achieve this we perform a number of sensitivity simulations and compare them with a control simulation (CTRL). All simulations carried out are done through a K-fold cross-validation to avoid over-fitting. K here is the number of summers in a time series at a given site. In each simulation, we thus remove one summer at a time when fitting the copula parameters but use the same marginal PDFs for each period. In this way we only cross-validate the PCC rather than the entire multivariate statistical model. For each simulation, we then produce a probabilistic forecast of h consisting of 1000 members through conditioning on specified values of Y.

2.3.1 Model Performance

The CTRL simulation is performed through sampling h conditioned on observed values of Y (equation 2.2.8). The performance of CTRL may be qualitatively gauged from Figure 2.3. Plots shown in panels (a) to (e) are results from wet sites while those from (f) to (k) are results from dry sites. The mean value of h from CTRL at each time step can be seen to follow the temporal evolution of observed soil moisture (h^{obs}) quite well while h^{obs} is generally found within the 95% confidence interval of CTRL. Also shown within each panel in Figure 2.3 are the order 1 persistence probabilities of low h for observed (PP_{obs}) and mean simulated h (PP_{sim}). PP_{sim} and PP_{obs} are found to

be very similar at all wet sites and most dry sites although PP_{sim} is generally less than PP_{obs} at dry sites. A comparison of the observed ACF, estimated up to order 10, with the ACF derived from the mean of the simulation also showed close correspondence at each site (not shown). Such results indicate good agreement between the observed h and simulated mean h in terms of temporal evolution and the persistence of low values.

To provide information of the performance of the model in terms of the probabilistic forecast of low soil moisture values, we calculate Brier scores (BS) and Brier Skill Scores (BSS) for CTRL at each site (Table 2.2). In general we see good BS and positive BSS that range from 0.06 to 0.12 and 0.04 to 0.51 respectively with medians of 0.09 and 0.25. These BSS indicate that the model is better than the climatology at predicting low soil moisture values. Low BSS values are seen at Site (c) where we also see poor correspondence between h^{obs} and the mean of CTRL. Optimising the performance of the model at this site through changing integration periods does not bring a noticeable improvement indicating that the proposed model and variables included do not predict soil moisture correctly at all sites. It should be noted that BSS is only evaluated for values below the 15th percentile and so no information is provided from BSS of the rest of the distribution. However, with satisfactory results generally obtained at most sites, we employ the model for use in sensitivity analysis in a number of tests presented below.

2.3.2 Assessment of Contributing Variables to Soil Moisture

We test the contribution of Y_{1ps} (short-term precipitation), Y_{2pl} (long-term precipitation), and Y_{3pet} (PET), to the estimation of h in three sensitivity simulations $SENS - Y_{1ps}$,

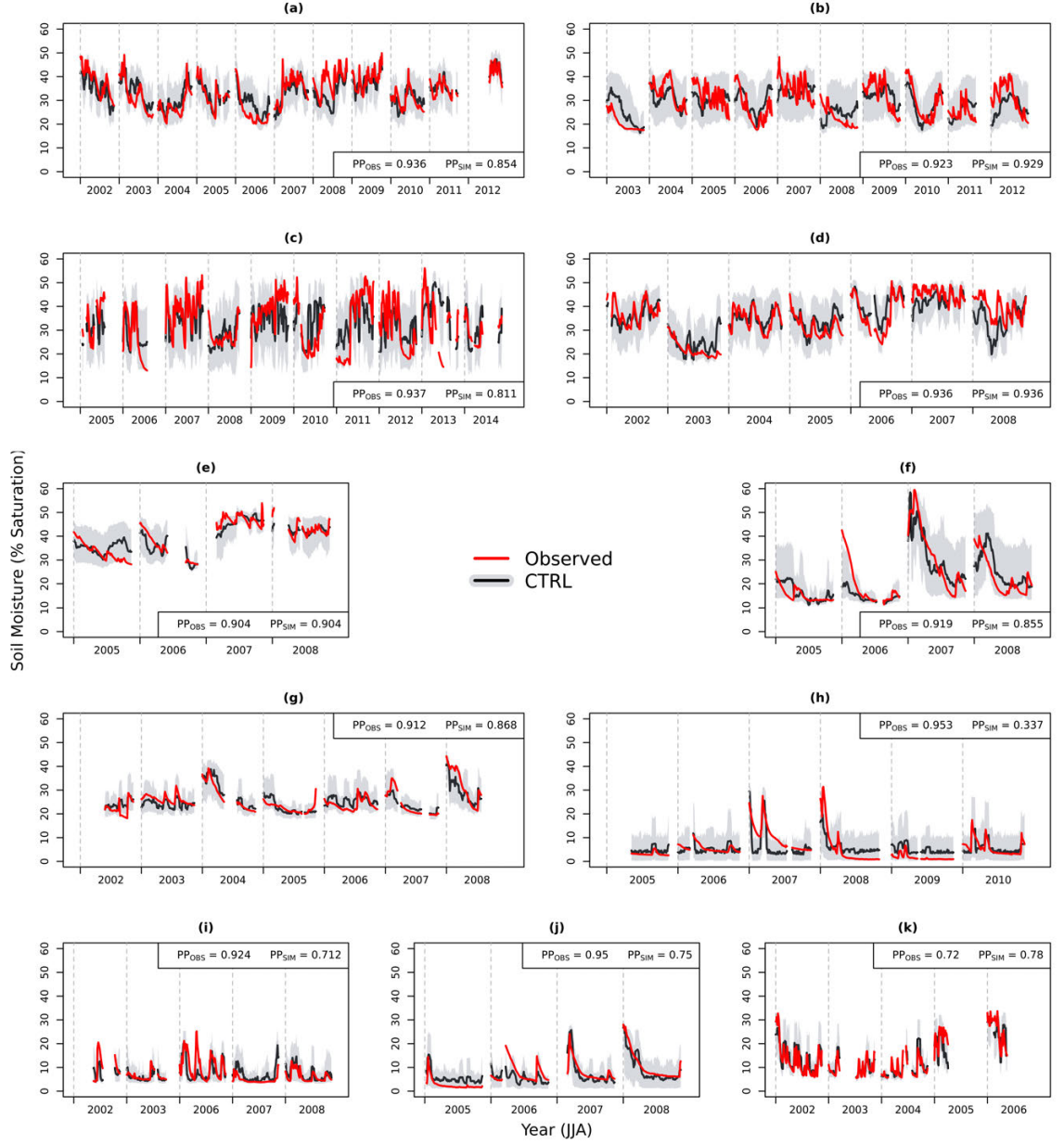


Figure 2.3: Observed time series (red) alongside the cross-validation time series of the CTRL mean (black) and the 95% prediction interval (grey), obtained from 1000 simulations, at wet sites are (a) to (e) and dry sites (f) to (k). Also provided within each panel are the order 1 persistence probabilities calculated from the observed (PP_{obs}) and CTRL mean (PP_{sim}) timeseries.

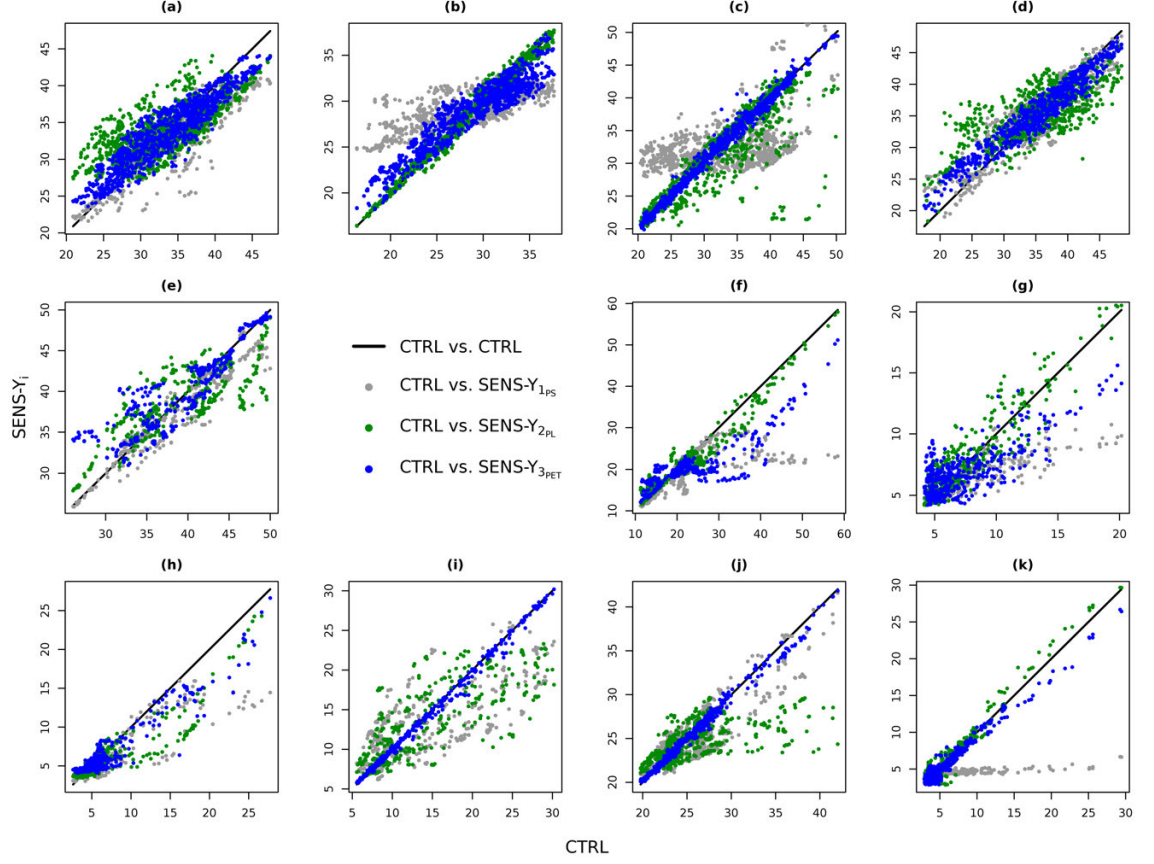


Figure 2.4: Comparison of the mean of the cross-validation simulations of CTRL with $\text{SENS} - Y_{1PS}$, $\text{SENS} - Y_{2PL}$ and $\text{SENS} - Y_{3PET}$ at wet sites (a) to (e) and dry sites (f) to (k). Values are ordered according to CTRL from low to high such that the closer the correspondence of points to the diagonal, the smaller the change in the estimation of soil moisture in the given sensitivity simulation.

$\text{SENS} - Y_{2PL}$, and $\text{SENS} - Y_{3PET}$ respectively. For each sensitivity simulation, h is sampled conditioning on the median value of the respective variable to be tested and the observed values of the other two Y variables. To assess the contributions of all variables, we compare the mean of each simulation with the CTRL mean. We also compare the probabilistic forecasts from $\text{SENS} - Y_i$ with CTRL using the BS, BSS and the mean ensemble bias computed for values of h below the observed 15th percentile (Table 2.2). At wet sites, precipitation is generally seen to have the most influence on low soil mois-

ture values while PET can act to amplify the low soil moisture anomaly during drought periods. Comparing the means of the three sensitivity simulations with the mean of CTRL (Figure 2.4), larger overestimations of low h values with respect to CTRL are generally seen in either of the simulations assessing the influence of a precipitation variable, $\text{SENS} - Y_{1_{\text{PS}}}$ or $\text{SENS} - Y_{2_{\text{PL}}}$, than is seen in $\text{SENS} - Y_{3_{\text{PET}}}$. Underlining this are larger changes in positive bias of low soil moisture values seen from $\text{SENS} - Y_{1_{\text{PS}}}$ or $\text{SENS} - Y_{2_{\text{PL}}}$ than from $\text{SENS} - Y_{3_{\text{PET}}}$ (Table 2.2). A comparison of BSS for each simulation in Table 2.2 also shows a larger reduction in skill of forecasting values below 15th percentile in either $\text{SENS} - Y_{1_{\text{PS}}}$ or $\text{SENS} - Y_{2_{\text{PL}}}$ than in $\text{SENS} - Y_{3_{\text{PET}}}$. Focusing on drought events at wet sites (a), (b) and (d) in 2003 and 2006, years in which heat waves have also occurred (Ciais et al., 2005; Rebetez et al., 2009), we see from the mean of the simulations (Figure 2.5) that removing the influence of precipitation can lead to the misspecification of a drought event with the green line largely above the black line (CTRL). On the other hand, removing the influence of PET can result in the underestimation of the severity of the event with the blue line only just higher than the black during a drought event.

At dry sites, we see that precipitation again holds the main influence over soil moisture while PET generally offers little added benefit to the estimation of soil moisture. The main differences of CTRL with $\text{SENS} - Y_{1_{\text{PS}}}$ and $\text{SENS} - Y_{2_{\text{PL}}}$ are found for high values of soil moisture (Figure 2.4). Low values in these sensitivity simulations are generally equivalent with CTRL as the medians of $Y_{1_{\text{PS}}}$ and $Y_{2_{\text{PL}}}$ are associated with relatively low values due to the positively skewed nature of the variables' distributions. Little or no difference is seen between $\text{SENS} - Y_{3_{\text{PET}}}$ and CTRL simulations for low values of soil moisture. Large percentage changes in bias for low soil moisture values are seen at sites (f) and (i), though the actual changes in soil moisture are relatively low

Table 2.2: Brier scores (BS), Brier Skill Scores (BSS) and mean bias for CTRL, SENS – Y_{1PS} , SENS – Y_{2PL} , and SENS – Y_{3PET} simulations calculated for soil moisture values below the observed 15th percentile. Bias values for SENS – Y_{1PS} , SENS – Y_{2PL} , and SENS – Y_{3PET} are given as percentage change relative to CTRL

Site	Score	CTRL	SENS – Y_{1PS}	SENS – Y_{2PL}	SENS – Y_{3PET}
(a)	BS	0.09	0.10	0.12	0.10
	BSS	0.25	0.21	0.01	0.18
	Bias	3.89	+5%	+113%	+45%
(b)	BS	0.11	0.13	0.10	0.11
	BSS	0.15	-0.01	0.17	0.15
	Bias	4.33	+107%	-1%	+33%
(c)	BS	0.12	0.14	0.11	0.12
	BSS	0.04	-0.1	0.13	0.06
	Bias	10.66	+51%	-24%	+2%
(d)	BS	0.06	0.06	0.09	0.08
	BSS	0.51	0.49	0.26	0.39
	Bias	3.52	+45%	+149%	+83%
(e)	BS	0.09	0.10	0.09	0.12
	BSS	0.28	0.25	0.27	0.03
	Bias	3.62	-15%	+78%	+81%
(f)	BS	0.08	0.07	0.06	0.13
	BSS	0.36	0.43	0.53	-0.01
	Bias	0.37	-215%	+207%	+720%
(g)	BS	0.09	0.09	0.11	0.09
	BSS	0.31	0.24	0.15	0.30
	Bias	1.48	+43%	+86%	+6%
(h)	BS	0.12	0.13	0.12	0.13
	BSS	0.04	0.00	0.05	0.003
	Bias	3.28	+9%	-3%	+4%
(i)	BS	0.12	0.13	0.12	0.13
	BSS	0.07	0.002	0.04	-0.06
	Bias	1.24	-9%	+5%	+52%
(j)	BS	0.12	0.12	0.12	0.12
	BSS	0.09	0.10	0.05	0.06
	Bias	2.8	-8%	+10%	+16%
(k)	BS	0.08	0.13	0.12	0.08
	BSS	0.36	0.01	0.09	0.37
	Bias	1.05	+205%	+146%	+10%

(Table 2.2). This would be expected at dry sites during summer where soil moisture normally reaches low levels such that ET is moisture-limited and will diverge from PET. Extremes of PET driven by extreme temperatures would then have little added effect to the severity of soil moisture drought in dry locations.

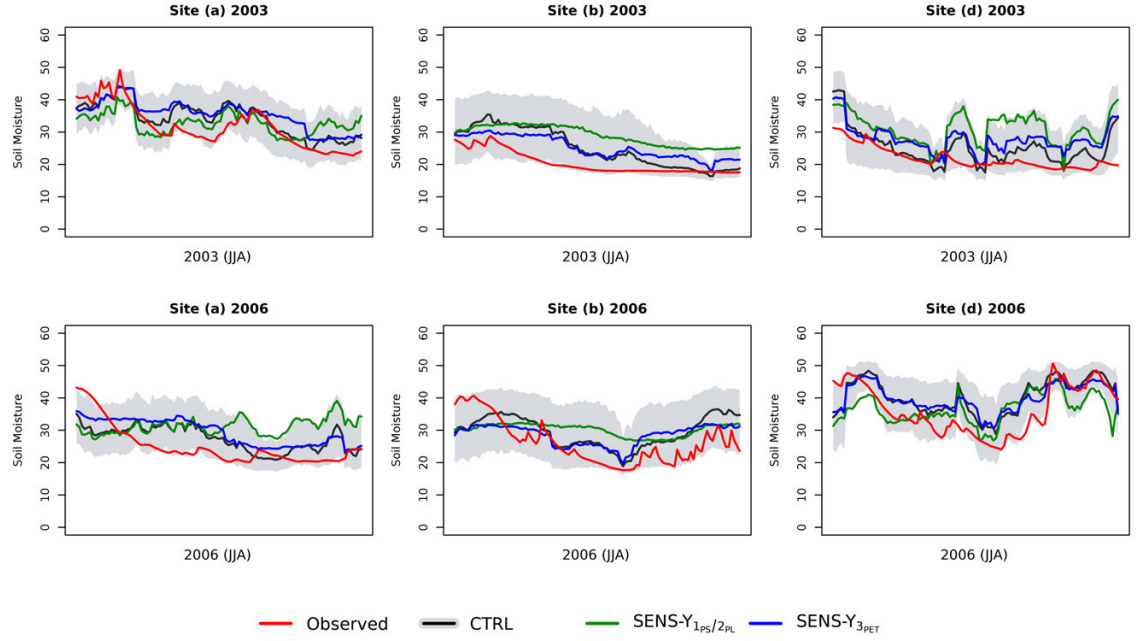


Figure 2.5: Mean cross-validated time series of simulations assessing the contributions of precipitation and PET to the estimation of soil moisture and CTRL (black) for the summers (JJA) of 2003 and 2006 at wet sites (a), (b) and (d). Time series of mean simulated values are presented for SENS-Y_{2PL} (green) and SENS-Y_{3PET} (blue) at wet sites (a) and (d) while time series of SENS-Y_{1PS} (green) and SENS-Y_{3PET} (blue) are presented for site (b).

2.3.3 Assessing the Relevance of Y Dependence Structure

The contribution of the dependence between Y_{2PL} and Y_{3PET} to the estimation of low h values is assessed using sensitivity simulation IND-Y_{2PL}. IND-Y_{2PL} is used to highlight where interactions between drought and heat wave conditions, arising through

land-atmosphere interactions, act to amplify drought conditions. To illustrate the dependence between $Y_{2_{PL}}$ and $Y_{3_{PET}}$, we calculate Spearman's ρ and a measure of tail dependence, λ_q , calculated as:

$$\lambda_q = Pr(Y_{3_{PET}} > F_3^{-1}(q) \mid Y_{2_{PL}} < F_2^{-1}(1 - q)) \quad (2.3.1)$$

where $q = 0.9$ in this case. λ_{90} can be interpreted as the fraction of days when $Y_{3_{PET}}$ was greater than its observed 90th percentile when $Y_{2_{PL}}$ was less than its 10th percentile. For two independent variables, the expected value of λ_q is $1 - q$. Values of ρ and λ_q for each site are given in Figure 2.6. At many sites we observe a negative dependence between $Y_{2_{PL}}$ and $Y_{3_{PET}}$, as measured by ρ , and an increased probability of extreme PET ($Y_{3_{PET}}$) when antecedent precipitation ($Y_{2_{PL}}$) had been extremely low.

To test the relevance of such dependence in $IND - Y_{2_{PL}}$, we break the dependence between $Y_{2_{PL}}$ and the short-term variables, $Y_{1_{PS}}$ and $Y_{3_{PET}}$. This is achieved by shuffling $Y_{2_{PL}}$ such that it is randomly associated with them. A probabilistic forecast of h , consisting of 1000 members, is then produced sampling from the multivariate distribution where we condition on the observed values of $Y_{1_{PS}}$ and $Y_{3_{PET}}$ and the shuffled $Y_{2_{PL}}$. To account for sampling variability of the shuffling process, we produce 1000 $IND - Y_{2_{PL}}$ probabilistic forecasts.

We obtain a kernel density estimate of the PDF produced from each of the 1000 $IND - Y_{2_{PL}}$ simulations. The mean density and the 95% confidence interval of $IND - Y_{2_{PL}}$ PDFs are calculated and presented alongside the PDFs of CTRL and h^{obs} (Figure 2.6). The statistical significance of the difference between the CDFs of CTRL and $IND - Y_{2_{PL}}$ is assessed at the 5th, 10th, and 15th percentiles of observed soil moisture. CTRL is considered significantly different for a given percentile if the associated soil moisture

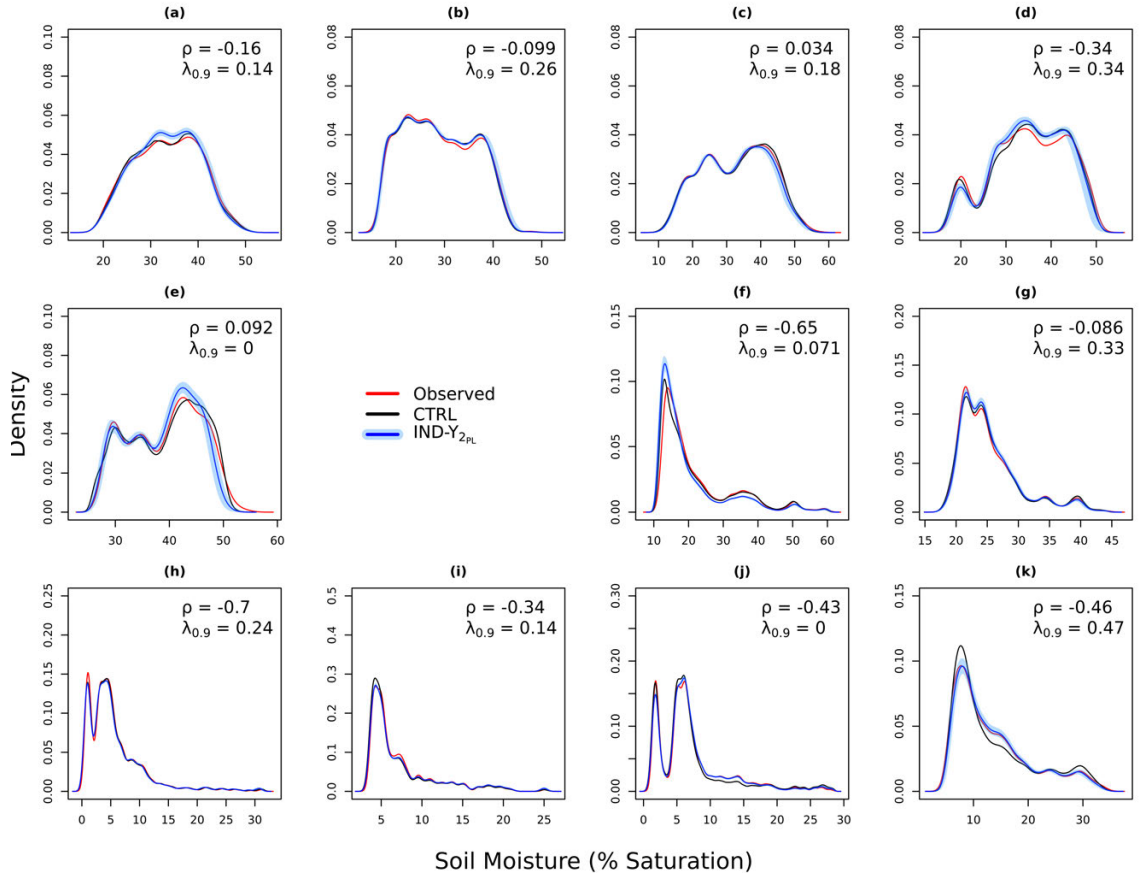


Figure 2.6: Kernel density estimates of observed soil moisture (red) and soil moisture simulated via cross-validation from probabilistic forecasts CTRL (black) IND – Y_{2PL} (blue) simulations. The blue line and shading respectively represent the mean density and 95% confidence interval obtained from the 1000 IND – Y_{2PL} simulations

value of CTRL is less than the lower bound of 95% confidence interval of that percentile from $IND - Y_{2_{PL}}$. This would signify that the probability of values below that percentile are underestimated when the dependence between $Y_{2_{PL}}$ and $Y_{3_{PET}}$ is broken.

Statistically significant differences are found between all three percentiles at Site (d) where we also see a noticeable difference between PDFs (Figure 2.6 (d)). A negative dependence as well as a significant dependence in the tails is also observed here. Site (d) lies in a transitional region where land-atmosphere interactions can lead to the mutual reinforcement of drought and heat wave events (Seneviratne et al., 2010). This result highlights the importance of the interplay between drought and heat wave conditions, driven by land-atmosphere interactions, to the reinforcement of drought conditions in such locations.

Statistically significant differences between the percentiles tested are also found at wet sites (a), (b) and (e) and dry sites (g) and (j), though relatively little difference is observed between CTRL and $IND - Y_{2_{PL}}$ PDFs at these sites for values below the tested percentiles (Figure 2.6). We observe negative dependencies (ρ) and tail dependencies (λ_q) at these sites which highlights that the concurrence of such conditions may be important for the estimation of low values of soil moisture. These dependencies are also observed at other dry sites but no significant differences between assessed percentiles are found. Such dependencies at these sites are perhaps of little relevance for soil moisture during summer as extremes of PET may be energy-limited in wet climates while soil in dry climates may have little available moisture for ET. In dry conditions then, extremes of PET in combination with extremely low antecedent precipitation will have little effect on moisture levels in soil.

2.3.4 Relevance of PET over Short and Long Integration Periods

The variable set S2, as described in the Meteorological Predictor Selection section, is used to demonstrate the relevance of PET, integrated over various durations LG_3 and LF_3 , to the estimation of soil moisture h . We fit two models at wet sites (a), (b) and (d) where we see contributions of PET to the estimation of soil moisture drought in variable set S1 (Figure 2.5). The integration periods used for precipitation variables, Y_{1ps} and Y_{2pl} , in S1 remain the same. For the simulation $PET - INT_S$, we set $LG_3 = LF_3 = 7$ and for the simulation $PET - INT_L$ we set $LG_3 = 70$ and $LF_3 = 90$.

Based on the mean of the simulations (Figure 2.7), better representation of drought onset can be seen at sites (a) and (d) in the $PET - INT_S$ simulations where the black line generally follows red (observed) at the beginning of an event when initial drying is taking place. On the other hand, drought persistence is generally captured better by the $PET - INT_L$ simulation where the blue line remains low with the red line in comparison to the black. Better BSS are found for simulations using a long-term integration of PET at sites (a) and (b). Increases of BSS, from $PET - INT_S$ to $PET - INT_L$, of 0.24 to 0.36 and 0.18 to 0.25 are found at each site respectively while little difference is seen between simulations at site (d) with BSS equal to 0.51 and 0.52.

Although these results are somewhat qualitative, they highlight that both short- and long-term integrations of PET are important for the estimation of drought events in this framework. Longer integrations are generally better in capturing the persistence of drought conditions as they can account for the memory soil moisture holds of drying during the event. Short-term integrations however, are better in capturing drought onset as they are able to account for short intense periods of drying that can accelerate the propagation of meteorological drought to soil moisture drought. With drought

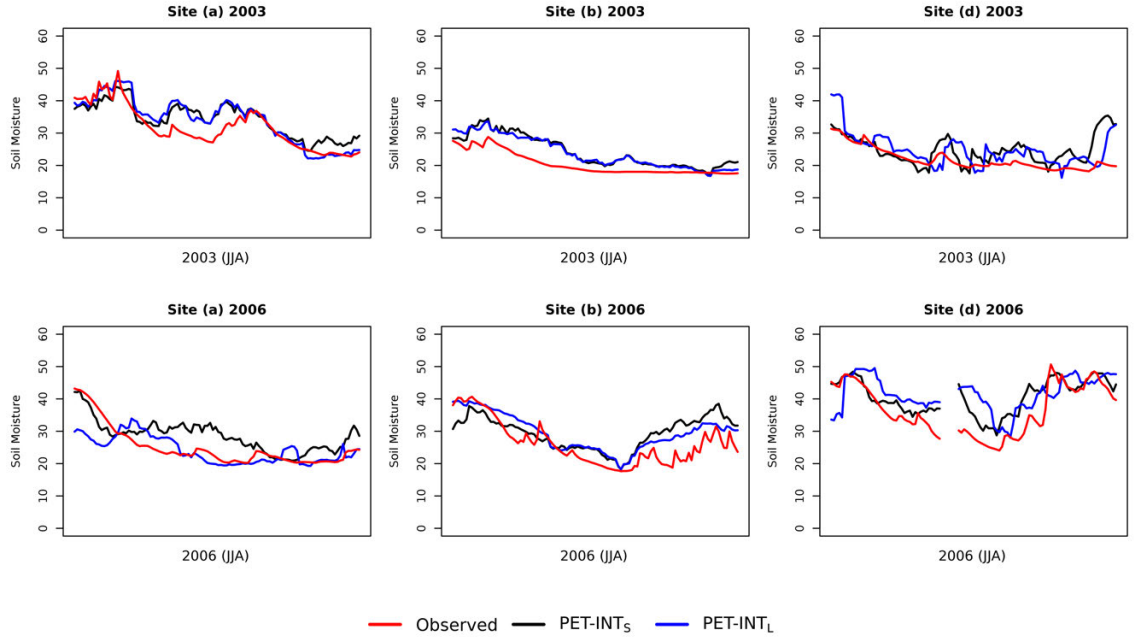


Figure 2.7: Mean cross-validation time series of simulations from models $PET - INT_S$ in which PET is considered over a short integration period (black) and $PET - INT_L$ in which PET is considered over a long integration period (blue) along with the observed time series (red) for the 2003 and 2006 drought events at wet sites (a), (b), and (d).

events expected to set in quicker in a warming climate (Trenberth et al., 2014), it will be important to detect such changes in the intensity of drying over short periods in spring and summer that are filtered out in longer integrations of PET . This may be of particular relevance in Europe where early onset of drought conditions can have large implications for extreme temperatures in summer (Vautard et al., 2007).

2.4 Summary and Conclusions

Compound events are multivariate extreme events in which the contributing variables need not be extreme themselves, but their joint, dependent, concurrence produces an extreme impact (Leonard et al., 2014; Bevacqua et al., 2017). We have analysed soil

moisture drought over Europe as a compound event of variables employed in common drought indices, namely precipitation and potential evapotranspiration (PET), and assessed the individual roles of these variables and that of their dependence structure to the estimation of soil moisture. The overall aim was to explore the compound nature of soil moisture drought and the differences that exist between wet and dry climates.

To achieve our aim, we developed a statistical model based on pair copula constructions. Within the model we considered precipitation and PET over timescales related to meteorological drought and heat waves respectively. These timescales were considered to assess the influence of heat wave conditions on soil moisture, as well as dependencies driven by land-atmosphere interactions that can cause a mutual reinforcement between drought and heat wave events in Europe. We applied the model to data from 11 Fluxnet sites situated in wet, transitional and dry climates in Europe and generally found satisfactory performance of the model. We thus employed it in a number of sensitivity experiments to assess the relevance of contributing variables and their dependence structure to the estimation of soil moisture drought.

Results obtained from sensitivity experiments were in line with previous studies. Precipitation was found to hold the main control over soil moisture drought. PET was required only when it departs from normal conditions (Vicente-Serrano et al., 2009) to partly explain the severity of drought conditions in wet climates (Seneviratne et al., 2012a; Teuling et al., 2013), while little or no contribution was found in dry climates (Luo et al., 2017) during summer. The concurrence of extremely low antecedent precipitation with extremely high PET was found to be most relevant at a site situated in a transitional climate region between wet and dry climates where land-atmosphere interactions are most relevant for the development of soil moisture drought (Senevi-

ratne et al., 2006, 2012b). The concurrence of these conditions was also seen at many dry sites though were found to have little relevance for soil moisture. This lack of relevance at dry sites is presumably related to the limited availability of moisture in soil for actual evapotranspiration (ET) to occur such that PET and Extremes of PET could have little influence to a low soil moisture anomaly.

The aforementioned contribution of PET is based on a short-term integration period that was used to capture the influence of heat waves on soil moisture. At wet sites, this short integration period is found to be effective in describing the onset of drought events as it can capture initial drying that occurs on a daily basis. It can however be ineffective in capturing the persistence of drought conditions, which longer integrations can better account for, as it neglects the memory soil moisture may hold of PET and the intense drying that may have occurred throughout a drought event. The differences found between short and long integrations of PET may become relevant in the analysis of changes in the onset of drought events using drought indices. A warmer climate may cause droughts to set in quicker (Trenberth et al., 2014) and lead to flash droughts (Mo and Lettenmaier, 2016). Such drying may be hidden through the use of longer integration periods of PET in an index such as the Standardised Precipitation Evapotranspiration Index (SPEI), or through a recursive model used for the Palmer Drought Severity Index (PDSI) that retains memory of PDSI values from previous time steps. Advantages of using drought indices include the simplicity they offer, as well as the widespread availability of meteorological datasets compared to those of soil moisture. Although they are not specifically designed to represent soil moisture (Seneviratne et al., 2010), indices such as the SPEI, PDSI and the Reconnaissance Drought Index (RDI) provide a convenient means of combining precipitation and PET into a kind of impact function that may be implicitly linked to soil moisture.

However, soil moisture drought is not a simple phenomenon to characterise with drought indices due to differing contributions and relevant integration periods of meteorological variables in wet and dry climates. The use of a climatic water balance (Precipitation - PET) in the SPEI and PDSI assumes over-simplified relationships between precipitation, PET and soil moisture (Seneviratne, 2012), and implies that the statistical relevance of precipitation and PET to the estimation of soil moisture are the same over a given integration period. With such simplifications comes a loss of information such as short intense periods of drying that may be filtered out through the inclusion of redundant information when using a long integration period for PET. Through the inclusion of PET, these indices are expected to provide a better picture of changes in drought conditions in a warming climate than indices that use precipitation alone such as the Standardised Precipitation Index (SPI). Ubiquitously applying indices, that incorporate PET, across different climates can provide a general overview of the response of drought conditions to global warming. It is however important to note that severe drought, as depicted by these indices, will have a different meaning for soil moisture drought in wet and dry climates. ET is limited by moisture availability and so will diverge from PET in dry conditions leading to an overestimation of the actual drying taking place with respect to soil. In contrast, land surface models account for this moisture limitation by capturing the physical relationship between PET and soil moisture, they can therefore provide a more reliable estimate. Their use within coupled climate models to study changes in soil moisture drought is particularly advocated for by Berg et al. (2017), who also demonstrate the added complexity of diverging changes to soil moisture at different soil depths that cannot be disentangled using drought indices.

Despite discrepancies between PET and ET in dry conditions, extremes of PET will still

be indicative of the drying potential of the atmosphere, provided it is calculated using a reliable physically based method such as the Penman-Monteith equation. Such atmospheric drying potential may possibly have adverse effects on crop yields and contribute to other environmental hazards such as wildfires that are mediated by the availability of moisture in vegetation (Gudmundsson et al., 2014; Ruffault et al., 2016).

Much information of soil moisture and other drought impacts may be deduced from drought indices and their response to a warming climate. To do so requires careful interpretation and detailed knowledge of the involved variables' influence on soil moisture in a given climate. It is therefore important that drought indices incorporating PET are interpreted within the context of the climate in which they are applied, whilst also keeping in mind the applications they are designed for.

In our impact focused approach, we have made use of the little soil moisture data that is available across different locations and climate types in Europe to demonstrate the compound nature of soil moisture drought during summer. These results provide further insight into the relationship between soil moisture and drought indices that incorporate PET. It is hoped that this insight will aid with the interpretation of drought indices in a given climate and season so that as much information as possible may be gained from their application.

Chapter 3

Long-Duration, Dry and Hot Events in Europe

3.1 Introduction

Soil moisture drought is a complex hazard (Seneviratne, 2012) that can adversely affect crop yields and natural ecosystems. Understanding its relationship with rising global temperatures is of significant importance. Sparse soil moisture data networks make it a difficult phenomenon to investigate empirically (Robock et al., 2000; Dorigo et al., 2011), and forces one to study output from land surface models (Mitchell et al., 2004; Sheffield et al., 2014) or the more widely available meteorological drivers. In this chapter we assess changes in meteorological droughts that co-occur with extreme temperatures. From here we term these events as long duration, dry and hot (*DH*) events. We characterise these events by their duration (*D*) and magnitude (*M*). *D* is defined as the number of consecutive dry days with precipitation below 1mm while *M* is the maximum daily temperature during the dry period.

The persistence of meteorological drought leads to the propagation of drought into soil moisture resulting in a negative moisture anomaly in the upper layers of soil known as the root zone. This propagation depends on both *D* and *M*. Longer dry periods allow for more drying of soil than shorter intermittent dry periods separated by wet days providing recharge, while high temperatures that increase evapotranspiration (ET) can accelerate this propagation of drought (Seneviratne et al., 2012a; Orlowsky and Seneviratne, 2012; Teuling et al., 2013). The joint occurrence of extremely long-duration and high magnitude events may thus lead to higher soil moisture deficits than events where only one characteristic is extreme. Larger deficits can produce longer lasting soil moisture droughts as higher amounts of precipitation are then required for drought recovery (Seneviratne et al., 2012a; Manning et al., 2018).

In this chapter, we aim here to provide insight into compound nature of *DH* events throughout Europe and how they may change in a warming climate. We estimate

the probability as well as change in probability *DH* events throughout Europe during June, July and August (JJA), both in terms of their duration and the co-occurrence of extremes in their duration and magnitude.

The chapter is structured as follows: In section 3.2, we present the data employed here as well as a description of the methods. The results are presented in section 3.3 while conclusions are outlined in section 3.4.

3.2 Methods

3.2.1 Data

For the identification of *DH* events, we use temperature and precipitation data from the EOBS dataset (Haylock et al., 2008) version 16.0 on a 0.25 degree grid. EOBS is the state of the art gridded dataset for Europe, although it is produced from a network of stations whose density is heterogeneous in both time and space. Herrera et al. (2018) point to a minimum number of stations required for reliable grid cell averages when assessing precipitation extremes, which is far higher than that used to produce EOBS in many regions (see Herrera et al. (2018)). However, the events studied here are driven by large-scale systems that will produce smoother fields than localised precipitation extremes, and so we consider EOBS to be adequate for identifying the events of interest.

The dataset is available from 1950 to 2017, although data is missing over Russia from 2014 onwards. We therefore analyse the period of 1950 until and including 2013 to keep a consistent time period throughout Europe. There are also many missing values of precipitation over Poland, Iceland and parts of Northern Africa throughout the observation period. These areas are therefore removed from the analysis. We also

employ the ERA Interim reanalysis dataset (Dee et al., 2011) to provide temperature data for the composite plots presented in Figure 3.1, as EOBS is a land-only dataset.

3.2.2 Event Definition

We characterise *DH* events by their duration (D) and magnitude (M) and identify events occurring within June, July and August (JJA). Events overlapping these months that begin before or end after this period are also included. D is defined as the number of days where precipitation is consecutively below 1mm. This threshold is chosen to remain consistent with previous studies (Orlowsky and Seneviratne, 2012; Donat et al., 2013; Sillmann et al., 2013; Lehtonen et al., 2014), as well as to be applicable to output from climate models which systematically overestimate the number of drizzle days. To ensure we obtain an independent event set (Coles et al., 2001) and capture events in their entirety (Fleig et al., 2006), we combine events longer than the 90th percentile of duration that are separated by $n_{sep} = 2$ days or less. Combining events shorter than the 90th percentile can result in events made up of intermittent dry and wet periods rather than the distinct dry events that we seek. The choice of two days is a subjective choice, and the sensitivity of the results to this choice was tested with values of $n_{sep} = 0, 1, 2, 3$, and 4 days. Little difference is seen between results obtained for each value of n_{sep} and so this choice will not affect the overall message of the paper. M is defined as the maximum daily maximum temperature observed during a dry period, it is thus defined independently of D . M is highly correlated with the mean of the maximum daily maximum temperatures during an event and so it is taken to represent the level of temperature throughout each event. Although temperature is not the sole driver of the atmospheric evaporative demand for water, it is the main driver of atmospheric evaporative demand through alterations to vapour pressure deficits

(Scheff and Frierson, 2014; Zhao and Dai, 2015b), and is more widely available than other variables. We therefore assume that it provides us with an indication of potential changes in the drying of soil moisture during DH events over time.

3.2.3 Estimation of Univariate and Bivariate Return Periods

Univariate return periods (RPs) are estimated for an exceedance of a given value of each characteristic separately. RPs are estimated through the application of stationary parametric models to exceedances of the thresholds d_{sel}^{uni} and m_{sel}^{uni} (sel : selected, uni : univariate) for D and M respectively. The default selection for each threshold is the 90th percentile of the given variable, though it is decreased in cases where there are not at least 20 events, but never below the 70th percentile. The sensitivity of estimated univariate RPs is tested for thresholds between the 90th and 70th percentiles, and little or differences are found for various thresholds. This implies that the distribution parameters are stable for thresholds within this range. Grid points with fewer than 20 events exceeding the 70th percentile are removed from the analysis. These cases are found in arid regions such as Southern Spain, Turkey and Northern Africa where dry events are generally very long lasting such that there can be very few events.

The univariate RP, T , of an event exceeding a duration d is estimated as (Coles et al., 2001):

$$T(d) = \frac{\mu_D}{1 - F(d)}, \quad (3.2.1)$$

where F is the cumulative distribution function (CDF) of the exceedances above d_{sel}^{uni} , while μ_D is the mean inter-arrival time between events with a duration exceeding d_{sel}^{uni} . This is estimated as $\mu_D = N_Y / N_E$, where N_Y is the number of years in the observation period and N_E is the total number of exceedances of d_{sel}^{uni} . The RP of an event exceeding

a magnitude of m , $T(m)$, is estimated in the same manner.

Following the approach developed in Bevacqua et al. (2018), bivariate RPs are estimated through the application of a parametric copula-based probability distribution to events in which D and M jointly exceed their respective thresholds d_{sel}^{bi} and m_{sel}^{bi} (*sel*: selected, *bi*: bivariate). This ensures we focus on long duration, dry and hot events. Again the default selection for each threshold is the 90th percentile though both are simultaneously decreased if there is not at least 20 events, but never below their 70th percentiles. The same sensitivity tests as above are carried out for bivariate RPs and little or no differences are found for various thresholds within this range.

A copula is a multivariate distribution function that models the dependence between random variables independent of the marginal distributions. According to Sklar (1959), the joint distribution of D and M may be written as:

$$F(D, M) = C(u_D, u_M) \quad (3.2.2)$$

where C is the copula modelling the dependence between the selected (D, M) pairs while $u_D = F_D(d)$ and $u_M = F_M(m)$ are uniformly distributed variables on $[0, 1]$. F_D and F_M are respectively the marginal CDFs of D and M from events with joint exceedances. The bivariate RP of an event exceeding D_q and M_q is then estimated as (Salvadori et al., 2007):

$$T(D_q, M_q) = \frac{\mu_E}{1 - u_{D_q} - u_{M_q} + C(u_{D_q}, u_{M_q})} \quad (3.2.3)$$

where $\mu_E = N_Y/N_E$ is the average inter-arrival time of events where D and M jointly exceed the thresholds d_{sel}^{bi} and m_{sel}^{bi} , and $u_{D_q} = F_D(D_q)$ (likewise for u_{M_q}).

Duration exceedances of the thresholds d_{sel}^{uni} and d_{sel}^{bi} are modelled using an exponen-

tial distribution. A geometric distribution is generally used for D but the application of copulas requires continuous marginals, and so we employ its continuous counterpart as done in Serinaldi et al. (2009). Magnitude exceedances of m_{sel}^{uni} and m_{sel}^{bi} are modelled using the generalised pareto distribution. Copulas were fitted to u_D and u_M (obtained via empirical marginal cumulative distribution function (CDF)), and selected using the Akaike Information Criterion (AIC) from the families Gaussian, t, Clayton, Gumbel, Frank, Joe, BB1, BB6, BB7, and BB8. Marginal distributions and copulas were fitted through a maximum likelihood estimator using the `fitdistrplus` (Delignette-Muller and Dutang, 2015), `ismev` (Heffernan and Stephenson, 2018) and `VineCopula` (Schepsmeier et al., 2017) R packages. The goodness of fit of marginals and copulas (one-tailed; $N_{boot} = 100$ for copulas) was tested using the CvM criterion with the `gofest` (Faraway et al., 2017), `eva` (Bader and Yan, 2018) and `VineCopula` R packages. We reject the null hypothesis that the selected distribution or copula family may not be rejected if the p-value is less than 0.05. This occurs at less than 5% of grid points for each case, which is in the acceptable range of tests that may fail by random chance (Zscheischler et al., 2017).

To illustrate the influence of the (D, M) dependence on the estimation of bivariate return periods, we compute $T(D_q, M_q)$ considering D and M independent of one another. In this case, an independent copula is chosen for C and $\mu_E = N_Y/N_{ind}$, where N_{ind} is the expected number of joint exceedances for two independent variables (the total number of events (including non-extremes) multiplied by the probability of a joint exceedance above q in the independent case). F_D and F_M are then fitted to all marginal exceedances of the thresholds d_{sel}^{uni} and m_{sel}^{uni} .

3.2.4 Estimation of Annual Trends and Return Period Variation

Linear trends are estimated for the annual maxima of D and M from DH events throughout the entire analysis period (1950-2013) using linear regression. Statistical significance of the trend is identified when the coefficient p-value for time is less than 0.05 such that we reject the null hypothesis that the coefficient has a value of zero.

We estimate changes in the RP for individual and joint exceedances of the 95th percentiles of D and M . The analysis period is split into two 30 year periods, a reference period (ref : 1950-1979) and a post-reference period ($pref$: 1984-2013), and RPs are estimated in each period separately. All thresholds including d_{sel}^{uni} , m_{sel}^{uni} , d_{sel}^{bi} and m_{sel}^{bi} , as well as the 95th percentiles, are estimated from ref while ensuring that at least twenty events are found in both ref and $pref$. The change in case $i =$ (a) $T(D_{95})$, (b) $T(M_{95})$, and (c) $T(D_{95}, M_{95})$, is calculated in $pref$ with respect to ref as:

$$\Delta T_i = \frac{T_i^{pref} - T_i^{ref}}{T_i^{ref}} \cdot 100 \quad (3.2.4)$$

where ΔT_i refers to the change of RP in $pref$ (T_i^{pref}) with respect to that estimated in ref (T_i^{ref}). The statistical significance of changes is identified through comparing T_i^{ref} with the 95% uncertainty interval surrounding T_i^{ref} . This uncertainty interval is constructed, via non-parametric bootstrapping, from 1000 values of T_i^{ref} obtained from 1000 event sets. These are created by resampling of the entire distribution such that we consider the uncertainties around μ_i also.

3.2.5 Contributions to Return Period Variation

Using a method developed in Bevacqua et al. (2018), we assess the relative contributions to changes in bivariate RPs arising from changes in the marginal distributions of (a) D , (b) M , and (c) the (D, M) dependence. The relative change in probability for each case is estimated as:

$$\Delta T_{exp_i} = \frac{T_{exp_i} - T^{ref}}{T^{ref}} \cdot 100 \quad (3.2.5)$$

where T^{ref} is the bivariate return period from *ref* while T_{exp_i} is calculated in the following manner:

Experiment (a): We estimate the bivariate RP specifying the marginal distribution of D (including non-exceedances) as that from *pref* but the marginal distribution of M and the (D, M) dependence as those from *ref*. Given the variable D^{ref} , we calculate the associated empirical CDF to obtain $U_{D^{ref}}$. From the variable D^{pref} we define the empirical CDF $F_{D^{pref}}$ that is used to obtain $D_a = F_{D^{pref}}^{-1}(U_{D^{ref}})$. We then compute the return period T_{exp_a} using the bivariate model fitted to (D_a, M^{ref}) pairs that jointly exceed d_{sel}^{bi} and m_{sel}^{bi} . The variables (D_a, M^{ref}) have the same Spearman correlations and tail dependence as during *ref* but the marginal distribution of D is that of *pref*.

Experiment (b): Similar to Experiment (a) but swapping D and M .

Experiment (c): We estimate the bivariate RP specifying the (D, M) dependence as that from *pref* but the marginal distributions are those of *ref*. Given variables (D^{pref}, M^{pref}) , their respective empirical CDFs are computed to obtain variables $(U_{D^{pref}}, U_{M^{pref}})$. With variables (D^{ref}, M^{ref}) we obtain their respective empirical CDFs from which we define $D_c = F_{D^{ref}}^{-1}(U_{D^{pref}})$ and $M_c = F_{M^{ref}}^{-1}(U_{M^{pref}})$. The variables (D_c, M_c) have the same Spearman correlation and tail dependence as (D^{pref}, M^{pref}) , but the marginal distributions are those of *ref*. The return period T_{exp_c} is then computed using the bivariate

model fitted to (D_c, M_c) pairs jointly exceeding d_{sel}^{bi} and m_{sel}^{bi} .

3.3 Results

The joint behaviour of D and M is demonstrated at five grid points near Stockholm, Paris, Belgrade, Moscow and Madrid using xy-scatter plots (Figure 3.1, left column). These illustrate the (D, M) dependence seen throughout Europe where long-duration events generally coincide with high temperatures. Such dependence is explained by the anti-cyclonic conditions underlying DH events, which suppress rainfall and allow for more incoming solar radiation that heats the Earth's surface and atmosphere causing high temperatures to build throughout an event (Miralles et al., 2014). The top 5 ranked events at each location, from the entire period available (1950-2016), are both provided in tables 3.1 to 3.5 shown in the appendix section at the end of this chapter and indicated in Figure 3.1 (left column). Such events have contributed to severe impacts in the affected regions. For example the 2010 event at Moscow was accompanied by extreme heat and wildfires that resulted in 50,000 excess deaths (Shaposhnikov et al., 2014), while the 1972 event was termed one of the worst modern droughts at the time (Federov, 1973; Buchinsky, 1976; Schubert et al., 2014). At Belgrade, the events of 1990 and 2012 brought respective estimated agricultural losses of USD 500 million (Sepulcre-Canto et al., 2012) and USD 2 billion (Zurovec et al., 2015). While at Madrid, the 1994 event formed part of Spain's worst 20th century drought event from 1991 to 1995 (Sheffield and Wood, 2012) which peaked during the 1994 event according to Stagge et al. (2013). Furthermore the 2012 event led to long-term negative impacts for trees that will have cascading effects on ecosystem services (Camarero et al., 2015) while the 2015 event covered the hottest July ever

recorded in Spain (Ionita et al., 2017). Further examples are detailed in the appendix which indicate the effectiveness of the characteristics in identifying important events. The bivariate model, presented in Section 3.2.3, is applied to *DH* events that reside in the upper right hand corner defined by the dashed grey lines, representing m_{sel}^{bi} and d_{sel}^{bi} , in Figure 3.1, (left column). Although the characteristics of these events are calculated at a single grid point, they represent anti-cyclonic systems with large spatial extents. To give an idea of their spatial coverage, two types of composite plots of temperature anomalies are produced using ERA Interim data for events in *pres*. A daily temperature anomaly is defined with respect to the climatological mean temperature of all days within a 21-day window centred on the given day. The first composite is produced considering days on which the maximum temperature during an event was observed (Figure 3.1, middle column), while the second is produced considering all days throughout each event (Figure 3.1, right column). The number of days (n_{days}) used to produce the composite is given on each panel.

Stronger anomalies are of course seen for the first type of composite (Figure 3.1, middle column), but both types indicate the affected areas of these events. Within the composites, we also see alternating regions of warm and cold anomalies, particularly in Scandanavia and areas in Central Europe. This feature demonstrates the connection of the event characteristics to blocking systems and sub-tropical ridges, affecting these regions (Sousa et al., 2018), that are themselves embedded within planetary-scale Rossby waves.

The differences between Madrid and the other locations should be noted. In contrast to the more northern locations, events in Madrid are much longer-lasting, as persistent anticyclonic conditions are common here in summer (Ulbrich et al., 2012), and no spatial signature is seen in the composite of temperature anomalies for all event

days (Figure 3.1 (o)). Thus, in Madrid, unlike the other locations where the characteristics are representative of distinct events, D is most likely representative of a normal summer season while M may represent a single hot event within that season.

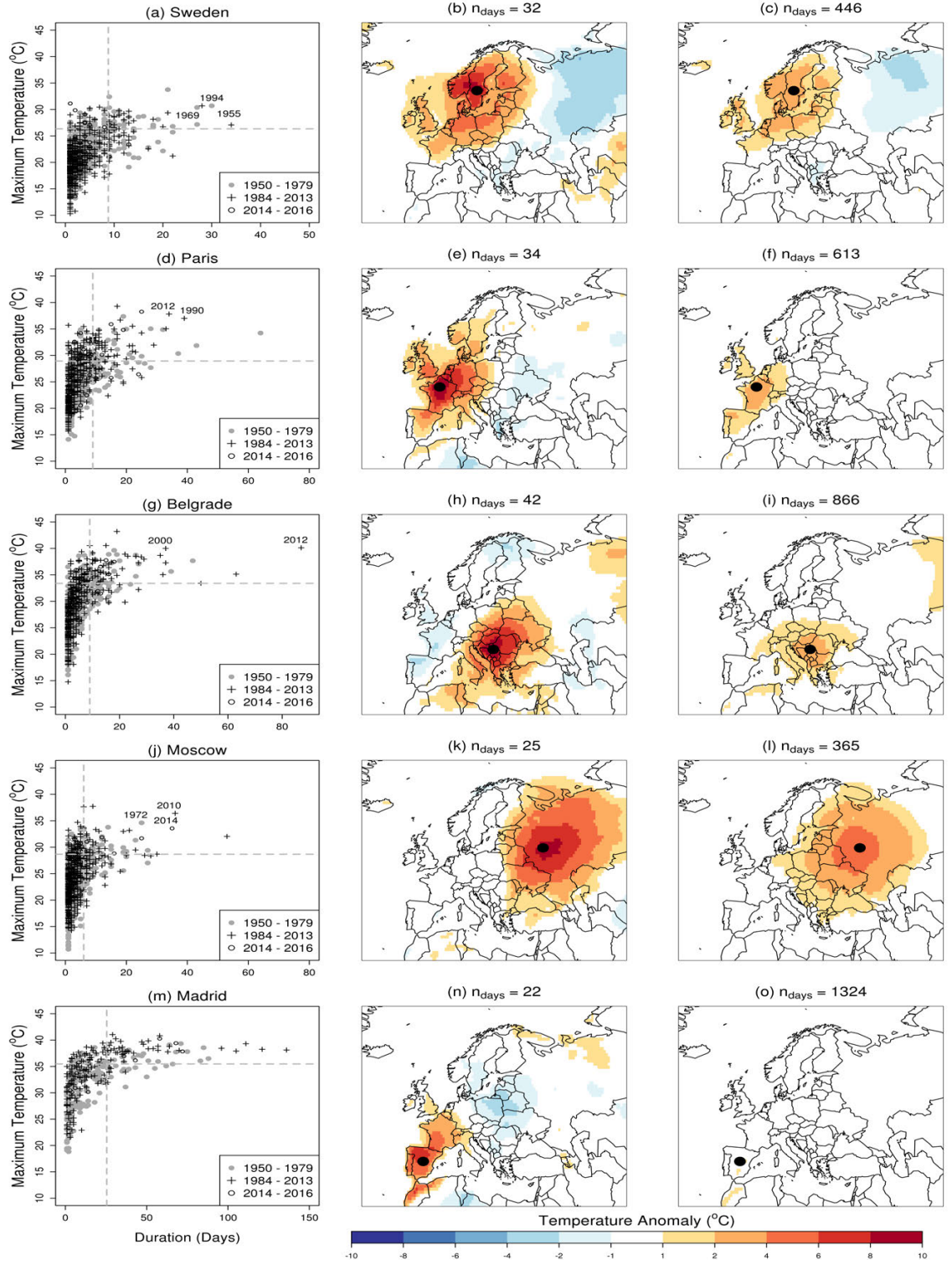


Figure 3.1: (Caption next page.)

Figure 3.1: (Previous page.) Summary of event characteristics taken from grid points near Stockholm (a, b, c), Paris (d, e, f), Belgrade (g, h, i), Moscow (j, k, l) and Madrid (m, n, o). Panels in the left column provide xy-scatter plots of Duration (D) and Magnitude (M) of events from *ref* (grey dots), *pref* (black crosses) and the period 2014-2016 (black circles). The dashed grey lines represent d_{sel}^{bi} and m_{sel}^{bi} for D and M respectively, the bivariate statistical model is fitted to all events that jointly exceed these thresholds in *ref* and *pref* separately. The years are shown next to the points representing events that jointly exceed the 99th percentiles estimated from *ref*. Panels in the center column provide temperature anomaly composites considering days on which the maximum temperature was observed during events jointly exceeding d_{sel}^{bi} and m_{sel}^{bi} . And panels in the right column provide temperature composites considering all days during the events jointly exceeding d_{sel}^{bi} and m_{sel}^{bi} . Composites are produced using the ERA Interim dataset.

3.3.1 Return Periods for Long Duration and Bivariate Extreme Events

Univariate RPs ($T(d)$) of long duration dry periods exceeding a duration $d = 15, 20, 30$ and 40 days are presented in Figure 3.2. The spatial distribution of $T(d)$ identifies the differences in synoptic variability seen across Europe during summer. Persistent anti-cyclonic conditions that are common in Southern Europe (Ulbrich et al., 2012) explain the low values of $T(d)$ seen there, while higher values in more northern parts of Europe are due to a higher synoptic variability between cyclonic and anti-cyclonic conditions.

Figure 3.3 shows the D and M values associated with their 95th and 99th percentiles throughout Europe. Bivariate RPs ($T(D_q, M_q)$), computed from *pref*, for joint exceedances of $q = 95^{th}$ and 99^{th} percentiles respectively are presented in Figure 3.4. The dependence of the event characteristics can influence the estimation of $T(D_q, M_q)$. This influence is quantified using the Likelihood Multiplication Factor (LMF) (Zscheischler and Seneviratne, 2017) and is estimated as the ratio between $T(D_q, M_q)$ considering (D, M) dependent (T_{dep}) and independent (T_{ind}) of one another, $LMF = T_{ind}/T_{dep}$.

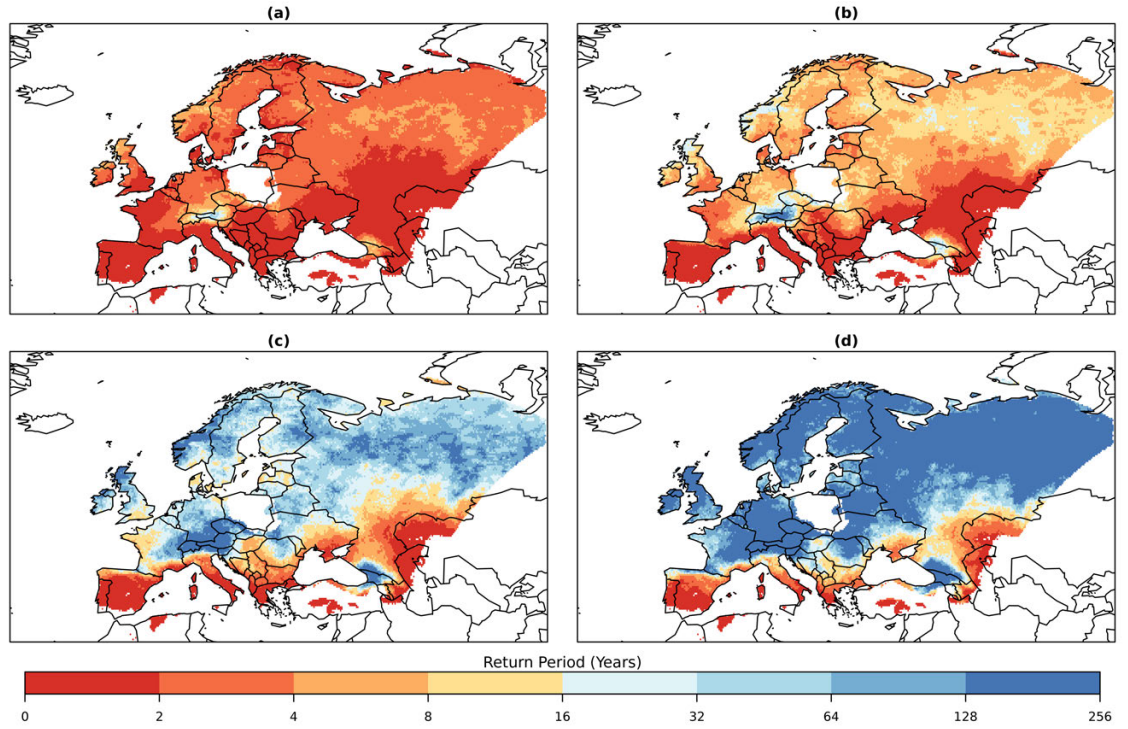


Figure 3.2: Return periods ($T(d)$) of dry events from $pref$ with durations (d) exceeding (a) 15; (b) 20; (c) 30; and (d) 40 days.

The dependence is seen to have a large influence across Europe (Figure 3.4 (b) and (d)). For example, treating D and M as independent results in an overestimation of $T(D_{95}, M_{95})$ of up to 8 times the RP when accounting for their dependence.

The spatial distribution of $T(D_{95}, M_{95})$ is mostly homogeneous throughout Western and Eastern Europe (Figure 3.4 (a)). Lowest RPs are seen in the Balkans while higher RPs are found in southern areas such as Spain. The interpretation of $T(D_{95}, M_{95})$ requires careful consideration of both $T(d)$, shown in Figure 3.2, and the local climate. For instance, event characteristics in areas of higher synoptic variability are most likely associated with distinct blocking events or sub-tropical ridges (Sousa et al., 2018). In areas such as the Balkan region that also lie in a transitional climate zone with strong land-atmosphere interactions (Hirschi et al., 2011; Schwingshackl et al., 2017),

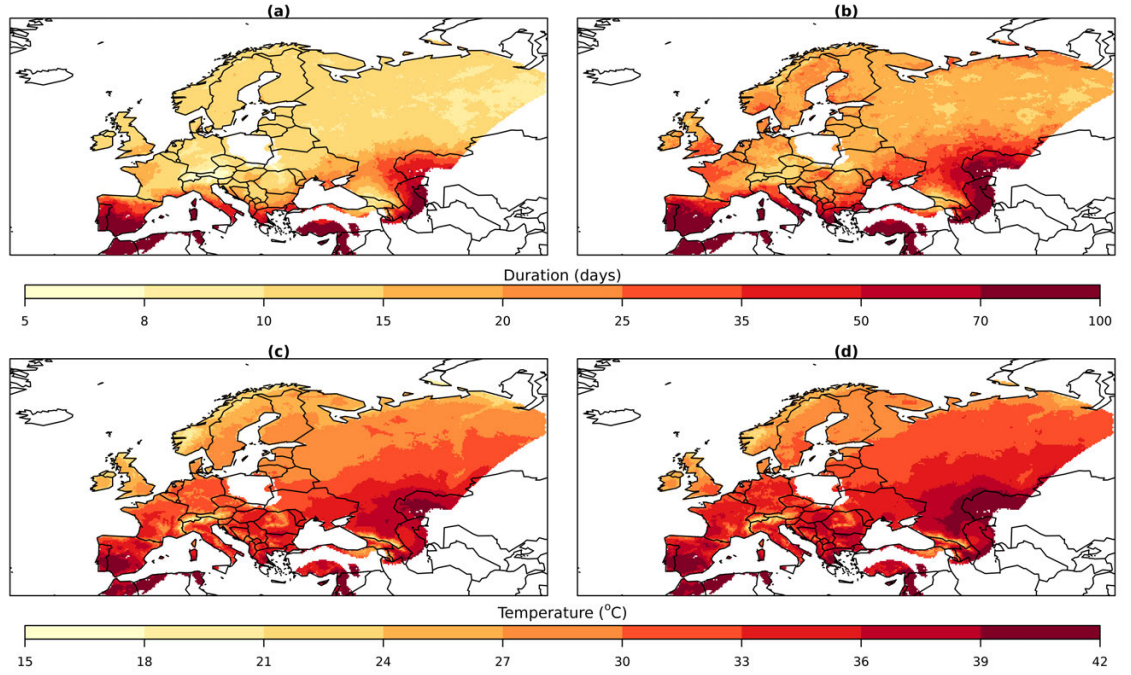


Figure 3.3: Absolute values at the 95th and 99th percentiles throughout Europe for D (a and c) and M (b and d).

drying of soil during a dry period can in turn intensify temperatures (Seneviratne et al., 2010). This combination may in part explain why the lowest RPs are found in the Balkan region. Meanwhile, in Southern Europe, D can be representative of the normal situation during a large part of the summer season while M may be representative of a single hot event within that season. This results in high values of $T(D_{95}, M_{95})$ due to a smaller number of events that are each very long-lasting.

The occurrence of events with joint exceedances of the 99th percentiles have led to severe impacts in parts of Europe, these events are indicated by the years in red in Figure 3.1. Due to the rare occurrence of such events, the estimation of $T(D_{99}, M_{99})$ is highly sensitive to the occurrence of a single event and as such is subject to large uncertainties. Figure 3.4 (c) provides an indication of where such events have and have not occurred during *pres* and where such events may be more likely to occur

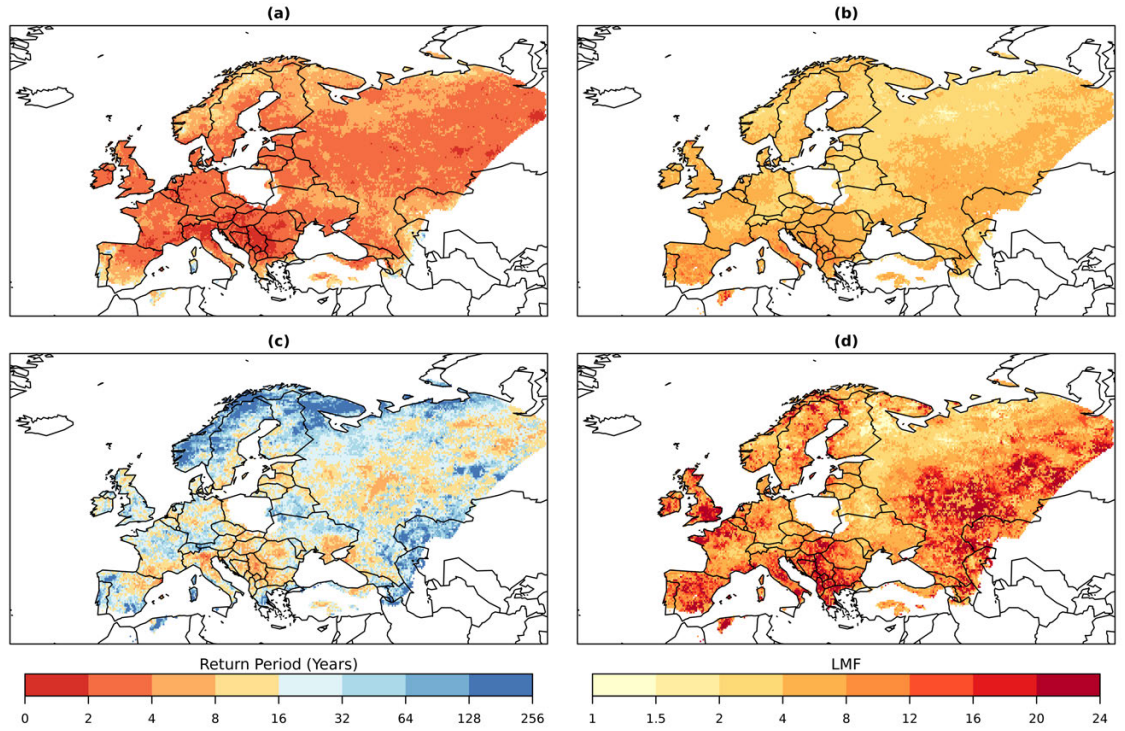


Figure 3.4: Bivariate return periods of DH events from $pref$ with joint exceedances of (a) the 95th percentiles ($T(D_{95}, M_{95})$) and (c) 99th percentiles ($T(D_{99}, M_{99})$), along with the Likelihood Multiplication Factor (LMF) that quantifies the influence of the (D, M) dependence on the estimation of (b) $T(D_{95}, M_{95})$ and (d) $T(D_{99}, M_{99})$, a value greater than one signifies that the bivariate return period is overestimated when considering the D and M independent of one another.

again. For example, the areas of 2010 and 2012 events in Russia and South-East Europe are highlighted by lower values of $T(D_{99}, M_{99})$ (Figure 3.4 (c)). However, it does not provide robust information of locations where such extreme events are unlikely to occur. This is emphasised by the recent record breaking 2018 dry and hot period that had severe impacts in much of Northern Europe, where large RPs are found (3.4 (c)). Robust estimates of the probability of such rare events are not obtainable using empirical data, particularly with non-stationarities imposed by a changing climate. Such estimates require ensembles of suitable climate models that provide a larger sample of events and perhaps more creative methods to understand the changing probabil-

ity and future likelihood of such rare events (Hazeleger et al., 2015; Bevacqua et al., 2017). For these reasons, we present the analysis of changes to $T(D_{95}, M_{95})$ in the next sections as we have greater confidence in its estimation.

3.3.2 Variations in Duration and Magnitude

Figure 3.5 presents the linear trends, estimated via linear regression, in the annual maxima of D and M over the entire observation period (1950-2013), as well as the percentage change in $T(D_{95})$ and $T(M_{95})$ estimated via Equation 3.2.4.

Between D and M , the strongest changes in both the annual maxima and 95th percentile exceedances are seen for M across Europe. Positive linear trends are seen in the annual maxima of M in much of Western Europe and parts of Eastern Europe (Figure 3.5 (b)). These trends can be between 0.25°C to 0.5°C per decade, meaning that the annual maximum of M in DH events may have warmed by 1.5 to 3°C over the 64 year observation period. Large differences in $T(M_{95})$ between *ref* and *pref* are found across Europe (Figure 3.5 (d)). The frequency of exceedances has almost doubled in many locations while much of Northern Scandinavia has seen a halving in frequency.

Weak variations are observed for D . Significant trends in the annual maximum duration are found only in a particular region of Russia and Southeastern Europe (Figure 3.5 (a)). These trends can be between 1 to 2 days per decade such that the annual maximum duration may have increased by between 6 and 12 days over the 64 years in these locations. Variations in D_{95} are also mostly small. The strongest increases are found in South-Eastern Europe and parts of Russia while the strongest decreases are seen across much of the UK, Scandinavia and Russia.

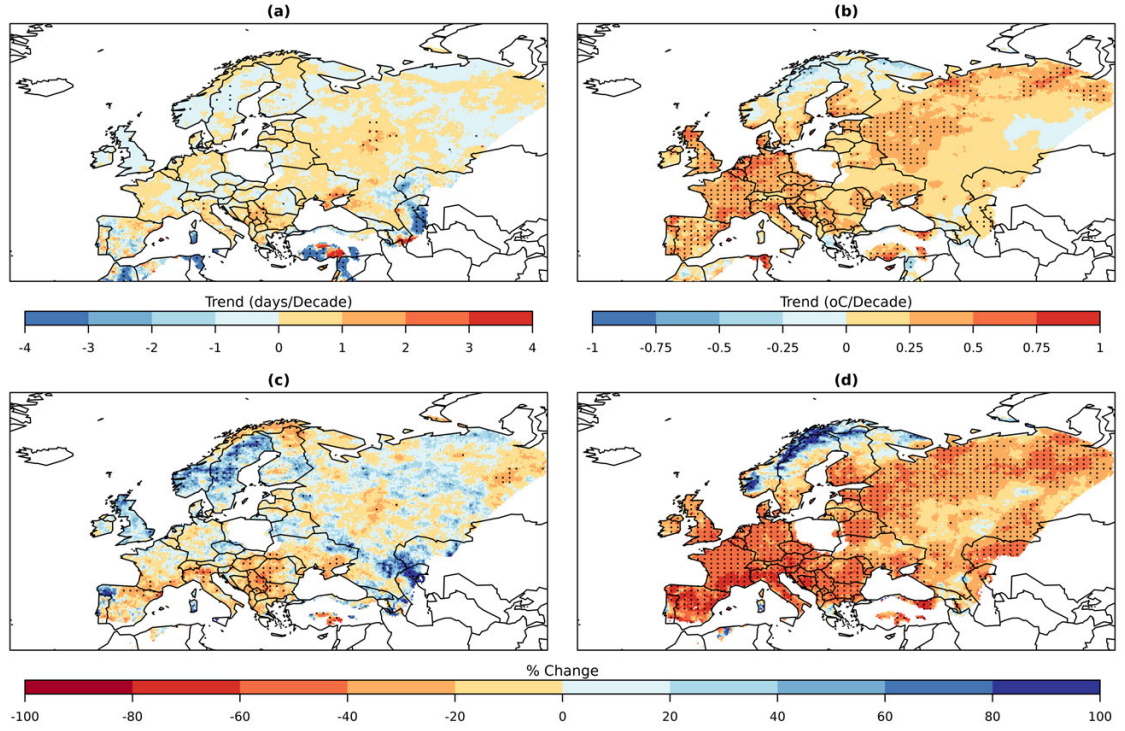


Figure 3.5: Estimated linear trends in the annual maxima of (a) Duration and (b) Magnitude. Statistically significant trends are indicated by stippling. Also given are the change in univariate RPs in *pref* (1984-2013) with respect to *ref* (1950-1979) of (c) Duration and (d) Magnitude for exceedances of their respective 95th percentiles. Statistically significant differences to the 95% uncertainty interval, estimated via non-parametric bootstrap, are shown by stippling. For all cases, only every 3rd and 5th latitudinal and longitudinal grid point are selected for showing the stippling, showing all points would hide the magnitude of change due to the high resolution of the dataset.

3.3.3 Variations in Bivariate Return Periods

The change in $T^{pref}(D_{95}, M_{95})$ with respect to $T^{ref}(D_{95}, M_{95})$, estimated via Equation 3.2.4, is provided in Figure 3.6 (a). Statistically significant differences between *pref* and *ref*, indicated by the stippling in Figure 3.6 (a), are identified when $T^{pref}(D_{95}, M_{95})$ is outside the 95% uncertainty interval of $T^{ref}(D_{95}, M_{95})$. The strongest changes are seen just north of the Mediterranean, particularly in South-Eastern Europe, and across much of Western Russia. Statistically significant negative changes (increased probabil-

ity) are found throughout these regions and amount to 17% of the total area covered by the dataset. Figure 3.6 (b) presents the kernel density estimates of $T^{ref}(D_{95}, M_{95})$ and $T^{pref}(D_{95}, M_{95})$ from each grid point throughout Europe. Comparing these highlights the general shift across Europe to lower bivariate RPs and thus a higher frequency of compound long, dry and hot events during *pref* compared to *ref*. To give an idea of whether or not the results may be affected by the event parameter n_{sep} , we show the results obtained when using a value of $n_{sep} = 1, 2$, and 3 in the Supplementary Information section at the end of this chapter. The results presented in Figure 3.8 show only subtle differences between the results obtained, and so defining $n_{sep} = 2$ will not affect the message of this paper.

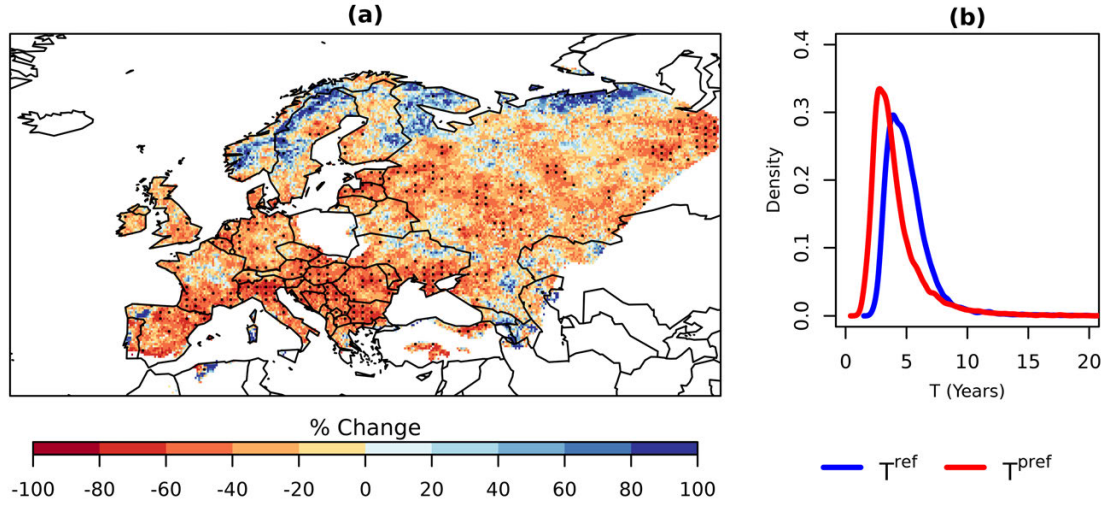


Figure 3.6: Estimated change in bivariate RPs in *pref* (1984-2013) with respect to *ref* (1950-1979) for joint exceedances of their respective 95th percentiles. Shown in (a) are the % changes across Europe, stippling indicates statistically significant differences between *pref* and the 95% uncertainty interval from *ref* estimated via non-parametric bootstrap. Only every 3rd and 5th latitudinal and longitudinal grid point are selected for showing the stippling. Alongside in (b) are the kernel densities estimated using the RPs from all grid points for *ref* (blue) and *pref* (red).

These changes in $T(D_{95}, M_{95})$, shown in Figure 3.6, can arise due to changes in the marginal distributions of (a) D and (b) M as well as changes in (c) the dependence be-

tween D and M . Using methods outlined in Section 3.2.5, we decompose the changes in bivariate RPs to quantify the contribution of these three components to the variation in $T(D_{95}, M_{95})$. Changes in marginal density of M have the largest contributions as indicated by the higher amount of stippling (Figure 3.7 (b)), while changes in duration are seen to have a contribution in some areas of Europe (Figure 3.7 (a)), most specifically in the Balkans where the largest changes in D are seen (Figure 3.5 (a)). Large contributions are also seen from variations in the (D, M) dependence (Figure 3.7 (c)) owing to an increase in the dependence between D and M . The physical reasoning behind this increase is unclear. It is possible that with longer events becoming warmer, higher levels of ET due to increased temperatures may dry out soil moisture and induce land-atmosphere interactions that further amplify temperature extremes. Though as there are very few significant differences, it is possible that the contribution from a variation in dependence is dominated by a single event such as the 2010 Russian heat wave which coincides with the region where the largest contribution from dependence is seen. However, removing this event from the estimation of this contribution did not affect the results (see Figure 3.9 in supplementary information at the end of this chapter).

Overall, with large variations in M and only small variations found in D , the results illustrate the predominant influence of temperature on the increase in compound probability seen across Europe and there is little evidence to suggest that events are more prolonged in *pref*. Thus, DH events are, in general, becoming warmer but not longer.

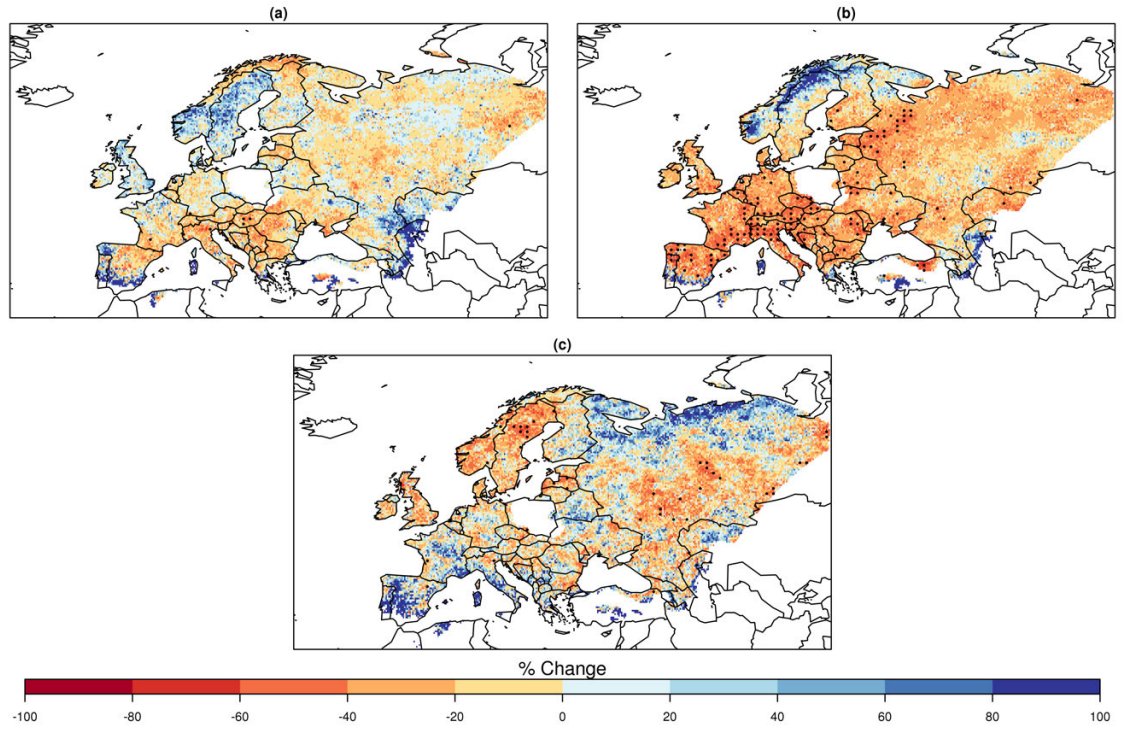


Figure 3.7: Contributions to the variation in bivariate RPs from changes in the marginal densities of (a) Duration, and (b) Magnitude, as well as changes in (c) dependence. Statistically significant differences between T_{exp_i} and T^{ref} are indicated by stippling. Again, only every 3rd and 5th latitudinal and longitudinal grid point are selected for showing the stippling.

3.4 Summary and Conclusions

We have investigated long-duration dry events that co-occur with extreme temperatures in Europe, as well as changes in these events over the period 1950-2013. This paper proposes a framework to characterise such events and quantify their probability and return periods (RPs) through the application of a copula-based approach introduced by Bevacqua et al. (2018). The events are denoted as long-duration dry and hot (DH) events and are characterised by their duration D (consecutive number of day with precipitation less than 1mm), and magnitude M (maximum daily maximum temperature during event). These characteristics combined are shown here to be ef-

fective in highlighting important events that have brought severe impacts to affected regions.

The probability of such compound events, with respect to joint exceedances of the respective 95th percentiles of D and M , has increased across much of Europe between *ref* (1950-1979) and *pres* (1984-2013) periods. The main driver of this change in probability is increasing temperatures throughout Europe. Little change is seen in the duration of events, leading us to conclude that DH events have mostly become warmer during *pres* rather than longer. An exception to this is found in South-East Europe where events appear to have increased in temperature and duration.

Return periods were also estimated for events in which D and M jointly exceed their 99th percentiles. However, robust estimations of their probability are not possible to obtain due to the rarity of their occurrence. For this reason, we cannot assess changes in these return periods. Such events have brought severe impacts to the affected regions and so it is important that efforts are made to better quantify their probability such that possible future changes in their occurrence may be better understood (Coumou et al., 2018). It is hoped that the methodology used in characterising these events and quantifying their probability will provide a platform for further research, particularly in extracting information of their current and future risk from climate models.

The implications of the increased probability of DH events found here mainly pertain to the acceleration of drought propagation from meteorological drought to soil moisture drought. The results complement other findings with respect to the relationship between drought and climate change. For example, soil moisture drought events are expected to set in quicker and become more severe (Trenberth et al., 2014; Samaniego et al., 2018), owing to increases in evaporation during dry periods (Dai et al., 2004)

that are driven by rising temperatures (Scheff and Frierson, 2014; Zhao and Dai, 2015b). Furthermore, given the weak historical trends found in global land precipitation (New et al., 2001; Lambert et al., 2004; Ren et al., 2013; Adler et al., 2017), the dominant temperature signal behind the increased probability of *DH* events may also largely explain changes in global drought conditions, as shown in Marvel et al. (2019), which closely resemble changes in global mean temperature (e.g. Pachauri et al. (2014)). The results may also have implications for the persistence of soil moisture drought conditions. High amounts of precipitation are required for recovery from large moisture deficits induced by intense drying (Seneviratne et al., 2012a; Manning et al., 2018) while general increases in evaporation can push environments towards a climatically drier state (Samaniego et al., 2018).

The response of *D* and *M* to climate change can also be linked to that of blocking events. The weak variations seen in *D* align with studies on changes in blocking frequency which is expected to be dominated by natural variability in the coming decades (Woollings et al., 2018). Consistent with the changes in *M* shown here, blocking events have become warmer and are expected to become more extreme in the future (Sousa et al., 2018) due to increasing temperatures and decreasing soil moisture that can strengthen temperature extremes through land-atmosphere interactions (Seneviratne et al., 2006).

One should note that these results are derived from a gridded dataset which may introduce errors through interpolation of station observations whose spatial density can be too low for adequate representation of extremes (Haylock et al., 2008; Herrera et al., 2018). Although we have more confidence in this dataset for large-scale events investigated here than for localised precipitation extremes, as investigated in (Herrera et al., 2018) for instance, it would be interesting to investigate the influence of inter-

polarization and the spatial density of stations on the representation of characteristics of *DH* events in gridded products. This would provide important information for climate model validation studies that incorporate EOBS and other gridded datasets.

Finally, the comparison made here between *ref* and *pres* shows differences in the multi-decadal variability of *DH* events. Direct attribution of these events to anthropogenic climate change is not possible with an empirical analysis. However, our finding that temperature changes are the main cause for changes in bivariate probability is in line with trends of increasing temperature due to rising greenhouse gas concentrations. One can therefore hypothesise, alongside forewarnings from Samaniego et al. (2018), that such increases in probability will continue into the future leading to more severe long-lasting soil moisture droughts that can lead to negative impacts such as reduced crop yields and increased wildfire risk.

3.5 Supplementary Information

Table 3.1: *Top 5 Events from Stockholm grid cell. The top 5 events at each site are selected based on a combined ranking, r_{DM} , based on a sum of the individual ranks of duration (r_D) and magnitude r_M , i.e. $r_{DM} = r_D + r_M$. The event with the highest combined ranking will be that with the largest r_{DM} value.*

D (days)	M ($^{\circ}\text{C}$)	Start Date	Reference
30	30.70	1955-07-06	Veryard (1956)
28	30.69	1994-06-30	Stagge et al. (2013)
21	33.75	1975-07-25	SPCCA (2016)
27	30.38	1969-07-25	Hannaford et al. (2011)
21	29.36	2008-05-20	Larsson (2017)

Table 3.2: Top 5 Events from Paris grid cell. Events ranked as described in the caption of Table 3.1.

<i>D</i> (days)	<i>M</i> (°C)	Start Date	Reference
39	37.00	1990-07-06	Stagge et al. (2013)
34	37.82	2012-08-06	No Information
25	38.26	2015-06-23	Ionita et al. (2017)
33	35.03	1986-07-07	No Information
28	35.04	1959-07-01	Stagge et al. (2013)

Table 3.3: Top 5 Events from Belgrade grid cell. Events ranked as described in the caption of Table 3.1.

<i>D</i> (days)	<i>M</i> (°C)	Start Date	Reference
87	40.12	2012-07-30	Zurovec et al. (2015)
37	40.00	2000-07-21	Sepulcre-Canto et al. (2012)
35	38.67	1988-07-17	No Information
26	38.74	1950-08-06	Tošić and Unkašević (2014)
19	43.20	2007-07-12	Sepulcre-Canto et al. (2012)

Table 3.4: Top 5 Events from Moscow grid cell. Events ranked as described in the caption of Table 3.1.

<i>D</i> (days)	<i>M</i> (°C)	Start Date	Reference
36	36.40	2010-06-17	Mokhov (2011)
25	34.61	1972-07-29	Schubert et al. (2014)
35	33.56	2014-07-03	Russo et al. (2015)
53	32.04	1999-06-01	Schubert et al. (2014)
21	33.18	2007-08-08	Schubert et al. (2014)

Table 3.5: Top 5 Events from Madrid grid cell. Events ranked as described in the caption of Table 3.1.

<i>D</i> (days)	<i>M</i> (°C)	Start Date	Reference
111	39.31	1994-06-02	Stagge et al. (2013)
58	40.83	2012-07-27	Camarero et al. (2015)
71	39.33	1966-07-03	Cantos et al. (2000)
58	40.28	2015-06-24	Ionita et al. (2017)
68	39.41	2016-07-07	Vázquez et al. (2016)

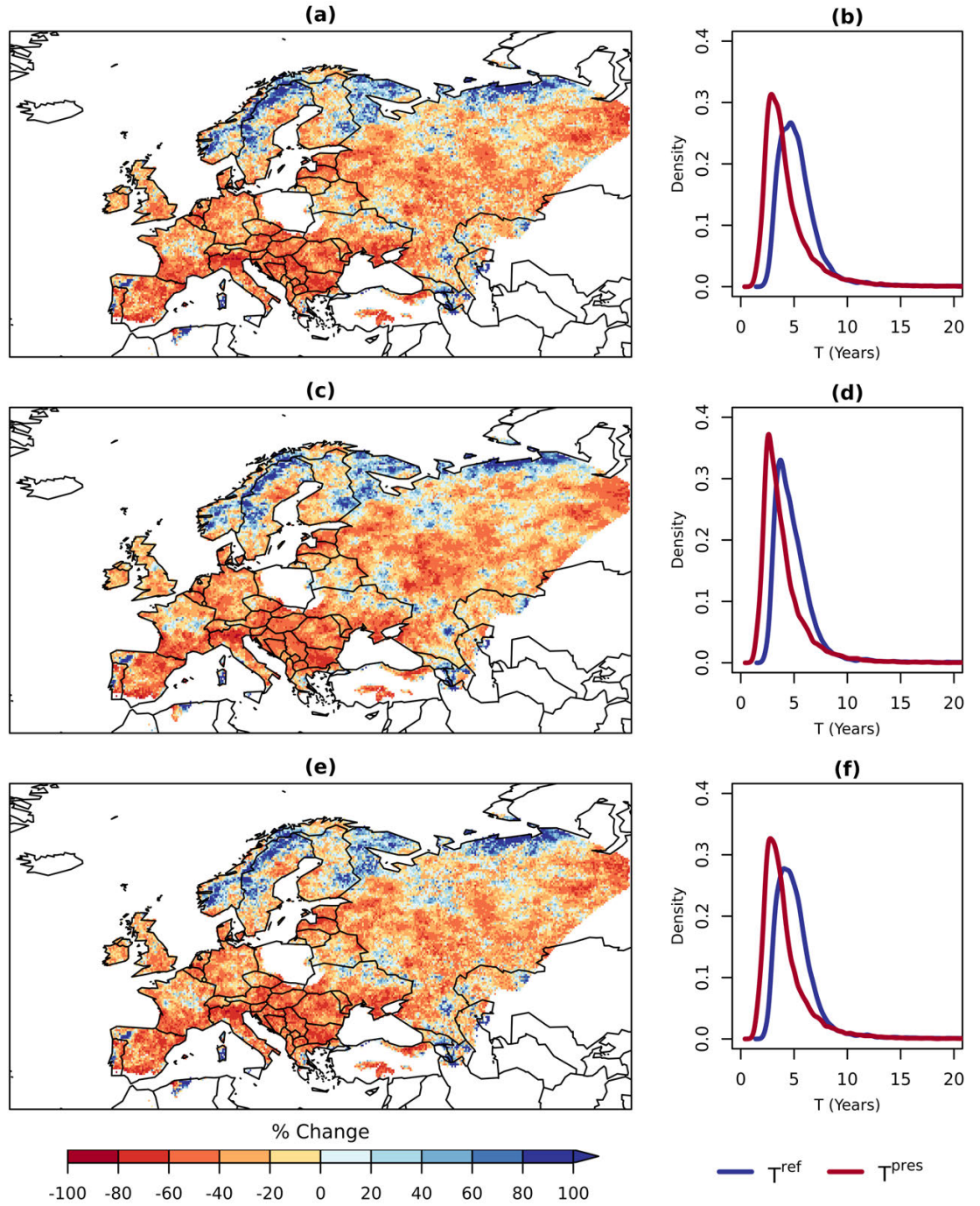


Figure 3.8: Estimated change in bivariate RPs in pref (1984-2013) with respect to ref (1950-1979) for joint exceedances of their respective 95th percentiles for $n_{\text{sep}} = 1$ (a, b), 2 (c, d), and 3 (e, f). Shown in (a), (c), and (e) are the % changes across Europe. Alongside in (b), (d), and (f) are the kernel densities estimated using the RPs from all grid points for ref (blue) and pref (red).

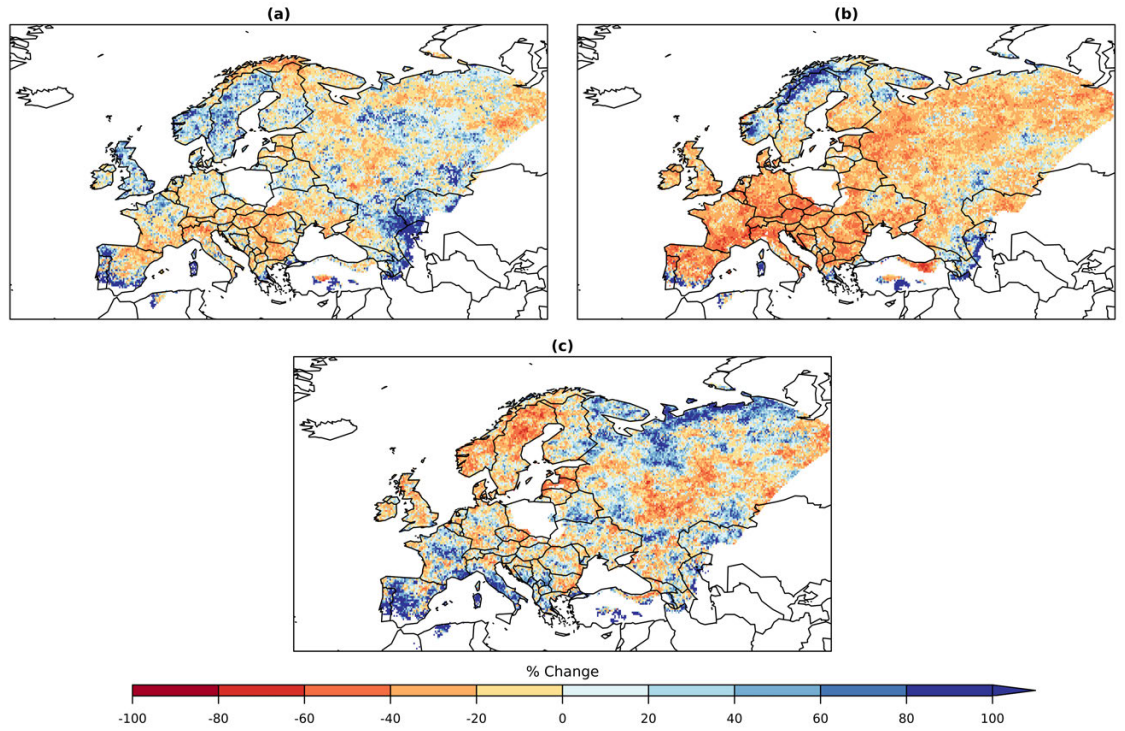


Figure 3.9: This figure is the same as Figure 3.7 but with the year 2010 removed from the analysis. Contributions to the variation in bivariate RPs from changes in the marginal densities of (a) Duration, and (b) Magnitude, as well as changes in (c) dependence. Statistically significant differences between T_{exp_i} and T^{ref} are indicated by stippling. Only every 3rd and 5th latitudinal and longitudinal grid point are selected for showing the stippling.

Chapter 4

Long Duration, Dry and Hot Events in CMIP5

4.1 Introduction

Climate models are central to our understanding of how climate change will alter the probability of extreme events. As planning of adaptation and mitigation measures for a future climate are mostly based on their projections, it is important to assess their skill in representing these extreme events. In this chapter we assess the characteristics of *DH* events, namely their duration D and magnitude M in a set of CMIP5 (Coupled Model Intercomparison Project Phase 5) models. Again, D is defined as the consecutive number of days with precipitation less than 1mm, and long duration events exceeding a given threshold are combined if they are separated by two days or less. M is then defined as the maximum daily temperature over the duration of an event. Much attention has been given to soil moisture in climate models and its potential evolution in a future warmer climate (e.g. (Berg et al., 2017; Sheffield and Wood, 2008; Samaniego et al., 2018; Vogel et al., 2018; Zhao and Dai, 2015a; Hoerling et al., 2012; Burke, 2011)). Much of this attention has focussed on the changes in the mean soil state and background aridity which point to a drier future (Berg et al., 2017; Zhao and Dai, 2015a; Hoerling et al., 2012; Burke, 2011), while Samaniego et al. (2018) showed that CMIP5 models project longer lasting soil moisture drought events with greater spatial extents that each worsen with the degree of warming. Changes in soil moisture are also linked to temperature through land-atmosphere interactions where drier soil moisture projections are also accompanied with higher temperature variability and hotter extremes (Seneviratne et al., 2006; Berg et al., 2015; Vogel et al., 2018, 2017).

It is strongly thought that vegetation response will play a large role in the amount of drying that will take place in a warmer climate. For instance, increases in atmospheric CO₂ concentration can improve water use efficiency in vegetation as it stimulates car-

bon assimilation in plants leading to reduced stomal conductance and loss of water vapour as a result (Field et al., 1995; Hungate et al., 2002; Long et al., 2006). In fact, global greening has been observed (Zhu et al., 2016; Fensholt et al., 2012) and projected in the future (mahowald2016projections) as a result of increased carbon fertilisation and water use efficiency (Berg and Sheffield, 2018). This suggests a large adaptive capacity of vegetation to changes in background aridity. Furthermore, Berg et al. (2017) studied future projections of soil moisture in climate models which exhibit a gradient in changes of soil moisture with depth, where upper layers show largest decreases. They argue that these changes may not have large implications for vegetation as moisture availability at lower levels still remains high enough in the root zone to support moisture demand.

However, these studies do not address changes in extremes and potential risks posed to vegetation during extreme drought events. Those that have addressed changes in soil moisture droughts project increases in long duration events in the Mediterranean using a set of CMIP4 models Sheffield and Wood (2008) while Samaniego et al. (2018) project increases throughout Europe using a set of CMIP5 models. The reduced moisture levels in surface layers of soil projected by climate models (Berg et al., 2017; Zhao and Dai, 2015a; Hoerling et al., 2012; Burke, 2011) suggest that moisture in lower soil layers will be more susceptible to decreases during high evapotranspiration (ET) driven by temperature extremes, as there will be less moisture in the surface layers to act as a buffer. Hence the likelihood of drought conditions may become higher at lower soil depths during meteorological drought, regardless of any potential changes in the meteorological hazards such as the duration and magnitude of long-duration dry and hot (*DH*) events. Although, as changes in these hazards will likely have direct implications for soil moisture drought, it is important to gain knowledge of their rep-

resentation in climate models, as poor representation of such hazards will limit our confidence in climate model projections of soil moisture drought.

The representation of the duration of events, defined in this manner, has not been studied in climate models in depth. Other studies have compared the maximum duration event as a wider analysis of indices of climate extremes (Orlowsky and Seneviratne, 2012; Sillmann et al., 2013; Lehtonen et al., 2014), but not in terms of their frequency or relationship with extreme temperatures. These characteristics are representative of anti-cyclonic systems such as blockings and sub-tropical ridges and so there are similarities between this study and others investigating blocking frequency. The majority of literature has focussed on the representation of winter blocking in climate models (Lucarini et al., 2007; Scaife et al., 2011; Anstey et al., 2013; Berckmans et al., 2013; Hoskins and Woollings, 2015; Woollings et al., 2018). Those that have studied the representation of blocking frequency during summer in CMIP5 models have found mixed results. In general, the frequency of events lasting longer than 5 days is underestimated over Scandanavia and northern parts of Russia (Masato et al., 2013; Dunn-Sigouin and Son, 2013; Scaife et al., 2010). However, Masato et al. (2013) find a varied performance between CMIP5 models in that some underestimate blocking frequency, others overestimate it while a few models show a good comparison with the observed blocking frequency. While Dunn-Sigouin and Son (2013) find that the multi-model mean of summer blocking frequency compares well with the observed frequency of events lasting up to 15 days but underestimate the frequency of events lasting longer than 5 days.

The persistence of anti-cyclonic systems such as blocking events and sub-tropical ridges leads to the occurrence of dry conditions and extremely high temperatures during summer (Pfahl and Wernli, 2012; Sousa et al., 2018). In Chapter 3, we have quantified

the probability long duration dry periods co-occurring with extremely high temperatures, and shown that this probability is largely underestimated when not accounting for the dependence between the two. Thus it is important to know whether models can adequately represent these characteristics and their dependence. Although the limitations of climate models in representing single variables has been widely investigated, it is not clear how well climate models can capture the multivariate nature of compound events (Fischer and Knutti, 2013; Collins et al., 2013), and there is lack of literature focusing on this aspect.

In this chapter, for the reasons given above, we assess the representation of the duration of dry periods as well as the frequency of *DH* events throughout Europe. The chapter is laid out as follows: the data employed is described in Section 4.2, the methods, which are mostly the same as those in Chapter 3, are outlined in Section 4.3, while a summary of the results as well as conclusions drawn are presented in Section 4.5.

4.2 Data

4.2.1 Observed Data

As in Chapter 3, we employ temperature and precipitation data from the EOBS dataset (Haylock et al., 2008) version 16.0 on a 0.25 degree grid. We analyse the same time period from 1950 to 2013 and remove grid points over areas of Poland and Iceland where many missing values are found throughout the analysis period.

4.2.2 Global Climate Models

Daily maximum temperatures and daily precipitation accumulations were obtained from the Earth System Grid data portal for 12 fully coupled CMIP5 earth system mod-

Table 4.1: *Summary of CMIP5 Models Employed in this Study*

Model	Institution	Members
ACCESS1-3	Commonwealth Scientific and Industrial Research Organisation and Bureau of Meteorology, Australia	1
CanESM2	Canadian Climate Center for Climate Modelling and Analysis	5
CNRM-CM5	Centre National de Recherches Meteorologiques, Meteo-France, France	1
CSIRO-MK3-6-0	Australian Commonwealth Scientific and Industrial Research Organisation, Australia	10
EC-EARTH	Royal Netherlands Meteorological Institute, The Netherlands	2
HadCM3	Met Office Hadley Centre, UK	10
INMCM4	Institute for Numerical Mathematics, Russia	1
IPSL-CM5A-LR	Institut Pierre-Simon Laplace, France	4
MIROC5	AORI (Atmosphere and Ocean Research Institute), NIES (National Institute for Environmental Studies), JAMSTEC (Japan Agency for Marine-Earth Science and Technology), Japan	5
MIROC-ESM	AORI, NIES, JAMSTEC, Japan	1
MPI-ESM-LR	Max Planck Institute for Meteorology, Germany	3
NorESM1-M	Norwegian Climate Centre, Norway	1

els (ESMs). Each model has a varying number of ensemble members available, as indicated in Table 4.1. The same time (1984-2013) period is assessed for each model and observations. As CMIP5 historical simulations are run up to 2005, the remaining 8 years are obtained from RCP4.5 scenario runs. All calculations are carried out on the native model grids, the results are then interpolated to the EOBS grid for comparison.

4.3 Methods

4.3.1 Event Definition

We characterise long duration, dry and hot (*DH*) events by their duration D and Magnitude M . D is defined as number of consecutive days with precipitation below 1mm. Events with a duration greater than the 90th percentile of D are combined if separated by two days or less. M is then defined as the maximum daily temperature reached during an event.

A precipitation threshold of 1mm is chosen for identifying dry days to remain consistent with previous studies and remain comparable to climate models which systematically overestimate the number of drizzle days (Orlowsky and Seneviratne, 2012; Donat et al., 2013; Lehtonen et al., 2014). Applying a threshold of 0mm results in a large underestimation in the frequency dry periods and their duration in each model (not shown). The selection of a 1mm threshold to account for the drizzle day bias may be seen as a subjective choice. We therefore analysed the sensitivity of results to this choice. To do so, we select thresholds in each model based on a probability density function (pdf) mapping procedure in which a threshold is selected based on a selected percentile of daily precipitation (including zero and non-zero values) in the model. This percentile is the percentage of observed days with precipitation below 1mm at a given location. This ensures that the model will have the same number of dry days as observed. We find differences between some results and no differences for other results. We decide to use a threshold of 1mm, as it is unclear whether or not the changes seen pdf mapping procedure are coherent with the large-scale physical drivers or a statistical artefact, the latter being important issue in the context of bias correction (Maraun et al., 2017). We discuss results obtained from both methods in

the results section.

4.3.2 Estimation of Duration Return Levels

Univariate return levels (RLs) of D are estimated via application of the stationary parametric model, as defined in Chapter 3, to exceedances of a selected threshold d_{sel}^{uni} (*uni*: univariate, *sel*: selected). The default selection for d_{sel}^{uni} is the 90th percentile of D , though it is reduced if there are not at least 20 exceedances, but never below the 70th percentile. The threshold selection is carried out within each GCM separately. The RL (d) for a return period (RP) of T years is estimated as (Coles et al., 2001):

$$d = F^{-1}\left(\frac{1 - \mu_D}{T(d)}\right), \quad (4.3.1)$$

where F^{-1} is the inverse CDF of D and μ_D is the mean inter-arrival time for exceedances above the selected threshold d_{sel}^{uni} .

4.3.3 Estimation of Bivariate Return Periods

We follow the same approach here as laid out in Section 3.2.3 of Chapter 3. We fit the bivariate statistical model to joint exceedances of the selected thresholds d_{sel}^{bi} and m_{sel}^{bi} . The default selection of these thresholds is the 90th percentile of D and M respectively, and the thresholds are reduced simultaneously if there is not at least 20 events, but never below the 70th percentile. The selection of these threshold is done for each model simulation separately, and so the 90th percentile refers to that of the marginal distributions produced from each model simulation.

Bivariate RPs are estimated, via Equation 3.2.3 of Chapter 3, for joint exceedances of the respective 95th percentiles of D and M , D_{95} and M_{95} . As described in above

paragraph, the percentiles refer to that of the marginal distributions within each model simulation. The bivariate RPs, estimated in this manner, allow for comparison of the dependence between the ranks of D and M within the observations and each model run individually. This is essentially a bias correction via quantile mapping (Maraun et al., 2010). We therefore ignore biases in the marginal distributions and compare the likelihood of events having joint exceedances of D and M above their 95th percentiles in the respective observed or modelled climates.

Similarly to chapter 3, duration exceedances of the thresholds d_{sel}^{uni} and d_{sel}^{bi} are modelled using an exponential distribution, while magnitude exceedances of m_{sel}^{uni} and m_{sel}^{bi} are modelled using the generalised pareto distribution. Copulas were fitted to u_D and u_M (obtained via empirical marginal cumulative distribution function (CDF)), and selected using the Akaike Information Criterion (AIC) from the families Gaussian, t, Clayton, Gumbel, Frank, Joe, BB1, BB6, BB7, and BB8. The goodness of fit of marginals and copulas (one-tailed; $N_{boot} = 100$ for copulas) was tested using the CvM criterion with the goftest (Faraway et al., 2017), eva (Bader and Yan, 2018) and VineCopula R packages. We reject the null hypothesis that the selected distribution or copula family may not be rejected if the p-value is less than 0.05. Each model simulation has been checked, and this occurs at less than 5% of grid points for each case, which is in the acceptable range of tests that may fail by random chance (Zscheischler et al., 2017).

4.4 Results

Before any analysis was carried out, The EOBS data as well as the raw precipitation and temperature output from each model simulation has been regridded via conser-

vative remapping to a 2.5° lon-lat grid. This ensures that the grid cell averages are the same across models and observations. To remain consistent with the results in Chapter 3, all thresholds including d_{sel}^{uni} , d_{sel}^{bi} , m_{sel}^{bi} and D_{95} and M_{95} , are estimated from a reference period (*ref*: 1950-1979). Comparisons of univariate RLs and Bivariate RPs are made between those estimated in a post-reference period (*pref*: 1984-2013) for observations and models. The percentiles are also estimated according to each model separately, meaning an extreme is defined relative to the climate simulated by a given model. The results in this chapter are presented as follows: firstly a comparison is made between EOBS and the multi-model mean as well as the individual model ensemble means that the multi-model mean is calculated from. Secondly, we study individual ensemble members of all models and in more detail for a single model. This process is used for both duration RLs and bivariate RPs.

4.4.1 Representation of Long Duration Events in CMIP5 Models

The return levels (RLs) of duration (D) across Europe for an event with an average return period of 5 years, estimated via Equation 4.3.1, are presented for EOBS, the multi-model median and the ensemble median of each model in Figure 4.1. The median is preferred to the mean here as it prevents any undue weighting towards any single model simulation that may be largely different to others. The duration RL represents the duration that is expected to be exceeded on average at least once every 5 years, or 6 times in the 30 year period studied here. The spatial distribution of RLs, shown for the observations (Figure 4.1 (a)) indicate the differences in synoptic variability seen across Europe. Persistent anticyclonic conditions in the south explain the longer events expected once every 5 years while the shorter durations in more northern locations result from a higher synoptic variability between cyclonic and an-

tycliconic conditions.

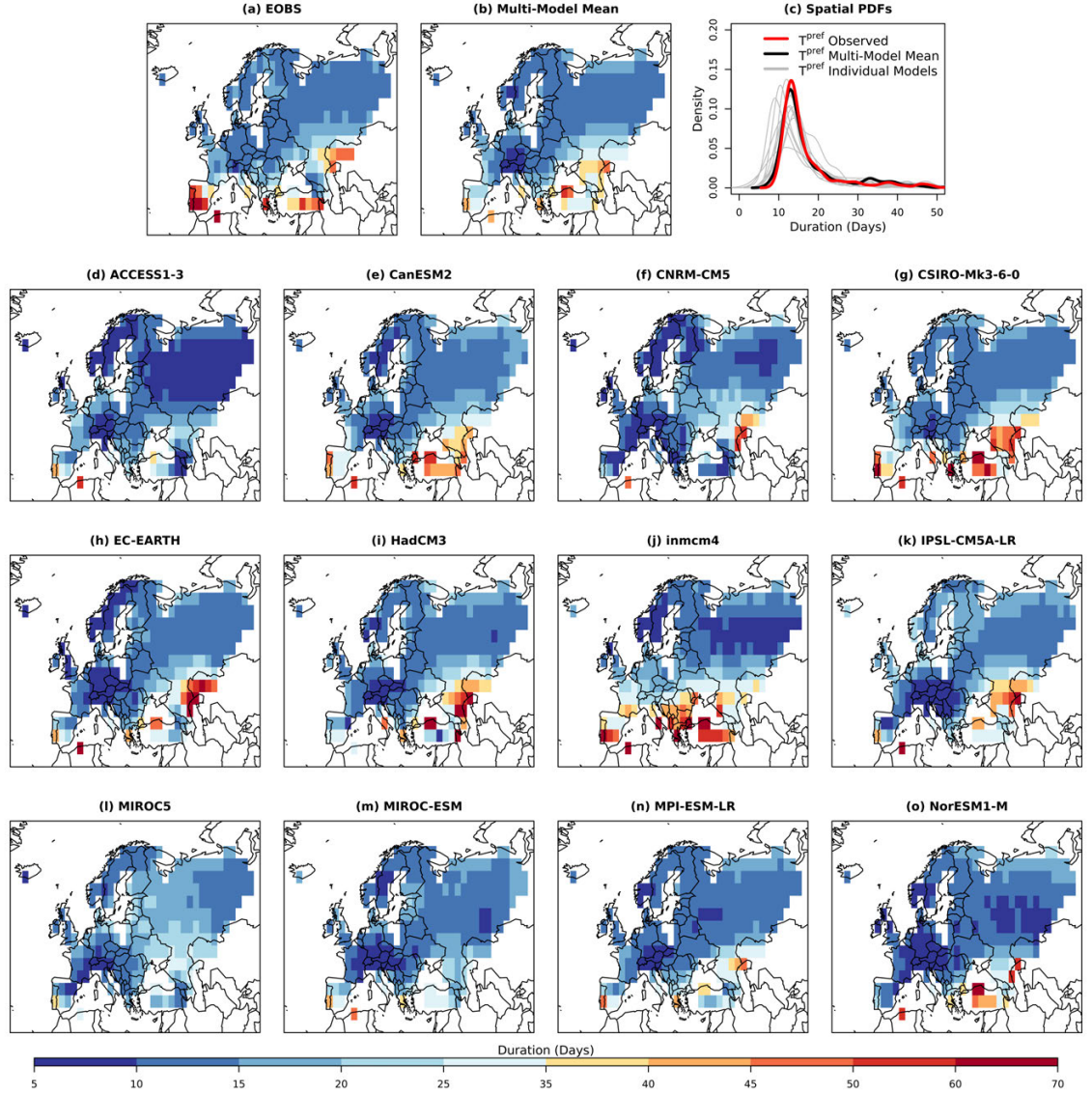


Figure 4.1: Return levels (d) of events with durations that have an expected return period of 5 years based on p_{ref} for (a) observations across Europe, (b) multi-model mean across Europe, (c) kernel density estimates of the pdf of d from all grid points across Europe for the observations (red line), the multi-model mean (black line) and the ensemble mean of each model (grey lines). Panels (d) to (o) provide the ensemble mean of each model which is labelled on each of these panels.

The multi-model median (Figure 4.1 (b)) is constructed from the individual model

ensemble medians. By doing so, we lose all information of the variability of the individual events which are averaged out in this process. However, it is useful to view as it gives us a general tendency of the models in their representation of events. Figure 4.1 (b) shows similar features to Figure 4.1 (a) in that longer duration RLs are seen in the south while shorter durations are found in the north giving the impression that the models generally capture the differences in synoptic variability between north and south. However, some notable differences can be seen in areas such as the Iberian peninsula and in Scandinavia where the Duration RLs are largely underestimated according to the Multi-model median.

The individual model ensemble medians are provided in Figure 4.1 (c) to (n). The ensemble median suffers from the same issue as the multi-model median in that differences in the frequency of events in individual simulations may be averaged out. However, as stated above it is useful to study in order to see the general tendency of each model. Some similarities and noteworthy differences can be seen between the models. In terms of similarities, models generally tend to get the differences between north and south as seen in observations. However, some models are notably better than others while others really misrepresent the spatial variability throughout Europe. Those that show best comparison with EOBS include CanESM2 (d), CSIRO-MK3-6-0 (f), EC-Earth (g), and HadCM3 (g). However, in agreement with the multi-model median, each of these models shows an underestimation of duration RLs on the Iberian peninsula. This underestimation is mirrored across each of the 12 model ensemble medians except for INCM4 (i). However this model shows large overestimations across the whole of southern Europe which might suggest that synoptic persistence is too strong over the south in the model that might compensate for errors driving the underestimation of duration RLs there in other models, although this is mere

speculation at this point and needs further investigation. Another noteworthy area is Scandinavia where only the model IPSL-CM5A-LR (i) seems to compare well with Duration RLs from EOBS. All other models tend to underestimate the RLs in the region which may be linked to problems in the representation of blocking in climate models (Scaife et al., 2010; Masato et al., 2013; Dunn-Sigouin and Son, 2013), although it is difficult to compare with these as they only assess the models in terms of their frequency of blocking events that exceed a 5 days. Quite variable results are found across Central Europe and Russia with some models comparing well and others not. The pdf mapping procedure used to select an alternative threshold that ensures the same number of "dry days" in the model as in the observations shows differing and contrasting results to those obtained using a threshold of 1mm. These results are given in the Supplementary Information section at the end of this chapter in Figure 4.7. The comparison between EOBS and the models is largely improved in Southern Europe but over much of Northern and Central Europe, the duration RLs are overestimated. It is difficult to say if these differences are due to the removal of drizzle days or due to a statistical artefact of the method. To decipher this, an additional analysis is needed to link the biases in D RLs in wither case to biases in large-scale drivers. To use the pdf mapping procedure, it necessary to ensure the differences coming from it arise in a physically consistent way, such that the duration would be linked to the persistence of anti-cyclonic systems over a given area.

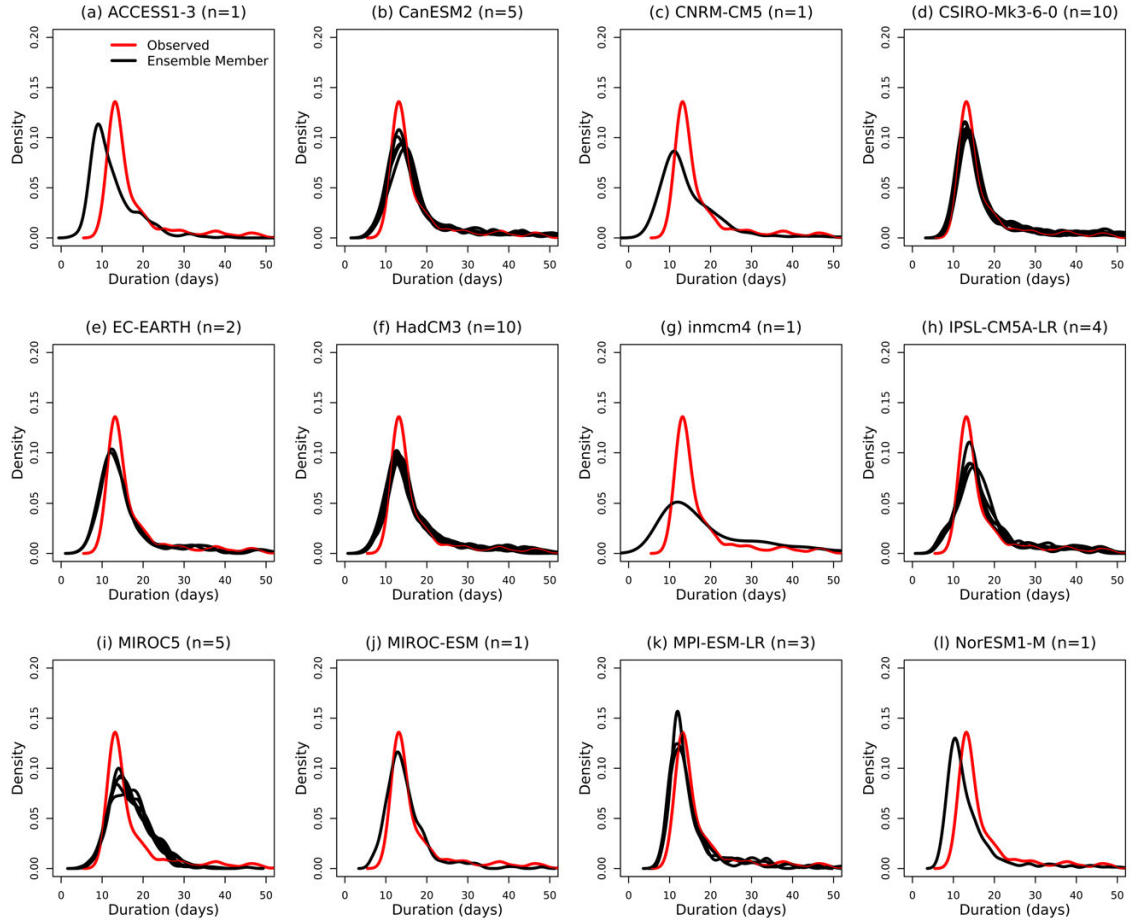


Figure 4.2: Kernel density estimates of the pdf of duration return levels from all grid points across Europe for each ensemble member within a model's ensemble. Each panel provides the ensemble members of one model represented with the black lines while EOBS is represented with a red line.

As mentioned in above paragraphs, the information gained from comparisons of the multi-model mean model ensemble means is limited as it may average out differences between individual model ensemble members and loses information of internal variability. To give an idea of the differences between individual simulations from each model, we present the duration RLs across Europe as probability density functions (pdfs) in which the area beneath the curve represents the area (or number of grid points) across the studied region with a given duration RL (Figure 4.2). The observed

pdf is also given in each panel in red for comparison. In general, the pdfs within each model ensemble are very similar to one another. Although in 5 of the cases, we only have one ensemble member. The similarities shown within ensembles with multiple members gives an indication that internal variability of these events is similar across the models, and that there is no decadal or multi-decadal oscillation that would cause events of shorter or longer durations, at least not in the models. However, this comparison for the whole of Europe will not give information on the internal variability of events regionally which is likely to be higher (Hawkins et al.).

To give an idea of the regional variability of duration RLs within a model's ensemble simulations, we present the duration RLs obtained from each member of the HadCM3 ensemble (Figure 4.3 (c) to (l)), the duration RLs estimated from EOBS (a) as well as the ensemble median (b) are provide for comparison also. Little variability is seen between each of the ensemble members which are all very similar to the ensemble median. This indicates the suitability of analysing model ensemble means of duration RLs as the similarities shown indicate a low internal variability of duration RLs in HadCM3.

The variation in D RLs between models can arise due to different individual model specifications, such as model cores, resolution and parameterisations, or due to internal variability of the climate of each model during the analysed time period. The results presented in Figures 4.2 and 4.3 indicate a low internal variability of the duration RLs. This firstly suggests that the ensemble medians presented Figure 4.1 are reflective of their ensemble members. Secondly, given that there is little difference between the estimated duration RLs within individual model ensembles, the estimated RLs are robust and are a good reflection of the RL that is expected to be exceeded every 5 years on average within the climate simulated by a given model. A poor/good

comparison with observations is thus reflective of the models ability to represent the duration of dry periods.

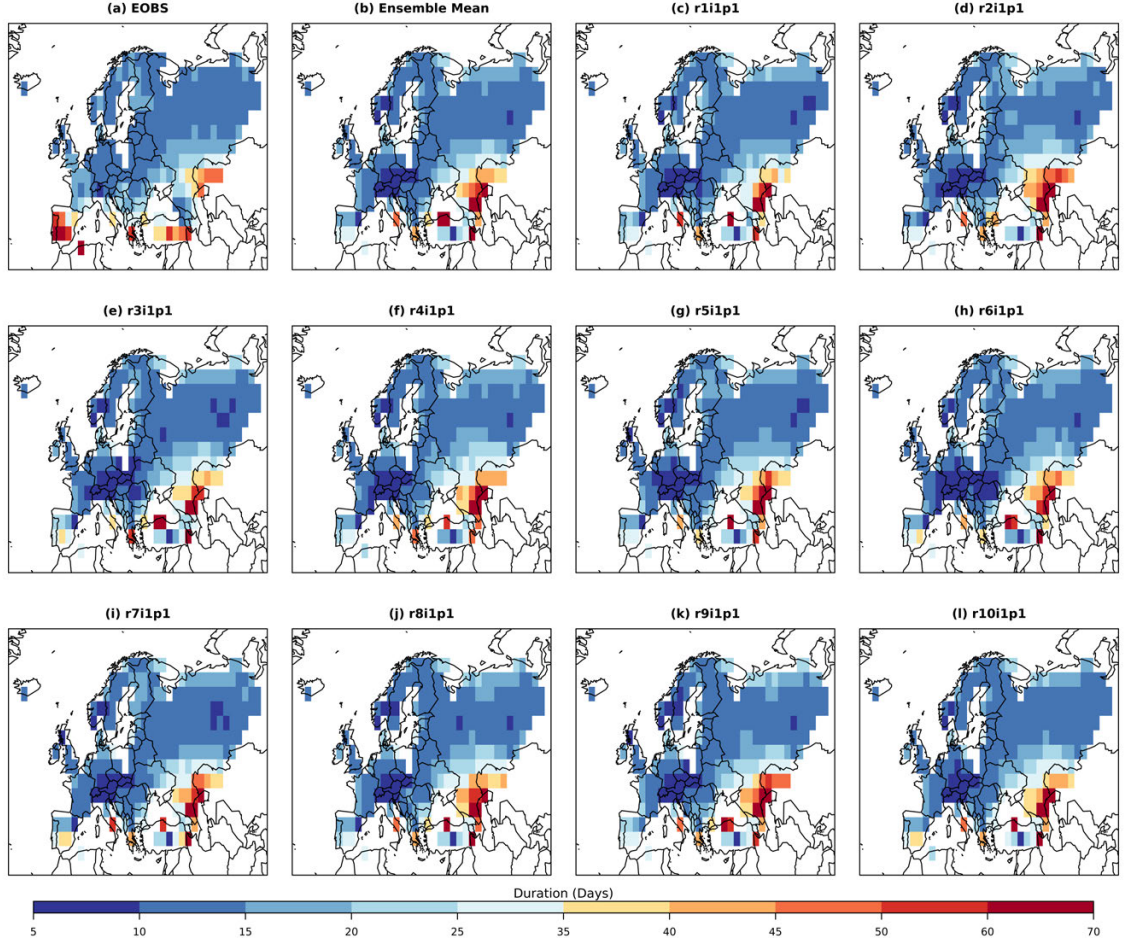


Figure 4.3: Return levels (d) of events with durations that have an expected return period of 5 years based on $pref$ for (a) EOBS, (b) the HadCM3 ensemble mean, and each of the HadCM3 ensemble members shown in (c) to (l).

4.4.2 Representation of Bivariate Return Periods in CMIP5

Bivariate RPs are estimated via Equation 3.2.3, of Chapter 3, for joint exceedances of the 95th percentiles of D (D_{95}) and M (M_{95}) for $pref$ in the observations and in each model. The 95th percentiles are estimated from ref within the observations and each

model separately, such that extremes are defined relative to the observed or modelled climates. The estimated bivariate RP therefore provides a metric with which we can compare the (D, M) rank correlation between observations and models, and more specifically, the probability of D and M jointly exceeding D_{95} and M_{95} respectively.

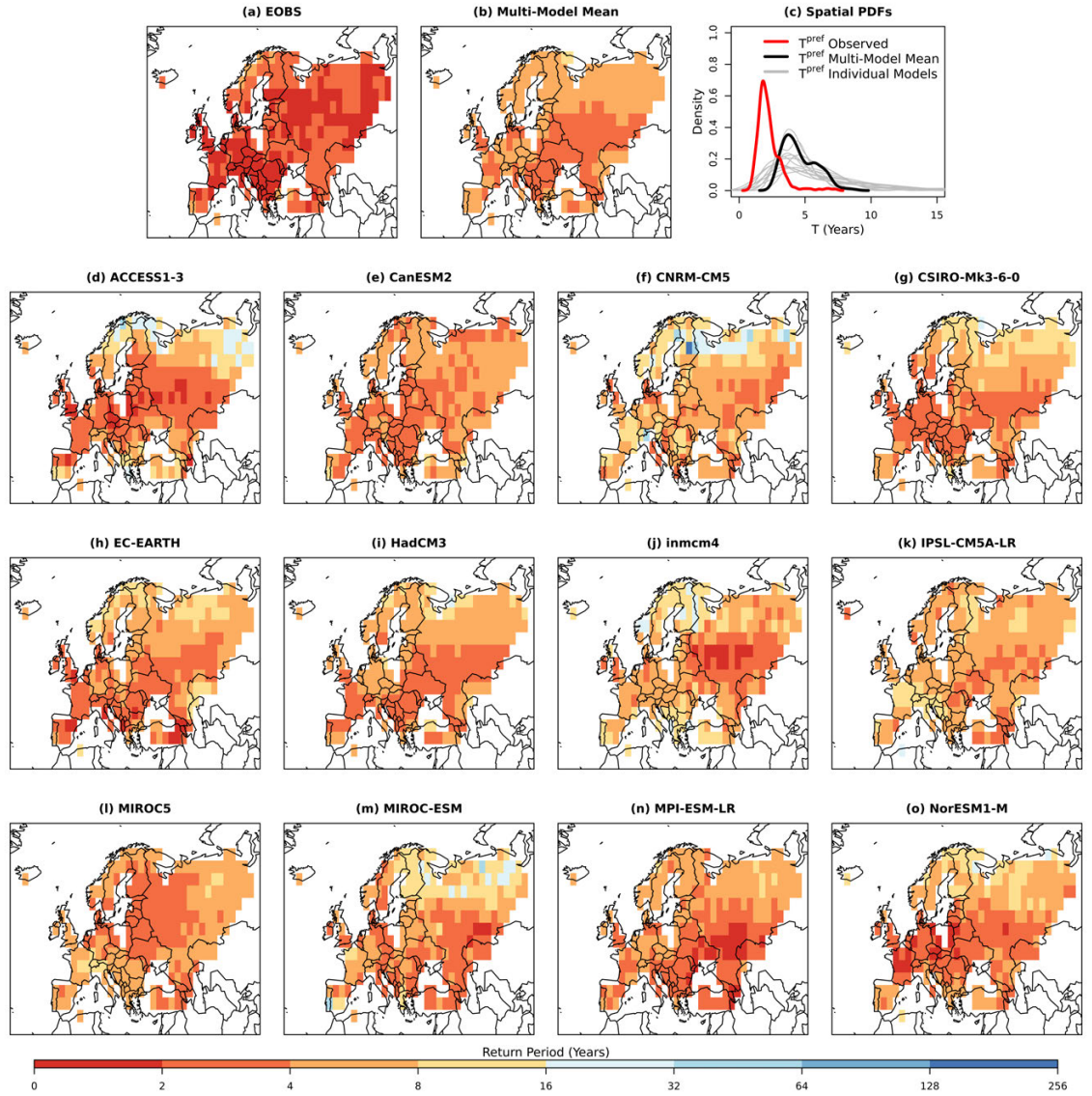


Figure 4.4: Bivariate return periods ($T(D_{95}, M_{95})$) of events from $pref$ for (a) the observations across Europe, (b) the multi-model mean across Europe, (c) kernel density estimates of the pdf of $T(D_{95}, M_{95})$ from all grid points across Europe for the observations (red line), the multi-model mean (black line) and all ensemble means for each model (grey lines). Panels (d) to (o) provide the ensemble mean of each model which is labelled on each of these panels.

Figure 4.4 (a) provides the bivariate RPs ($T(D_{95}, M_{95})$) estimated from EOBS. The multi-model mean of $T(D_{95}, M_{95})$ is calculated from each individual models' ensemble mean, that are in turn calculated from $T(D_{95}, M_{95})$ estimated from each ensemble

member for the given model. The observed $T(D_{95}, M_{95})$ is generally homogeneous throughout Europe but with lowest RPs found in South-east and Central Europe and higher RPs found in Southern Europe such as the Iberian peninsula. A similar homogeneous spatial distribution is also found in the multi-model mean (Figure 4.4). However, the RPs are generally over-estimated throughout Europe. This indicates a weaker rank correlation between D and M in the models than found in the observations leading to fewer joint exceedances of D_{95} and M_{95} . The kernel densities in Figure 4.4 (c) show the distribution of $T(D_{95}, M_{95})$ across Europe for observations, the multi-model median and each individual model's ensemble median. Comparing the distributions of $T(D_{95}, M_{95})$ estimated from observations (red line) highlights the large overestimation of bivariate RPs in each model, and thus underestimation in the probability of long duration dry and hot events. In fact no model is able to reproduce a similar pdf as found for EOBS.

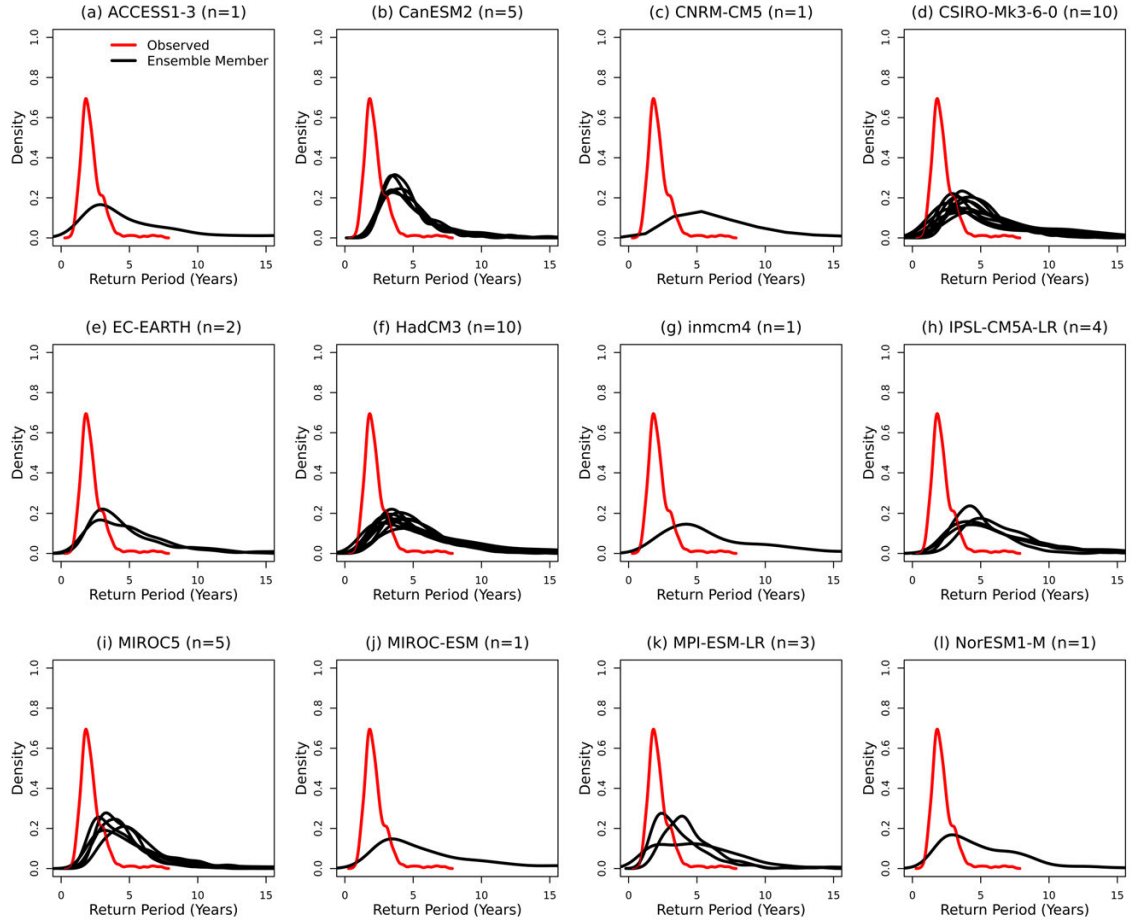


Figure 4.5: Kernel density estimates of the pdf of bivariate return periods ($T(D_{95}, M_{95})$) from all grid points across Europe for each ensemble member within a model's ensemble. Each panel provides the ensemble members of one model represented with the black lines while EOBS is represented with a red line.

The spatial distribution of $T(D_{95}, M_{95})$ across Europe is shown for each model ensemble mean in Figure 4.4 (d) to (o). Although the models can generally capture the homogeneous nature of $T(D_{95}, M_{95})$ as seen in EOBS across, it does vary between the models and $T(D_{95}, M_{95})$ is quite patchy in some models. To provide an idea of how $T(D_{95}, M_{95})$ varies for each ensemble member, the PDFs obtained from $T(D_{95}, M_{95})$ across Europe in each individual model ensemble member are provided in Figure 4.5. Large differences are seen between the individual ensemble members of each model

which can largely vary in the peak of the PDF, while no model exhibits an ensemble member that is comparable to EOBs. To give further insight into the spread within a given model's ensemble, the spatial distribution of $T(D_{95}, M_{95})$ is plotted for each of the HadCM3 ensemble members. Within this ensemble, a large differences are seen in the spatial distribution of $T(D_{95}, M_{95})$, in particular where the lowest values occur. The large variability seen within model ensembles shows that a robust estimation of $T(D_{95}, M_{95})$ cannot be obtained for any models, and thus indicates that events that are represented by $T(D_{95}, M_{95})$ are subject to a large random variability. However, the one common feature between all models is their overestimation of $T(D_{95}, M_{95})$ suggesting that there is a systematic failure in climate models to represent long-duration dry and hot events.

Results for $T(D_{95}, M_{95})$ from the approach using a threshold obtained from a pdf mapping procedure are also provided in the Supplementary Information section at the end of this chapter in Figure 4.8. Unlike the results obtained for D RLs however, there is little or no difference for $T(D_{95}, M_{95})$ obtained using the pdf mapping procedure and using a threshold of 1mm. Thus, even with increases to D RLs shown in 4.7, no improvement can be found for $T(D_{95}, M_{95})$, such that the poor representation of these events cannot be attributed to the threshold used to define dry days.

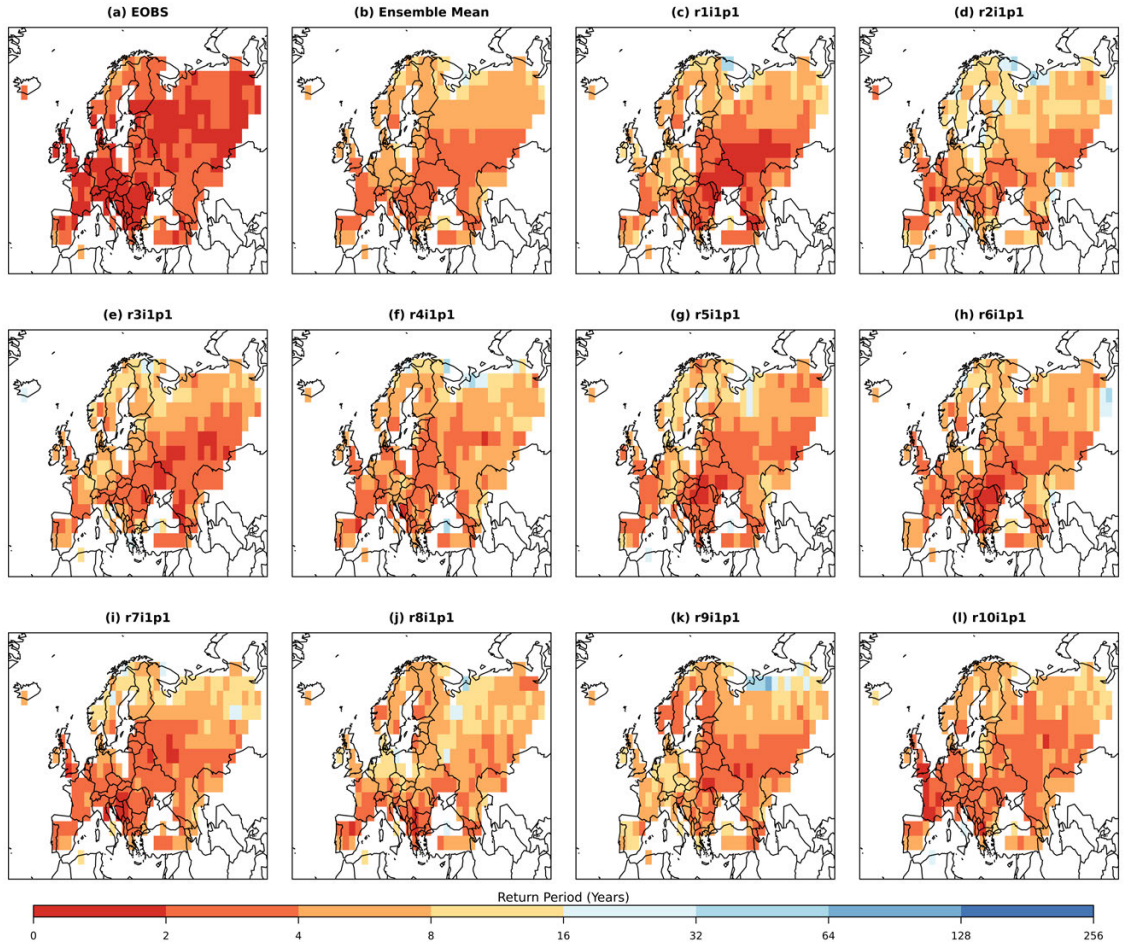


Figure 4.6: Return levels (d) of events with durations that have an expected return period of 5 years based on pr_{ef} for (a) EOBS, (b) the HadCM3 ensemble mean, and each of the HadCM3 ensemble members shown in (c) to (l).

4.5 Summary and Conclusions

Within this chapter, we have studied the representation of long duration, dry and hot (DH) events in a selection of CMIP5 models. We have compared characteristics of these events in terms of their spatial extent, their duration (D) and the joint occurrence of extremes in their duration and magnitude (M). We compared the duration return levels (RLs) of events that correspond to a five year return period. We see

mixed results across the 12 models assessed here. An analysis of the spread between ensemble members of the individual models found little variability of D RLs within model ensembles. This indicates that we obtain a robust estimation of the RLs within each ensemble such that we are confident the resulting values are not a result of random internal variability in a given model simulation. It thus tell us that a comparison between the RLs in the models with EOBS will provide information of the ability of models to represent the duration of dry periods.

We found varying skill between models. Some compare well with observations while others show underestimations of duration and others overestimate the duration in particular areas. In particular we found that many models underestimate duration in Scandanavia, Northern Russia and the Iberiran peninsula. The findings in northern parts of Europe tie in well with assessing the persistence of blocking in CMIP5 models during summer (Scaife et al., 2010; Masato et al., 2013; Dunn-Sigouin and Son, 2013) who each found that the models underestimate the frequency of blocking events that exceed 5 days.

It should be noted that these results are obtained when defining a dry day in the model when daily precipitation is less than 1mm. Climate models have a known drizzle day issue that leads to an overestimation of wet day frequency which may contribute to the model's perceived performance above. To test whether the results are sensitive to this threshold, we estimated duration RLs using a threshold to define a dry day that is obtained via pdf mapping. This ensures that we have the same number of dry days in the model as in the observations at each grid point. We found contrasting results in that the duration RLs were overestimated in many cases in comparison to EOBS, indicating that the results are sensitive to the threshold such that the results obtained are uncertain. It is worth noting however that the results do align with

findings from previous studies, as outlined above. Furthermore, it is possible that the results obtained from the pdf mapping approach are a statistical artefact. It is therefore important that these results are checked along with the representation of large-scale processes, such as persistent anti-cyclonic conditions, in order to give more confidence to results. Otherwise, it is difficult to draw strong conclusions of the representation of the duration of dry periods in climate models.

Finally, we compare Bivariate RPs for events in which both D and M exceed their 95th percentiles. The bivariate RPs are estimated with respect to the distributions of D and M obtained from the observations and each model simulation separately. This is essentially a bias correction via quantile mapping and thus we focus on the dependence between the ranks of the variables rather than their absolute values. We find an underestimation in bivariate RPs across Europe in all models. This means that the probability of M exceeding its 95th percentile is underestimated when D has exceeded its 95th percentile is lower in the models than observed.

The poor comparison with $T(D_{95}, M_{95})$ indicates that the rank correlation of D and M is quite varied between models, and more specifically that the tail dependence between D and M is generally not captured. For models that overestimate $T(D_{95}, M_{95})$, the probability of M exceeding M_{95} when D is greater than D_{95} is underestimated. Therefore, by default, the probability for M exceeding M_{95} during events with lower durations than D_{95} is overestimated. The drivers of this systematic failure in representing this dependence is manifold. It may arise through incorrect specification of the marginal variables, their dependence, or indeed a combination of each. In terms of duration, if models cannot reproduce long-duration events, then the influence of the persistence of dry conditions on temperature will simply not be present in the model. Thus the dependence between ranks will be quite random and each event will be of

a low duration. If D is adequately represented by a model, then their dependence is likely misrepresented. It is of course plausible for extreme temperatures to occur during short duration events. However, if the probability of temperature extremes is too high during shorter events, it indicates that the influence of long duration dry periods on temperature extremes in climate models is not as relevant as found for observed temperature extremes. This can signify that a certain driver of temperature extremes has a larger contribution to extreme temperatures in the models than seen in reality. One such possibility is soil moisture, which generally dries out too quickly in climate models (Vautard et al., 2018), resulting in stronger land-atmosphere feedbacks than observed and the over-amplification of temperature extremes as well as the overestimation of temperature variability (Fischer et al., 2012b).

The sensitivity of the $T(D_{95}, M_{95})$ results to choice of threshold used to define a dry day were also checked using a threshold obtained via the pdf mapping procedure. Unlike duration RLs however, these results were found to be insensitive and little or no change was found for $T(D_{95}, M_{95})$ using either threshold. This highlights that the underestimation in $T(D_{95}, M_{95})$ cannot be attributed to the choice of threshold and is likely a result of a systematic bias within the models.

The relevance of these results mainly pertain to the representation of drivers of soil moisture drought. The results point to systematic failure within the set of climate models studied here to reproduce the observed dependence between D and M , and to represent long-duration dry periods that co-occur with extreme temperatures. As a result, models are thus missing the influence of these events on soil moisture, and their role in the propagation of meteorological drought conditions into soil moisture drought. This may limit our confidence in the portrayal of soil moisture drought in a present and future climate. Current studies using climate model projections point

to an increase in background aridity accompanied by a decrease in soil moisture in the future (Zhao and Dai, 2015a; Hoerling et al., 2012; Burke, 2011), while Berg et al. (2017) show a gradient in changes in soil moisture where the top layer of soil moisture changes are much greater than those at lower layers. Although they point out that assessing top layers alone will overestimate the impact of such changes to vegetation, as moisture availability will still be high at lower levels, the decrease in surface layers may remove a buffering effect on the lower layers leaving them more exposed to meteorological drought and temperature extremes. This may lead to a quicker onset of soil moisture drought and more extreme deficits in the future, as hypothesised by (Trenberth et al., 2014), and more importantly a higher exposure of vegetation to drought and lower moisture availability.

More work is needed to diagnose the exact reasoning behind the poor performance of climate models in their representation of long-duration dry, and hot events. On top of this, further investigation is needed to extract the importance of such events in climate models, i.e. do models that better represent long duration *DH* events show different soil moisture drought characteristics to those that show poor performance. This would be quite informative for studies such as (Samaniego et al., 2018) in terms of the confidence we can put in the projections of soil moisture drought events. Without such knowledge, our confidence is limited, while it is also possible that the projections underestimate future changes if the meteorological extreme events are not adequately represented.

4.6 Supplementary Information

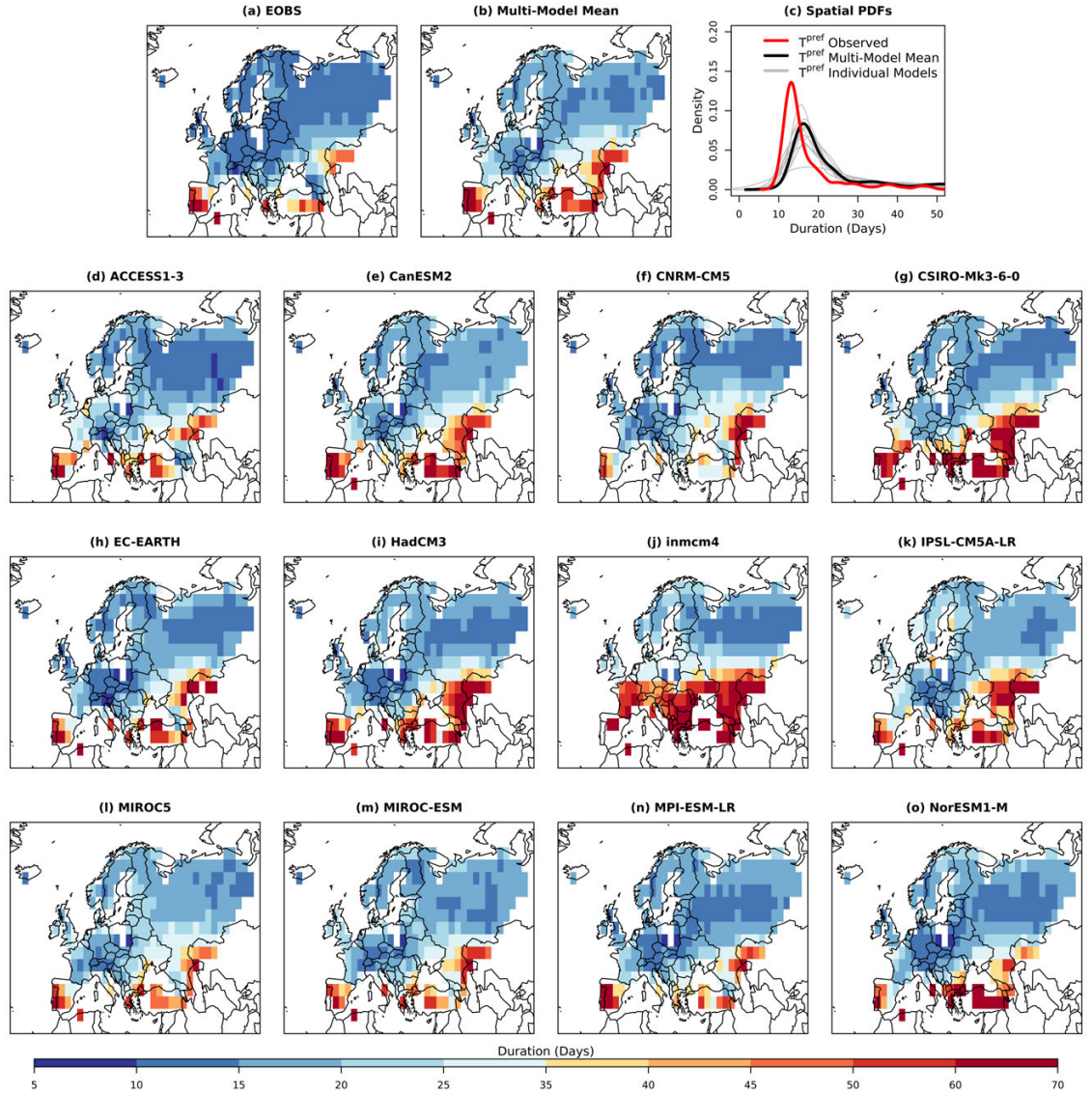


Figure 4.7: Return levels (d) of events with durations that have an expected return period of 5 years based on pref , obtained using pdf mapped threshold to define dry days, for (a) observations across Europe, (b) multi-model mean across Europe, (c) kernel density estimates of the pdf of d from all grid points across Europe for the observations (red line), the multi-model mean (black line) and the ensemble mean of each model (grey lines). Panels (d) to (o) provide the ensemble mean of each model which is labelled on each of these panels.

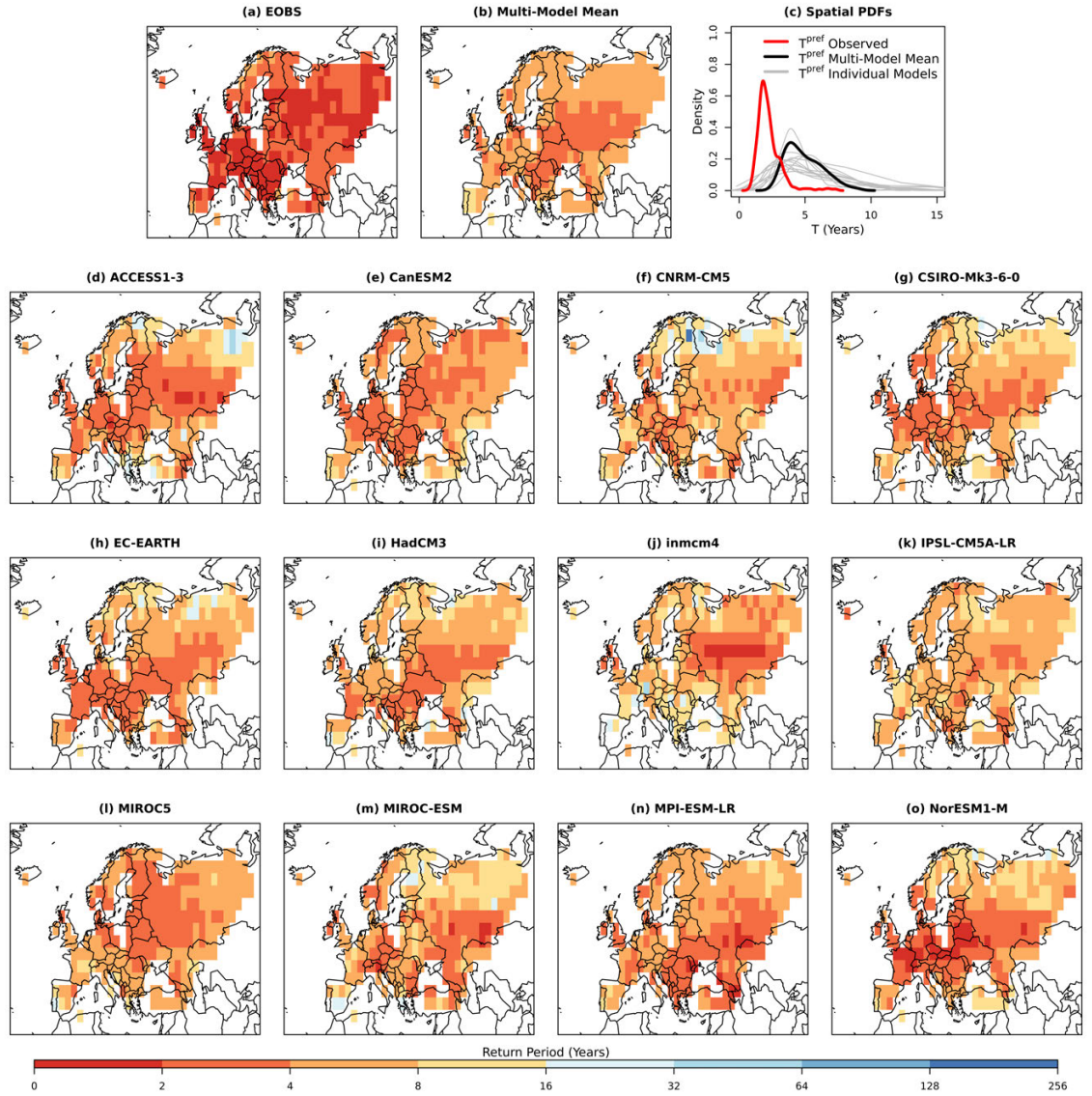


Figure 4.8: Bivariate return periods ($T(D_{95}, M_{95})$) of events from $pref$, obtained using pdf mapped threshold to define dry days, for (a) the observations across Europe, (b) the multi-model mean across Europe, (c) kernel density estimates of the pdf of $T(D_{95}, M_{95})$ from all grid points across Europe for the observations (red line), the multi-model mean (black line) and all ensemble means for each model (grey lines). Panels (d) to (o) provide the ensemble mean of each model which is labelled on each of these panels.

Chapter 5

Synthesis

5.1 Summary and Discussion

The main aim of this thesis is to increase our understanding of the meteorological hazards, namely meteorological drought and extremely high temperatures, that influence soil moisture drought, particularly in terms of their contributions to soil moisture over varying time-scales and the co-occurrence of their extremes. To do so, frameworks has been developed to firstly disentangle the influence of the meteorological hazards on soil moisture over varying time-scales, and secondly to characterise long-duration meteorological droughts that coincide with extremely high temperatures as well as quantify their probability.

The objectives, as laid out in Chapter 1, are to: (1) develop a framework that will provide a method to disentangle the influence of the meteorological hazards on soil moisture on varying time-scales and assess the contributions of precipitation and potential evapotranspiration (PET) to soil moisture drought at a local scale in wet, transitional and dry climates over various time-scales, (2) develop a framework to characterise and quantify the probability of compound long-duration dry and hot events, and assess changes in their probability over the historical period throughout Europe (3) assess the representation of compound long-duration, dry and hot events in Europe within CMIP5 global climate models (GCMs). In this section, with respect to these three objectives, I summarise the main findings and their implications.

In Chapter 2, we analysed the contribution of precipitation and potential evapotranspiration (PET) to soil moisture drought in wet, transitional and dry climates in Europe. Sparse soil moisture data networks make soil moisture a difficult phenomenon to investigate empirically, while an explicit representation via land surface models is challenging. Drought indices that incorporate precipitation and temperature via PET are therefore often employed as a proxy for soil moisture in studies that

assess the response of soil moisture drought to climate change.

The results presented in Chapter 2 show that precipitation holds the main control over soil moisture drought at all sites while PET contributed to the onset, severity and persistence of soil moisture drought at sites in wet climates. At sites in dry climates, PET shows little or no contribution and does not improve the estimation of soil moisture drought during summer. This is most likely explained by the lack of moisture available for actual evapotranspiration (ET) to take place.

The contributions of PET to the onset and persistence of soil moisture drought is highlighted when integrated over short and long time scales respectively. The short-term integration, that contributes to the onset, captures the influence of daily temperature extremes on the drying soil moisture, which are filtered out in a long-term integration. The long-term integration, which contributes to the persistence, holds information of the intensity of drying within its considered time-period that soil moisture holds memory of, this is lost when using a short-term integration. The differences between these short- and long-term integrations of PET may become relevant in the analysis of changes in the onset of soil moisture drought events when using drought indices. A warmer climate may cause droughts to set in quicker (Trenberth et al., 2014) and lead to flash droughts (Mo and Lettenmaier, 2016). Such quick drying may be hidden through the use of longer integration periods of PET in an index such as the Standardised Precipitation Evapotranspiration Index (SPEI), or through a recursive model used for the Palmer Drought Severity Index (PDSI) that retains memory of PDSI values from previous time steps.

Although drought indices were not specifically designed to represent soil moisture (Seneviratne et al., 2010), they do provide a convenient means of combining precipitation and PET into a kind of impact function that may be implicitly linked to soil

moisture. However, soil moisture drought is not a simple phenomenon to characterise with drought indices alone; the assumed relationships are over-simplified and may not hold in a future climate. It is thus difficult to extract tangible information of future soil moisture drought changes from drought indices, and any analysis incorporating them requires careful interpretation. With differing contributions of the meteorological variables over varying time scale, it is important to complement analyses of changes in drought indices with an analysis of changes in the meteorological variables over the relevant time scales, as well as with results from studies assessing changes in land surface models. Although there are issues in constraining these models due to a lack of observations, they may provide more reliable estimates when incorporated into coupled climate models (Berg et al., 2017). Furthermore, combining results from each approach may yield better knowledge of our confidence in projected changes of soil moisture in different regions.

In Chapter 3, we develop a framework to characterise long-duration, dry and hot events in Europe and quantify their probability. Using this framework, we estimate changes in this probability in Europe over the period 1950-2013. These events are termed *DH* events, and we characterise them by their Duration (*D*) and Magnitude (*M*). *D* is defined as the consecutive number of days where precipitation is below 1mm and we combine long duration events separated by two days or less. *M* is defined as the maximum daily temperature during an event. These are events in which we are most likely to see the largest reductions in soil moisture as a result of a lack of precipitation and high levels of ET due to extreme temperatures. Changes in their joint probability have direct implications for soil moisture drought.

We find an increase in the probability of *DH* events over much of Europe between a reference (*ref*: 1950-1979) and post-reference (*pref*: 1984-2013) period. The main

driver of this change in probability is increasing temperatures throughout Europe. Little change is seen in the duration of events, leading us to conclude that long-duration events have mostly become warmer during *pref* rather than longer. An exception to this is found in Southeast Europe in the Balkan region where events appear to have increased in temperature and duration. The strongest increase in probability of long duration dry and hot events over Europe is also found in here. This may be particularly eye-catching given the reliance of economies on agriculture there, which has a share of between 20 to 50% of employment in countries in this region (Volk, 2010). The implications of the increased probability of *DH* events found here mainly pertain to the acceleration of drought propagation from meteorological drought to soil moisture drought. The results complement other findings with respect to the relationship between drought and climate change. For example, soil moisture drought events are expected to set in quicker and become more severe (Trenberth et al., 2014; Samaniego et al., 2018), owing to increases in evaporation during dry periods (Dai et al., 2004) that are driven by rising temperatures (Scheff and Frierson, 2014; Zhao and Dai, 2015b). Furthermore, given the weak historical trends found in global land precipitation (New et al., 2001; Lambert et al., 2004; Ren et al., 2013; Adler et al., 2017), the dominant temperature signal behind the increased probability of *DH* events may also largely explain changes in global drought conditions, as shown in Marvel et al. (2019), which closely resemble changes in global mean temperature (e.g. Pachauri et al. (2014)). The results may also have implications for the persistence of soil moisture drought conditions. High amounts of precipitation are required for recovery from large moisture deficits induced by intense drying (Seneviratne et al., 2012a; Manning et al., 2018) while general increases in evaporation can push environments towards a climatically drier state (Samaniego et al., 2018). These results are in line with other

observational analyses (Dai et al., 2004; Trenberth et al., 2014; Scheff and Frierson, 2014; Zhao and Dai, 2015b) and add strength to results obtained from an analysis of land-surface models by Samaniego et al. (2018), who forewarn of longer-lasting and more severe soil moisture droughts in a future warmer climate.

Besides soil moisture drought, the occurrence of long-duration *DH* events can lead to severe impacts in many parts of society and has in the past led to large economic losses in agriculture (Sepulcre-Canto et al., 2012; Zurovec et al., 2015; van der Velde et al., 2012; Howitt et al., 2014) and subsequent losses of employment (Howitt et al., 2014). They have also contributed to events that have had large excesses in losses of life from the combinations of drought, extreme temperatures and wildfires (Shaposhnikov et al., 2014; Fouillet et al., 2006). Furthermore the occurrence of such events can influence the water supply for use in hydro-power production and public water supply, albeit the former is more related to longer variations in precipitation and reservoirs but the latter is more related to short-term anomalies (Stagge et al., 2015), as was seen in the recent 2018 event in much of Northern Europe. Thus the results of these findings have implications for various sectors including agriculture, health, energy and public water supply highlighting the need for more research in quantifying the risk of such sectors to long-duration *DH* events.

Meteorological droughts that co-occur with extremely high temperatures can bring large impacts to the affected regions, the recent 2018 summer drought and heat wave in Europe is a prime example. Quantifying the probability of these events can give us an idea of the regions which are most likely to suffer from such events. However, extreme events are rare by definition and return period estimations of such rare events can be sensitive to the occurrence of a single event. Such estimations are thus surrounded by large uncertainty intervals. Meteorological drought events are partic-

ularly subject to large uncertainties. Their long temporal persistence means there is automatically fewer events than other phenomena that vary over daily time-scales. A thirty-year period that is generally accepted as long enough to sample the distributions of variables such as precipitation or temperature may not be sufficient when estimating the probability of meteorological drought extremes. For example, high return periods of long-duration, dry and hot events were obtained in much of Northern Europe for the period 1984-2013. This might lead us to believe that we would not expect to see an event such as that in the summer of 2018. It is therefore highly important that we develop approaches to better quantify the probability of these events.

In Chapter 4 I assess the ability of a selection of CMIP5 models to represent *DH* events. We compared duration (D) return levels (RLs) corresponding to a return period (RP) of 5 years, and bivariate RPs for events in which both D and M of the event exceed their 95th percentiles. We found varying skill between models. Some compare well with observations while others show underestimations of duration and others overestimate the duration in particular areas. In particular we found that many models underestimate duration in Scandinavia, Northern Russia and the Iberian peninsula. The findings in northern parts of Europe tie in well with assessing the persistence of blocking in CMIP5 models during summer (Scaife et al., 2010; Masato et al., 2013; Dunn-Sigouin and Son, 2013) who each found that the models underestimate the frequency of blocking events that exceed 5 days.

A clear overestimation is found in the representation of bivariate RPs, meaning that combined extremes of D and M do not occur as frequently in the models as in the observations. It should be noted that bivariate RPs were estimated for exceedances of the 95th percentiles of D and M respectively. These percentiles were estimated within each model run separately. By doing so, we define extremes with respect to

the model climate and ignore model biases in the marginal distributions by focussing on the rank correlation of D and M . The underestimation in bivariate RPs highlights an underestimation in the dependence between extremes of D and M in the models. More specifically, it shows that models generally underestimate the probability of M exceeding its 95th percentile when D has also exceeded its 95th percentile. By default, this means that the probability of M exceeding its 95th during shorter duration events is too high.

The validation of extreme events in models requires not only that a given variable's distribution is well represented, but also that occurrences in its extremes occur for the right reasons (Trenberth and Fasullo, 2012). It is of course plausible for extreme temperatures to occur during short duration events. However, if the probability of temperature extremes is too high during shorter events, it would seem that long duration dry periods are not required for temperatures to reach high levels. This can signify that a certain driver of temperature extremes has a larger contribution to extreme temperatures in the models than seen in the reality. One such possibility is soil moisture, which generally dries out too quickly in climate models (Vautard et al., 2018), resulting in stronger land-atmosphere feedbacks than observed and the over-amplification of temperature extremes as well as the overestimation of temperature variability (Fischer et al., 2012b). If the contribution of land-atmosphere interactions to temperatures is far too high in the models, then questions may arise over the representation of the climate change signal in temperature extremes in climate models. This would have implications for attribution studies if extremes are not represented for the correct reasons (Trenberth and Fasullo, 2012). Our results do not fully answer this question, but do highlight the need for more in depth analysis of the representation of drivers of extremes in climate models.

Climate models project soil moisture to decrease in the future (Burke, 2011; Hoerling et al., 2012; Zhao and Dai, 2015a; Berg et al., 2017), with larger reductions in the upper layers than lower layers (Berg et al., 2017). The reduced upper layer may leave lower layers more exposed to ET (Teuling et al., 2013) and thus more vulnerable to large reductions in soil moisture during meteorological drought events. Samaniego et al. (2018) project soil moisture drought events to be longer and more severe in a future warmer climate, however, if the meteorological drivers of extreme events are not adequately represented in models, its possible that this result is arising for the wrong reasons or indeed it may be that their projections actually underestimate the risk of soil moisture drought in the future, particularly if the increased probability found in chapter 3 is to continue into the future. More research will be required to extract the importance of such events in climate models, i.e. do models that better represent long duration *DH* events show different soil moisture drought characteristics to those that show poor performance. Without such knowledge, our confidence in such projections is limited, and we will not fully their uncertainties.

5.1.1 Limitations of Findings

The findings presented within this thesis are not without uncertainty and have their limitations. For example, in Chapter 2 we have studied the contribution of precipitation and PET to soil moisture defined as the column integral over 3 layers within the top 30cm. However ET and therefore PET may have contributions to soil moisture at lower depths. For instance, Teuling et al. (2013) showed the contribution of ET to a depth of 1.5 metres during the 1976 drought event, whereby upper layers are firstly depleted followed by the propagation of drought into lower layers of soil as the drought persisted. Thus, our conclusion that PET has little contribution to soil mois-

ture drought at dry sites is limited to the upper layer of soil. However, sites within dry climates still exhibit moisture limiting ET regimes during summer (Stegehuis et al., 2012; Schwingshackl et al., 2017) and so PET is still likely to largely overestimate ET in such climates, and thus have a limited contribution to soil moisture at lower soil layers also.

In chapter 3, we employed the EOBS dataset to study long-duration, dry and hot events. EOBS is the state-of-the-art gridded dataset for Europe and is produced through the interpolation of station observations whose spatial density can be too low for adequate representation of extremes (Haylock et al., 2008; Herrera et al., 2018). This was particularly found by (Herrera et al., 2018) who investigated the influence of the underlying station density on grid point estimates of precipitation, finding that there is a need to have at least six stations for a reliable grid estimate. However, its worth noting that these results were obtained for precipitation extremes which will exhibit a much higher spatial variability than dry periods and temperature extremes that are driven by large-scale anticyclonic systems which will produce smoother fields. As such we expect EOBS to be reliable dataset for the study of long-duration *DH* events. This is evidenced in chapter 3 by 3.1 to 3.5 that indicate the ability of EOBS dataset in representing important extreme events. Nonetheless, it would be interesting to investigate the influence of interpolation and the spatial density of stations on the representation of characteristics of *DH* events in gridded products. This would provide important information for climate model validation studies that incorporate EOBS and other gridded datasets.

Climate models typically overestimate the number of wet days leading to the use of a 1mm threshold for defining dry days (Orlowsky and Seneviratne, 2012; Donat et al., 2013; Sillmann et al., 2013; Lehtonen et al., 2014). Alternatively one could use a pdf

mapping procedure to adjust the number of dry days to that of the observed time series (i.e. days below 1mm in EOBS). Both of these approaches were employed to define dry days from which to estimate duration return levels and differing results were found between them. It is difficult to say which is a better approach. On one hand, the 1mm threshold may include too many wet days due to the drizzle day bias in climate models, but on the other the pdf mapping procedure can produce a statistical artefact if it is not physically consistent with the large-scale drivers of long-duration dry periods (Maraun et al., 2017). For this reason, drawing strong conclusions from this analysis is difficult and to do so will require an additional analysis of variables representing the large-scale flow such that the representation of duration in climate models may be linked to the representation of the large-scale conditions, such as persistent anti-cyclones.

5.2 Outlook

It is argued that future soil moisture drought projections should be based directly on climate model simulations rather than on off-line metrics such as drought indices (Roderick et al., 2015; Milly and Dunne, 2016; Swann et al., 2016; Berg et al., 2017). Although the diversity of model soil schemes and vegetation parameterisations play a role in creating the large spread between model projections of soil moisture drought, the inter-model differences are largely explained by differences in climate model projections of variables such as precipitation and ET (Orlowsky and Seneviratne, 2013; Berg et al., 2017). Besides the limitations arising from land-surface models due to a lack of observational constraints, our confidence in future projections of drought risk is ultimately limited by the representation of contributing meteorological variables, such as *DH* event characteristics, and their large-scale drivers in climate models.

A logical next step would be to study the large-scale drivers of *DH* events in terms of their individual contributions as well as the relevance of their interactions for the occurrence of *DH* events. Such knowledge would shed light on the relative importance of drivers and what their future changes may hold for *DH* events (Shaw and Voigt, 2015; Coumou et al., 2018). Over recent years, much knowledge has been gained of the large-scale drivers behind *DH* events. For example, studies have indicated the role of land-atmosphere interactions in amplifying extreme temperatures and prolonging events (Seneviratne et al., 2006; Coumou et al., 2018). Others have identified the role of teleconnections triggered by sea surface temperature (SST) anomalies in the tropical Atlantic and Northern Indian Ocean that generate Rossby wave trains that lead to persistent dry and hot extremes over Europe (Cassou et al., 2005; Trenberth and Fasullo, 2012). Also the role of Arctic Amplification (the larger temperature increases in the Arctic relative to the whole northern hemisphere) in reducing zonal winds and amplifying Rossby waves has been unravelled in a number of recent studies (Francis and Vavrus, 2012; Petoukhov et al., 2013; Coumou et al., 2015; Petoukhov et al., 2016; Coumou et al., 2018).

Alongside the evaluation of *DH* event characteristics and their dependence in climate models, a process-based validation of climate models in terms of the large-scale drivers of *DH* events is required. This is required in terms of their link to *DH* event characteristics (Trenberth and Fasullo, 2012), their interactions with other drivers (Zscheischler et al., 2018) as well as the drivers relationship with climate change (Coumou et al., 2018). Misrepresentation of the above dependencies can result in the misrepresentation of the future risk posed by *DH* events. Through such a validation, we may identify reasons for model biases that may arise due to incorrect representation of drivers, or improvements that may be obtained from higher resolution simulations (Scaife et al.,

2011). Ultimately, limitations found in models will feedback into their improvement. Such validations may allow one to identify suitable climate models to provide long simulations or large ensembles for a given forcing, from which we may increase the sample size of events and reduce sampling uncertainties for estimates of event statistics, such as their return periods. We may therefore obtain better estimates of the potential risk posed by extreme DH in a current and future climate.

It is also important that the climate change signal in contributing factors is reliably represented. Such examples include Arctic Amplification (Francis and Vavrus, 2012; Petoukhov et al., 2013; Coumou et al., 2015; Petoukhov et al., 2016; Coumou et al., 2018) as well as dependencies between variables such D and M as highlighted in Chapters 3 and 4. For instance if soil in GCMs dries out too quickly the observed dependence between long-duration events and high temperatures may be misrepresented. If soil is already dry, the observed influence of long-duration dry periods on extreme temperatures may be filtered out due to the amplification of temperatures by dry soils during short-duration dry periods. Such a misrepresentation will have implications for attribution studies as the climate change signal in temperature may not be captured, and bias corrections such as that used in Christidis et al. (2015) cannot fix this.

Going forward, it is important that we increase our appreciation for the multivariate nature of extreme events. This multivariate reasoning and notion of compound events is not necessarily a new concept, though the increased attention towards compound events in recent years is more a recognition of the requirement of a compound event oriented approach for advancing research on extreme events (Bevacqua, 2018). In some respect, all events are multivariate in nature as their occurrence arises from the continuous interaction of several components of the climate system over differ-

ent time and spatial scales. Whether such interactions between contributing variables or large-scale drivers are random occurrences or if there is an underlying dependence structure is an important question. Treating dependent events as independent of one another can result in the underestimation of societal and environmental risk. This thesis has characterised events such as soil moisture drought and meteorological drought in terms of their relationship with changing temperatures and the importance of analysing variables over the relevant time scales. This contributes to our understanding of these events and can act as a platform for future research. As highlighted in this discussion, the next steps are in assessing the large-scale drivers of long-duration meteorological droughts that occur with extreme temperatures and their representation in climate models. This may be achieved through a compound event oriented approach in which we may try to quantify their complex dependencies as well as their relative contributions to extreme events. This may allow us gain better risk estimates of extreme events in the present and future climate, providing invaluable benefits to society in future planning.

Bibliography

- Aas, K., Czado, C., Frigessi, A., and Bakken, H. (2009). Pair-copula constructions of multiple dependence. *Insurance: Mathematics and Economics*, 44(2):182–198.
- Acar, E. F., Genest, C., and Nešlehová, J. (2012). Beyond simplified pair-copula constructions. *Journal of Multivariate Analysis*, 110:74–90.
- Adler, R. F., Gu, G., Sapiano, M., Wang, J.-J., and Huffman, G. J. (2017). Global precipitation: means, variations and trends during the satellite era (1979–2014). *Surveys in Geophysics*, 38(4):679–699.
- AghaKouchak, A., Cheng, L., Mazdiyasni, O., and Farahmand, A. (2014). Global warming and changes in risk of concurrent climate extremes: Insights from the 2014 California drought. *Geophysical Research Letters*, 41(24):2014GL062308.
- Anstey, J. A., Davini, P., Gray, L. J., Woollings, T. J., Butchart, N., Cagnazzo, C., Christiansen, B., Hardiman, S. C., Osprey, S. M., and Yang, S. (2013). Multi-model analysis of northern hemisphere winter blocking: Model biases and the role of resolution. *Journal of Geophysical Research: Atmospheres*, 118(10):3956–3971.
- Bader, B. and Yan, J. (2018). *eva: Extreme Value Analysis with Goodness-of-Fit Testing*.
- Baldocchi, D., Falge, E., Gu, L., Olson, R., Hollinger, D., Running, S., Anthoni, P.,

- Bernhofer, C., Davis, K., Evans, R., et al. (2001). Fluxnet: A new tool to study the temporal and spatial variability of ecosystem-scale carbon dioxide, water vapor, and energy flux densities. *Bulletin of the American Meteorological Society*, 82(11):2415–2434.
- Beniston, M. (2009). Trends in joint quantiles of temperature and precipitation in Europe since 1901 and projected for 2100. *Geophysical Research Letters*, 36(7):L07707.
- Berckmans, J., Woollings, T., Demory, M.-E., Vidale, P.-L., and Roberts, M. (2013). Atmospheric blocking in a high resolution climate model: Influences of mean state, orography and eddy forcing. *Atmospheric Science Letters*, 14(1):34–40.
- Berg, A., Findell, K., Lintner, B., Giannini, A., Seneviratne, S. I., Hurk, B. v. d., Lorenz, R., Pitman, A., Hagemann, S., Meier, A., Cheruy, F., Ducharne, A., Malyshev, S., and Milly, P. C. D. (2016a). Land-atmosphere feedbacks amplify aridity increase over land under global warming. *Nature Climate Change*, 6(9):869–874.
- Berg, A., Findell, K., Lintner, B., Giannini, A., Seneviratne, S. I., Van den Hurk, B., Lorenz, R., Pitman, A., Hagemann, S., Meier, A., et al. (2016b). Land-atmosphere feedbacks amplify aridity increase over land under global warming. *Nature Climate Change*, 6(9):869.
- Berg, A., Lintner, B. R., Findell, K., Seneviratne, S. I., van den Hurk, B., Ducharne, A., Chéruey, F., Hagemann, S., Lawrence, D. M., Malyshev, S., et al. (2015). Interannual coupling between summertime surface temperature and precipitation over land: Processes and implications for climate change. *Journal of Climate*, 28(3):1308–1328.

- Berg, A. and Sheffield, J. (2018). Climate change and drought: the soil moisture perspective. *Current Climate Change Reports*, 4(2):180–191.
- Berg, A., Sheffield, J., and Milly, P. C. (2017). Divergent surface and total soil moisture projections under global warming. *Geophysical Research Letters*, 44(1):236–244.
- Bernard, C. and Czado, C. (2015). Conditional quantiles and tail dependence. *Journal of Multivariate Analysis*, 138:104–126.
- Bevacqua, E. (2017). *CDVineCopulaConditional: Sampling from Conditional C- and D-Vine Copulas*. R package version 0.1.0.
- Bevacqua, E. (2018). Multivariate statistical modelling and analysis of compound events. *PhD Thesis*.
- Bevacqua, E., Maraun, D., Hobæk Haff, I., Widmann, M., and Vrac, M. (2017). Multivariate statistical modelling of compound events via pair-copula constructions: analysis of floods in Ravenna (Italy). *Hydrol. Earth Syst. Sci.*, 21(6):2701–2723.
- Bevacqua, E., Maraun, D., Voudoukas, M. I., Voukouvalas, E., Vrac, M., Mentaschi, L., and Widmann, M. (2018). Higher potential compound flood risk in northern europe under anthropogenic climate change. *EarthArXiv*.
- Buchinsky, I. E. (1976). Droughts and dry winds (in russian). *Gidrometeoizdat*, page 214.
- Burke, E. J. (2011). Understanding the sensitivity of different drought metrics to the drivers of drought under increased atmospheric co₂. *Journal of Hydrometeorology*, 12(6):1378–1394.

- Byrne, M. P. and O’Gorman, P. A. (2013). Link between land-ocean warming contrast and surface relative humidities in simulations with coupled climate models. *Geophysical Research Letters*, 40(19):5223–5227.
- Camarero, J. J., Gazol, A., Sangüesa-Barreda, G., Oliva, J., and Vicente-Serrano, S. M. (2015). To die or not to die: early warnings of tree dieback in response to a severe drought. *Journal of Ecology*, 103(1):44–57.
- Cantos, J. O., Gil, A. M., and Amorós, A. M. R. (2000). Diferentes percepciones de la sequía en españa: adaptación, catastrofismo e intentos de corrección. *Investigaciones Geográficas*, (23):5–46.
- Cassou, C., Terray, L., and Phillips, A. S. (2005). Tropical atlantic influence on european heat waves. *Journal of climate*, 18(15):2805–2811.
- Christidis, N., Jones, G. S., and Stott, P. A. (2015). Dramatically increasing chance of extremely hot summers since the 2003 european heatwave. *Nature Climate Change*, 5(1):46.
- Ciais, P., Reichstein, M., Viovy, N., Granier, A., Ogée, J., Allard, V., Aubinet, M., Buchmann, N., Bernhofer, C., Carrara, A., Chevallier, F., De Noblet, N., Friend, A. D., Friedlingstein, P., Grünwald, T., Heinesch, B., Keronen, P., Knohl, A., Krinner, G., Loustau, D., Manca, G., Matteucci, G., Miglietta, F., Ourcival, J. M., Papale, D., Pilegaard, K., Rambal, S., Seufert, G., Soussana, J. F., Sanz, M. J., Schulze, E. D., Vesala, T., and Valentini, R. (2005). Europe-wide reduction in primary productivity caused by the heat and drought in 2003. *Nature*, 437(7058):529–533.
- Coles, S., Bawa, J., Trenner, L., and Dorazio, P. (2001). *An introduction to statistical modeling of extreme values*, volume 208. Springer.

- Collins, M., Knutti, R., Arblaster, J., Dufresne, J.-L., Fichefet, T., Friedlingstein, P., Gao, X., Gutowski, W., Johns, T., Krinner, G., et al. (2013). Long-term climate change: projections, commitments and irreversibility.
- Coumou, D., Di Capua, G., Vavrus, S., Wang, L., and Wang, S. (2018). The influence of arctic amplification on mid-latitude summer circulation. *Nature communications*, 9(1):2959.
- Coumou, D., Lehmann, J., and Beckmann, J. (2015). The weakening summer circulation in the northern hemisphere mid-latitudes. *Science*, 348(6232):324–327.
- Dai, A. (2011). Drought under global warming: a review. *Wiley Interdisciplinary Reviews: Climate Change*, 2(1):45–65.
- Dai, A. (2013). Increasing drought under global warming in observations and models. *Nature Climate Change*, 3(1):52–58.
- Dai, A., Trenberth, K. E., and Qian, T. (2004). A Global Dataset of Palmer Drought Severity Index for 1870–2002: Relationship with Soil Moisture and Effects of Surface Warming. *Journal of Hydrometeorology*, 5(6):1117–1130.
- D’Andrea, F., Provenzale, A., Vautard, R., and De Noblet-Decoudré, N. (2006). Hot and cool summers: Multiple equilibria of the continental water cycle. *Geophysical Research Letters*, 33(24):L24807.
- Davin, E. L., Maisonnave, E., and Seneviratne, S. I. (2016). Is land surface processes representation a possible weak link in current regional climate models? *Environmental Research Letters*, 11(7):074027.
- Dee, D. P., Uppala, S. M., Simmons, A., Berrisford, P., Poli, P., Kobayashi, S., Andrae, U., Balmaseda, M., Balsamo, G., Bauer, d. P., et al. (2011). The era-interim reanalysis:

- Configuration and performance of the data assimilation system. *Quarterly Journal of the royal meteorological society*, 137(656):553–597.
- Delignette-Muller, M. L. and Dutang, C. (2015). *fitdistrplus*: An R package for fitting distributions. *Journal of Statistical Software*, 64(4):1–34.
- Dirmeyer, P. A., Gao, X., Zhao, M., Guo, Z., Oki, T., and Hanasaki, N. (2006). Gswp-2: Multimodel analysis and implications for our perception of the land surface. *Bulletin of the American Meteorological Society*, 87(10):1381–1398.
- Donat, M., Alexander, L., Yang, H., Durre, I., Vose, R., Dunn, R., Willett, K., Aguilar, E., Brunet, M., Caesar, J., et al. (2013). Updated analyses of temperature and precipitation extreme indices since the beginning of the twentieth century: the hadex2 dataset. *Journal of Geophysical Research: Atmospheres*, 118(5):2098–2118.
- Dorigo, W., Wagner, W., Hohensinn, R., Hahn, S., Paulik, C., Xaver, A., Gruber, A., Drusch, M., Mecklenburg, S., Oevelen, P. v., et al. (2011). The international soil moisture network: a data hosting facility for global in situ soil moisture measurements. *Hydrology and Earth System Sciences*, 15(5):1675–1698.
- Dunn-Sigouin, E. and Son, S.-W. (2013). Northern hemisphere blocking frequency and duration in the cmip5 models. *Journal of Geophysical Research: Atmospheres*, 118(3):1179–1188.
- Duong, T. (2017). *ks: Kernel Smoothing*. R package version 1.10.7.
- Faraway, J., Marsaglia, G., Marsaglia, J., and Baddeley, A. (2017). *goftest: Classical Goodness-of-Fit Tests for Univariate Distributions*. R package version 1.1-1.
- Federov, E. K. (1973). Weather and yield (in russian). *Gidrometeoizdat*, page 55.

- Fensholt, R., Langanke, T., Rasmussen, K., Reenberg, A., Prince, S. D., Tucker, C., Scholes, R. J., Le, Q. B., Bondeau, A., Eastman, R., et al. (2012). Greenness in semi-arid areas across the globe 1981–2007—an earth observing satellite based analysis of trends and drivers. *Remote sensing of environment*, 121:144–158.
- Field, C. B., Jackson, R. B., and Mooney, H. A. (1995). Stomatal responses to increased co₂: implications from the plant to the global scale. *Plant, Cell & Environment*, 18(10):1214–1225.
- Fischer, E. M. and Knutti, R. (2013). Robust projections of combined humidity and temperature extremes. *Nature Climate Change*, 3(2):126.
- Fischer, E. M., Rajczak, J., and Schär, C. (2012a). Changes in european summer temperature variability revisited. *Geophysical Research Letters*, 39(19).
- Fischer, E. M., Rajczak, J., and Schär, C. (2012b). Changes in European summer temperature variability revisited. *Geophysical Research Letters*, 39(19):L19702.
- Fischer, E. M., Seneviratne, S. I., Lüthi, D., and Schär, C. (2007a). Contribution of land-atmosphere coupling to recent european summer heat waves. *Geophysical Research Letters*, 34(6).
- Fischer, E. M., Seneviratne, S. I., Vidale, P. L., Lüthi, D., and Schär, C. (2007b). Soil moisture–atmosphere interactions during the 2003 european summer heat wave. *Journal of Climate*, 20(20):5081–5099.
- Fischer, M., Kraus, D., Pfeuffer, M., and Czado, C. (2017). Stress Testing German Industry Sectors: Results from a Vine Copula Based Quantile Regression. *arXiv:1704.00953 [stat]*. arXiv: 1704.00953.

- Fleig, A. K., Tallaksen, L. M., Hisdal, H., and Demuth, S. (2006). A global evaluation of streamflow drought characteristics. *Hydrology and Earth System Sciences*, 10(4):535–552.
- Ford, T. W. and Quiring, S. M. (2014). In situ soil moisture coupled with extreme temperatures: A study based on the Oklahoma Mesonet. *Geophysical Research Letters*, 41(13):2014GL060949.
- Fouillet, A., Rey, G., Laurent, F., Pavillon, G., Bellec, S., Guihenneuc-Jouyaux, C., Clavel, J., Jouglu, E., and Hémon, D. (2006). Excess mortality related to the august 2003 heat wave in france. *International archives of occupational and environmental health*, 80(1):16–24.
- Francis, J. A. and Vavrus, S. J. (2012). Evidence linking arctic amplification to extreme weather in mid-latitudes. *Geophysical Research Letters*, 39(6).
- Genest, C. and Favre, A.-C. (2007). Everything you always wanted to know about copula modeling but were afraid to ask. *Journal of hydrologic engineering*, 12(4):347–368.
- Gudmundsson, L., Rego, F., Rocha, M., and Seneviratne, S. I. (2014). Predicting above normal wildfire activity in southern europe as a function of meteorological drought. *Environmental Research Letters*, 9(8):084008.
- Gudmundsson, L. and Seneviratne, S. I. (2016). Anthropogenic climate change affects meteorological drought risk in Europe. *Environmental Research Letters*, 11(4):044005.
- Hannaford, J., Lloyd-Hughes, B., Keef, C., Parry, S., and Prudhomme, C. (2011). Examining the large-scale spatial coherence of european drought using regional indi-

- cators of precipitation and streamflow deficit. *Hydrological Processes*, 25(7):1146–1162.
- Hauser, M., Orth, R., and Seneviratne, S. I. (2016). Role of soil moisture versus recent climate change for the 2010 heat wave in western russia. *Geophysical Research Letters*, 43(6):2819–2826.
- Haylock, M., Hofstra, N., Tank, A. K., Klok, E., Jones, P., and New, M. (2008). A european daily high-resolution gridded data set of surface temperature and precipitation for 1950–2006. *Journal of Geophysical Research: Atmospheres*, 113(D20).
- Hazeleger, W., Van den Hurk, B., Min, E., Van Oldenborgh, G., Petersen, A., Stainforth, D., Vasileiadou, E., and Smith, L. (2015). Tales of future weather. *Nature Climate Change*, 5(2):107.
- Heffernan, J. E. and Stephenson, A. G. (2018). *ismev: An Introduction to Statistical Modeling of Extreme Values*. R package version 1.42.
- Hegerl, G. C., Hanlon, H., and Beierkuhnlein, C. (2011). Climate science: Elusive extremes. *Nature Geoscience*, 4(3):142–143.
- Herrera, S., Kotlarski, S., Soares, P. M., Cardoso, R. M., Jaczewski, A., Gutiérrez, J. M., and Maraun, D. (2018). Uncertainty in gridded precipitation products: Influence of station density, interpolation method and grid resolution. *International Journal of Climatology*.
- Hirschi, M., Seneviratne, S. I., Alexandrov, V., Boberg, F., Boroneant, C., Christensen, O. B., Formayer, H., Orłowsky, B., and Stepanek, P. (2011). Observational evidence for soil-moisture impact on hot extremes in southeastern Europe. *Nature Geoscience*, 4(1):17–21.

- Hoerling, M. P., Eischeid, J. K., Quan, X.-W., Diaz, H. F., Webb, R. S., Dole, R. M., and Easterling, D. R. (2012). Is a transition to semipermanent drought conditions imminent in the us great plains? *Journal of Climate*, 25(24):8380–8386.
- Hoskins, B. and Woollings, T. (2015). Persistent extratropical regimes and climate extremes. *Current Climate Change Reports*, 1(3):115–124.
- Howitt, R., Medellín-Azuara, J., MacEwan, D., Lund, J. R., and Sumner, D. (2014). *Economic analysis of the 2014 drought for California agriculture*. Center for Watershed Sciences University of California, Davis, CA.
- Hungate, B. A., Reichstein, M., Dijkstra, P., Johnson, D., Hymus, G., Tenhunen, J., Hinkle, C., and Drake, B. (2002). Evapotranspiration and soil water content in a scrub-oak woodland under carbon dioxide enrichment. *Global Change Biology*, 8(3):289–298.
- Ionita, M., Tallaksen, L., Kingston, D., Stagge, J., Laaha, G., Van Lanen, H., Scholz, P., Chelcea, S., and Haslinger, K. (2017). The european 2015 drought from a climatological perspective. *Hydrology and Earth System Sciences*, 21:1397–1419.
- Joe, H. (1997). *Multivariate models and multivariate dependence concepts*. CRC Press.
- Koster, R. D., Guo, Z., Yang, R., Dirmeyer, P. A., Mitchell, K., and Puma, M. J. (2009). On the nature of soil moisture in land surface models. *Journal of Climate*, 22(16):4322–4335.
- Kraus, D. and Czado, C. (2017). D-vine copula based quantile regression. *Computational Statistics & Data Analysis*, 110:1–18.
- Kurowicka, D. and Cooke, R. M. (2005). Distribution-free continuous bayesian belief. *Modern statistical and mathematical methods in reliability*, 10:309.

- Lambert, F. H., Stott, P. A., Allen, M. R., and Palmer, M. A. (2004). Detection and attribution of changes in 20th century land precipitation. *Geophysical Research Letters*, 31(10).
- Larsson, J. (2017). A historical analysis of hydrological drought in sweden.
- Lehtonen, I., Ruosteenoja, K., and Jylhä, K. (2014). Projected changes in european extreme precipitation indices on the basis of global and regional climate model ensembles. *International Journal of Climatology*, 34(4):1208–1222.
- Leonard, M., Westra, S., Phatak, A., Lambert, M., van den Hurk, B., McInnes, K., Risbey, J., Schuster, S., Jakob, D., and Stafford-Smith, M. (2014). A compound event framework for understanding extreme impacts. *Wiley Interdisciplinary Reviews: Climate Change*, 5(1):113–128.
- Lhotka, O., Kysely, J., and Plavcová, E. (2018). Evaluation of major heat waves' mechanisms in euro-cordex rcms over central europe. *Climate dynamics*, 50(11-12):4249–4262.
- Long, S. P., Ainsworth, E. A., Leakey, A. D., Nösberger, J., and Ort, D. R. (2006). Food for thought: lower-than-expected crop yield stimulation with rising co2 concentrations. *science*, 312(5782):1918–1921.
- Lorenz, R., Davin, E. L., and Seneviratne, S. I. (2012). Modeling land-climate coupling in Europe: Impact of land surface representation on climate variability and extremes. *Journal of Geophysical Research: Atmospheres*, 117(D20):D20109.
- Lorenz, R., Jaeger, E. B., and Seneviratne, S. I. (2010). Persistence of heat waves and its link to soil moisture memory. *Geophysical Research Letters*, 37(9):L09703.

- Lucarini, V., Calmanti, S., Dell'Aquila, A., Ruti, P. M., and Speranza, A. (2007). Inter-comparison of the northern hemisphere winter mid-latitude atmospheric variability of the ipcc models. *Climate Dynamics*, 28(7-8):829–848.
- Luo, L., Apps, D., Arcand, S., Xu, H., Pan, M., and Hoerling, M. (2017). Contribution of temperature and precipitation anomalies to the California drought during 2012–2015. *Geophysical Research Letters*, 44(7):2016GL072027.
- Manning, C., Widmann, M., Bevacqua, E., Van Loon, A. F., Maraun, D., and Vrac, M. (2018). Soil moisture drought in europe: A compound event of precipitation and potential evapotranspiration on multiple time scales. *Journal of Hydrometeorology*, 19(8):1255–1271.
- Maraun, D., Shepherd, T. G., Widmann, M., Zappa, G., Walton, D., Gutiérrez, J. M., Hagemann, S., Richter, I., Soares, P. M., Hall, A., et al. (2017). Towards process-informed bias correction of climate change simulations. *Nature Climate Change*, 7(11):764.
- Maraun, D., Wetterhall, F., Ireson, A., Chandler, R., Kendon, E., Widmann, M., Brienen, S., Rust, H., Sauter, T., Themeßl, M., et al. (2010). Precipitation downscaling under climate change: Recent developments to bridge the gap between dynamical models and the end user. *Reviews of Geophysics*, 48(3).
- Marvel, K., Cook, B. I., Bonfils, C. J., Durack, P. J., Smerdon, J. E., and Williams, A. P. (2019). Twentieth-century hydroclimate changes consistent with human influence. *Nature*, 569(7754):59.
- Masato, G., Hoskins, B. J., and Woollings, T. (2013). Winter and summer northern hemisphere blocking in cmip5 models. *Journal of Climate*, 26(18):7044–7059.

- Milly, P. C. D. and Dunne, K. A. (2016). Potential evapotranspiration and continental drying. *Nature Climate Change*, 6(10):946–949.
- Miralles, D. G., Teuling, A. J., van Heerwaarden, C. C., and Vilà-Guerau de Arellano, J. (2014). Mega-heatwave temperatures due to combined soil desiccation and atmospheric heat accumulation. *Nature Geoscience*, 7(5):345–349.
- Mitchell, K. E., Lohmann, D., Houser, P. R., Wood, E. F., Schaake, J. C., Robock, A., Cosgrove, B. A., Sheffield, J., Duan, Q., Luo, L., et al. (2004). The multi-institution north american land data assimilation system (nldas): Utilizing multiple gcip products and partners in a continental distributed hydrological modeling system. *Journal of Geophysical Research: Atmospheres*, 109(D7).
- Mittelbach, H. and Seneviratne, S. I. (2012). A new perspective on the spatio-temporal variability of soil moisture: temporal dynamics versus time-invariant contributions. *Hydrol. Earth Syst. Sci.*, 16(7):2169–2179.
- Mo, K. C. and Lettenmaier, D. P. (2016). Precipitation deficit flash droughts over the united states. *Journal of Hydrometeorology*, 17(4):1169–1184.
- Mokhov, I. (2011). Specific features of the 2010 summer heat formation in the european territory of russia in the context of general climate changes and climate anomalies. *Izvestiya, Atmospheric and Oceanic Physics*, 47(6):653–660.
- Mueller, B. and Seneviratne, S. I. (2012). Hot days induced by precipitation deficits at the global scale. *Proceedings of the National Academy of Sciences*, 109(31):12398–12403.
- New, M., Todd, M., Hulme, M., and Jones, P. (2001). Precipitation measurements and

- trends in the twentieth century. *International journal of climatology*, 21(15):1889–1922.
- Noh, H., Ghouch, A. E., and Bouezmarni, T. (2013). Copula-Based Regression Estimation and Inference. *Journal of the American Statistical Association*, 108(502):676–688.
- Orlowsky, B. and Seneviratne, S. I. (2012). Global changes in extreme events: regional and seasonal dimension. *Climatic Change*, 110(3-4):669–696.
- Orlowsky, B. and Seneviratne, S. I. (2013). Elusive drought: uncertainty in observed trends and short-and long-term cmip5 projections. *Hydrology and Earth System Sciences*, 17(5):1765–1781.
- Orth, R., Dutra, E., and Pappenberger, F. (2016). Improving weather predictability by including land surface model parameter uncertainty. *Monthly Weather Review*, 144(4):1551–1569.
- Orth, R. and Seneviratne, S. I. (2014). Using soil moisture forecasts for sub-seasonal summer temperature predictions in Europe. *Climate Dynamics*, 43(12):3403–3418.
- Orth, R., Staudinger, M., Seneviratne, S. I., Seibert, J., and Zappa, M. (2015). Does model performance improve with complexity? a case study with three hydrological models. *Journal of Hydrology*, 523:147–159.
- Pachauri, R. K., Allen, M. R., Barros, V. R., Broome, J., Cramer, W., Christ, R., Church, J. A., Clarke, L., Dahe, Q., Dasgupta, P., et al. (2014). *Climate change 2014: synthesis report. Contribution of Working Groups I, II and III to the fifth assessment report of the Intergovernmental Panel on Climate Change*. Ipcc.

- Palmer, W. C. (1965). *Meteorological drought*, volume 30. US Department of Commerce, Weather Bureau Washington, DC.
- Petoukhov, V., Petri, S., Rahmstorf, S., Coumou, D., Kornhuber, K., and Schellnhuber, H. J. (2016). Role of quasiresonant planetary wave dynamics in recent boreal spring-to-autumn extreme events. *Proceedings of the National Academy of Sciences*, page 201606300.
- Petoukhov, V., Rahmstorf, S., Petri, S., and Schellnhuber, H. J. (2013). Quasiresonant amplification of planetary waves and recent northern hemisphere weather extremes. *Proceedings of the National Academy of Sciences*, 110(14):5336–5341.
- Pfahl, S. and Wernli, H. (2012). Quantifying the relevance of atmospheric blocking for co-located temperature extremes in the northern hemisphere on (sub-) daily time scales. *Geophysical Research Letters*, 39(12).
- Pham, M. T., Vernieuwe, H., De Baets, B., Willems, P., and Verhoest, N. (2016). Stochastic simulation of precipitation-consistent daily reference evapotranspiration using vine copulas. *Stochastic Environmental Research and Risk Assessment*, 30(8):2197–2214.
- Plavcová, E. and Kyselý, J. (2012). Atmospheric circulation in regional climate models over central europe: links to surface air temperature and the influence of driving data. *Climate dynamics*, 39(7-8):1681–1695.
- Porporato, A. and D’Odorico, P. (2004). Phase Transitions Driven by State-Dependent Poisson Noise. *Physical Review Letters*, 92(11):110601.
- Rebel, K. T., de Jeu, R. A. M., Ciais, P., Viovy, N., Piao, S. L., Kiely, G., and Dolman,

- A. J. (2012). A global analysis of soil moisture derived from satellite observations and a land surface model. *Hydrol. Earth Syst. Sci.*, 16(3):833–847.
- Rebetez, M., Dupont, O., and Giroud, M. (2009). An analysis of the july 2006 heatwave extent in europe compared to the record year of 2003. *Theoretical and Applied Climatology*, 95(1):1–7.
- Ren, L., Arkin, P., Smith, T. M., and Shen, S. S. (2013). Global precipitation trends in 1900–2005 from a reconstruction and coupled model simulations. *Journal of Geophysical Research: Atmospheres*, 118(4):1679–1689.
- Robock, A., Vinnikov, K. Y., Srinivasan, G., Entin, J. K., Hollinger, S. E., Speranskaya, N. A., Liu, S., and Namkhai, A. (2000). The global soil moisture data bank. *Bulletin of the American Meteorological Society*, 81(6):1281–1300.
- Roderick, M. L., Greve, P., and Farquhar, G. D. (2015). On the assessment of aridity with changes in atmospheric co₂. *Water Resources Research*, 51(7):5450–5463.
- Rowell, D. P. and Jones, R. G. (2006). Causes and uncertainty of future summer drying over europe. *Climate Dynamics*, 27(2-3):281–299.
- Ruffault, J., Moron, V., Trigo, R., and Curt, T. (2016). Objective identification of multiple large fire climatologies: an application to a mediterranean ecosystem. *Environmental Research Letters*, 11(7):075006.
- Russo, S., Sillmann, J., and Fischer, E. M. (2015). Top ten european heatwaves since 1950 and their occurrence in the coming decades. *Environmental Research Letters*, 10(12):124003.
- Salvadori, G., De Michele, C., Kottegoda, N. T., and Rosso, R. (2007). *Extremes in nature: an approach using copulas*, volume 56. Springer Science & Business Media.

- Samaniego, L., Thober, S., Kumar, R., Wanders, N., Rakovec, O., Pan, M., Zink, M., Sheffield, J., Wood, E., and Marx, A. (2018). Anthropogenic warming exacerbates european soil moisture droughts. *Nature Climate Change*, 8(5):421.
- Scaife, A. A., Copsey, D., Gordon, C., Harris, C., Hinton, T., Keeley, S., O'Neill, A., Roberts, M., and Williams, K. (2011). Improved atlantic winter blocking in a climate model. *Geophysical Research Letters*, 38(23).
- Scaife, A. A., Woollings, T., Knight, J., Martin, G., and Hinton, T. (2010). Atmospheric blocking and mean biases in climate models. *Journal of Climate*, 23(23):6143–6152.
- Scheff, J. and Frierson, D. M. (2014). Scaling potential evapotranspiration with greenhouse warming. *Journal of Climate*, 27(4):1539–1558.
- Schepsmeier, U., Stoeber, J., Brechmann, E. C., Graeler, B., Nagler, T., and Erhardt, T. (2017). *VineCopula: Statistical Inference of Vine Copulas*. R package version 2.1.1.
- Schoetter, R., Cattiaux, J., and Douville, H. (2015). Changes of western european heat wave characteristics projected by the cmip5 ensemble. *Climate dynamics*, 45(5-6):1601–1616.
- Schubert, S. D., Wang, H., Koster, R. D., Suarez, M. J., and Groisman, P. Y. (2014). Northern eurasian heat waves and droughts. *Journal of Climate*, 27(9):3169–3207.
- Schwingshackl, C., Hirschi, M., and Seneviratne, S. I. (2017). Quantifying spatiotemporal variations of soil moisture control on surface energy balance and near-surface air temperature. *Journal of Climate*, 30(18):7105–7124.
- Seneviratne, S. I. (2012). Climate science: Historical drought trends revisited. *Nature*, 491(7424):338–339.

- Seneviratne, S. I., Corti, T., Davin, E. L., Hirschi, M., Jaeger, E. B., Lehner, I., Orlowsky, B., and Teuling, A. J. (2010). Investigating soil moisture–climate interactions in a changing climate: A review. *Earth-Science Reviews*, 99(3–4):125–161.
- Seneviratne, S. I., Lehner, I., Gurtz, J., Teuling, A. J., Lang, H., Moser, U., Grebner, D., Menzel, L., Schrott, K., Vitvar, T., and Zappa, M. (2012a). Swiss prealpine Rietholzbach research catchment and lysimeter: 32 year time series and 2003 drought event. *Water Resources Research*, 48(6):W06526.
- Seneviratne, S. I., Lüthi, D., Litschi, M., and Schär, C. (2006). Land–atmosphere coupling and climate change in Europe. *Nature*, 443(7108):205–209.
- Seneviratne, S. I., Nicholls, N., Easterling, D., Goodess, C. M., Kanae, S., Kossin, J., Luo, Y., Marengo, J., Innes, K. M., Rahimi, M., Reichstein, M., Sorteberg, A., Vera, C., Zhang, X., Rusticucci, M., Semenov, V., Alexander, L. V., Allen, S., Benito, G., Cavazos, T., Clague, J., Conway, D., Della-Marta, P. M., Gerber, M., Gong, S., Goswami, B. N., Hemer, M., Huggel, C., den Hurk, B. V., Kharin, V. V., Kitoh, A., Tank, A. M. G. K., Li, G., Mason, S., Guire, W. M., Oldenborgh, G. J. V., Orlowsky, B., Smith, S., Thiaw, W., Velegrakis, A., Yiou, P., Zhang, T., Zhou, T., and Zwiers, F. W. (2012b). Changes in climate extremes and their impacts on the natural physical environment. In *Managing the Risks of Extreme Events and Disasters to Advance Climate Change Adaptation*, pages 109–230. Cambridge University Press, Cambridge.
- Sepulcre-Canto, G., Horion, S., Singleton, A., Carrao, H., and Vogt, J. (2012). Development of a combined drought indicator to detect agricultural drought in Europe. *Natural Hazards and Earth System Sciences*, 12(11):3519–3531.
- Serinaldi, F., Bonaccorso, B., Cancelliere, A., and Grimaldi, S. (2009). Probabilistic

- characterization of drought properties through copulas. *Physics and Chemistry of the Earth, Parts A/B/C*, 34(10–12):596–605.
- Shaposhnikov, D., Revich, B., Bellander, T., Bedada, G. B., Bottai, M., Kharkova, T., Kvasha, E., Lezina, E., Lind, T., Semutnikova, E., et al. (2014). Mortality related to air pollution with the moscow heat wave and wildfire of 2010. *Epidemiology (Cambridge, Mass.)*, 25(3):359.
- Shaw, T. and Voigt, A. (2015). Tug of war on summertime circulation between radiative forcing and sea surface warming. *Nature Geoscience*, 8(7):560.
- Sheffield, J. and Wood, E. F. (2008). Projected changes in drought occurrence under future global warming from multi-model, multi-scenario, ipcc ar4 simulations. *Climate dynamics*, 31(1):79–105.
- Sheffield, J. and Wood, E. F. (2012). *Drought: past problems and future scenarios*. Routledge.
- Sheffield, J., Wood, E. F., Chaney, N., Guan, K., Sadri, S., Yuan, X., Olang, L., Amani, A., Ali, A., Demuth, S., et al. (2014). A drought monitoring and forecasting system for sub-sahara african water resources and food security. *Bulletin of the American Meteorological Society*, 95(6):861–882.
- Sheffield, J., Wood, E. F., and Roderick, M. L. (2012). Little change in global drought over the past 60 years. *Nature*, 491(7424):435–438.
- Shepherd, T. G., Boyd, E., Calel, R. A., Chapman, S. C., Dessai, S., Dima-West, I. M., Fowler, H. J., James, R., Maraun, D., Martius, O., et al. (2018). Storylines: an alternative approach to representing uncertainty in physical aspects of climate change. *Climatic change*, 151(3-4):555–571.

- Sherwood, S. and Fu, Q. (2014). A drier future? *Science*, 343(6172):737–739.
- Sillmann, J., Kharin, V., Zwiers, F., Zhang, X., and Bronaugh, D. (2013). Climate extremes indices in the cmip5 multimodel ensemble: Part 2. future climate projections. *Journal of Geophysical Research: Atmospheres*, 118(6):2473–2493.
- Sklar, M. (1959). Fonctions de repartition an dimensions et leurs marges. *Publ. Inst. Statist. Univ. Paris*, 8:229–231.
- Sousa, P. M., Trigo, R. M., Barriopedro, D., Soares, P. M., and Santos, J. A. (2018). European temperature responses to blocking and ridge regional patterns. *Climate Dynamics*, 50(1-2):457–477.
- SPCCA (2016). Drought.
- Stagge, J. H., Kingston, D. G., Tallaksen, L. M., and Hannah, D. M. (2017). Observed drought indices show increasing divergence across europe. *Scientific Reports*, 7(1):14045.
- Stagge, J. H., Kohn, I., Tallaksen, L. M., and Stahl, K. (2015). Modeling drought impact occurrence based on meteorological drought indices in Europe. *Journal of Hydrology*, 530:37–50.
- Stagge, J. H., Tallaksen, L. M., Kohn, I., Stahl, K., and Van Loon, A. F. (2013). A european drought reference database: Design and online implementation.
- Stefanon, M., D’Andrea, F., and Drobinski, P. (2012). Heatwave classification over Europe and the Mediterranean region. *Environmental Research Letters*, 7(1):014023.
- Stegehuis, A. I., Teuling, A. J., Ciais, P., Vautard, R., and Jung, M. (2013). Future

- European temperature change uncertainties reduced by using land heat flux observations. *Geophysical Research Letters*, 40(10):2242–2245.
- Stegehuis, A. I., Vautard, R., Ciais, P., Teuling, A. J., Jung, M., and Yiou, P. (2012). Summer temperatures in Europe and land heat fluxes in observation-based data and regional climate model simulations. *Climate Dynamics*, 41(2):455–477.
- Stocker, T. F., Qin, D., Plattner, G.-K., Tignor, M., Allen, S. K., Boschung, J., Nauels, A., Xia, Y., Bex, V., Midgley, P. M., et al. (2014). *Climate change 2013: the physical science basis: Working Group I contribution to the Fifth assessment report of the Intergovernmental Panel on Climate Change*. Cambridge University Press.
- Swann, A. L., Hoffman, F. M., Koven, C. D., and Randerson, J. T. (2016). Plant responses to increasing co2 reduce estimates of climate impacts on drought severity. *Proceedings of the National Academy of Sciences*, 113(36):10019–10024.
- Teuling, A. J., Van Loon, A. F., Seneviratne, S. I., Lehner, I., Aubinet, M., Heinesch, B., Bernhofer, C., Grünwald, T., Prasse, H., and Spank, U. (2013). Evapotranspiration amplifies European summer drought. *Geophysical Research Letters*, 40(10):2071–2075.
- Thober, S., Kumar, R., Sheffield, J., Mai, J., Schäfer, D., and Samaniego, L. (2015). Seasonal soil moisture drought prediction over europe using the north american multi-model ensemble (nmme). *Journal of Hydrometeorology*, 16(6):2329–2344.
- Törnros, T. and Menzel, L. (2014). Addressing drought conditions under current and future climates in the Jordan River region. *Hydrol. Earth Syst. Sci.*, 18(1):305–318.
- Tošić, I. and Unkašević, M. (2014). Analysis of wet and dry periods in serbia. *International Journal of Climatology*, 34(5):1357–1368.

- Trenberth, K. E., Dai, A., Schier, G. v. d., Jones, P. D., Barichivich, J., Briffa, K. R., and Sheffield, J. (2014). Global warming and changes in drought. *Nature Climate Change*, 4(1):17–22.
- Trenberth, K. E. and Fasullo, J. T. (2012). Climate extremes and climate change: The russian heat wave and other climate extremes of 2010. *Journal of Geophysical Research: Atmospheres*, 117(D17).
- Tsakiris, G. and Vangelis, H. (2005). Establishing a drought index incorporating evapotranspiration. *European Water*, 9(10):3–11.
- Ulbrich, U., Lionello, P., Belušić, D., Jacobeit, J., Knippertz, P., Kuglitsch, F. G., Leckebusch, G. C., Luterbacher, J., Maugeri, M., Maheras, P., et al. (2012). Climate of the mediterranean: synoptic patterns, temperature, precipitation, winds, and their extremes. In *The Climate of the Mediterranean Region*, pages 301–346. Elsevier.
- Van Baars, S. (2004). Peat dike failure in the netherlands. *European water management online*, 3:1–11.
- Van Baars, S. (2005). The horizontal failure mechanism of the wilnis peat dyke. *Géotechnique*, 55(4):319–323.
- van der Velde, M., Tubiello, F. N., Vrieling, A., and Bouraoui, F. (2012). Impacts of extreme weather on wheat and maize in france: evaluating regional crop simulations against observed data. *Climatic change*, 113(3-4):751–765.
- Vautard, R., Christidis, N., Ciavarella, A., Alvarez-Castro, C., Bellprat, O., Christiansen, B., Colfescu, I., Cowan, T., Doblas-Reyes, F., Eden, J., et al. (2018). Evaluation of the hadgem3-a simulations in view of detection and attribution of human influence on extreme events in europe. *Climate Dynamics*, pages 1–24.

- Vautard, R., Gobiet, A., Jacob, D., Belda, M., Colette, A., Déqué, M., Fernández, J., García-Díez, M., Goergen, K., Güttler, I., et al. (2013). The simulation of european heat waves from an ensemble of regional climate models within the euro-cordex project. *Climate Dynamics*, 41(9-10):2555–2575.
- Vautard, R., Yiou, P., D'andrea, F., De Noblet, N., Viovy, N., Cassou, C., Polcher, J., Ciais, P., Kageyama, M., and Fan, Y. (2007). Summertime european heat and drought waves induced by wintertime mediterranean rainfall deficit. *Geophysical Research Letters*, 34(7).
- Veryard, R. (1956). Looking back on 1955. *Weather*, 11(3):83–88.
- Vicente-Serrano, S. M., Beguería, S., and López-Moreno, J. I. (2009). A Multiscalar Drought Index Sensitive to Global Warming: The Standardized Precipitation Evapotranspiration Index. *Journal of Climate*, 23(7):1696–1718.
- Vicente-Serrano, S. M., Lopez-Moreno, J.-I., Beguería, S., Lorenzo-Lacruz, J., Sanchez-Lorenzo, A., García-Ruiz, J. M., Azorin-Molina, C., Morán-Tejeda, E., Revuelto, J., Trigo, R., et al. (2014). Evidence of increasing drought severity caused by temperature rise in southern europe. *Environmental Research Letters*, 9(4):044001.
- Vogel, M. M., Orth, R., Cheruy, F., Hagemann, S., Lorenz, R., van den Hurk, B. J., and Seneviratne, S. I. (2017). Regional amplification of projected changes in extreme temperatures strongly controlled by soil moisture-temperature feedbacks. *Geophysical Research Letters*, 44(3):1511–1519.
- Vogel, M. M., Zscheischler, J., and Seneviratne, S. I. (2018). Varying soil moisture–atmosphere feedbacks explain divergent temperature extremes and precipitation projections in central europe. *Earth System Dynamics*, 9(3):1107–1125.

- Vogt, J., Barbosa, P., Hofer, B., Magni, D., Jager, A., Singleton, A., Horion, S., Sepulcre, G., Micale, F., Sokolova, E., et al. (2011). Developing a european drought observatory for monitoring, assessing and forecasting droughts across the european continent. In *AGU Fall Meeting Abstracts*.
- Volk, T. (2010). *Agriculture in the Western Balkan countries*. Number 57. Studies on the Agricultural and Food Sector in Central and Eastern Europe.
- von Buttlar, J., Zscheischler, J., Rammig, A., Sippel, S., Reichstein, M., Knohl, A., Jung, M., Menzer, O., Arain, M. A., Buchmann, N., Cescatti, A., Gianelle, D., Kiely, G., Law, B. E., Magliulo, V., Margolis, H., McCaughey, H., Merbold, L., Migliavacca, M., Montagnani, L., Oechel, W., Pavelka, M., Peichl, M., Rambal, S., Raschi, A., Scott, R. L., Vaccari, F. P., van Gorsel, E., Varlagin, A., Wohlfahrt, G., and Mahecha, M. D. (2018). Impacts of droughts and extreme-temperature events on gross primary production and ecosystem respiration: a systematic assessment across ecosystems and climate zones. *Biogeosciences*, 15(5):1293–1318.
- Vázquez, C., Zafra, I., and Olivares, P. (2016). Wildfire on spanish coast forces 1,000 people from their homes.
- Wand, M. P. and Jones, M. C. (1994). Multivariate plug-in bandwidth selection. *Computational Statistics*, 9(2):97–116.
- Wanders, N. and Wood, E. F. (2017). Assessing seasonal climate forecasts over africa to support decision-making. *Bridging Science and Policy Implication for Managing Climate Extremes; Hong-Sang Jung, BW, Ed*, pages 1–15.
- Weisheimer, A., Doblas-Reyes, F. J., Jung, T., and Palmer, T. N. (2011). On the pre-

- dictability of the extreme summer 2003 over Europe. *Geophysical Research Letters*, 38(5):L05704.
- Whan, K., Zscheischler, J., Orth, R., Shongwe, M., Rahimi, M., Asare, E. O., and Seneviratne, S. I. (2015). Impact of soil moisture on extreme maximum temperatures in Europe. *Weather and Climate Extremes*, 9:57–67.
- Woollings, T., Barriopedro, D., Methven, J., Son, S.-W., Martius, O., Harvey, B., Sillmann, J., Lupo, A. R., and Seneviratne, S. (2018). Blocking and its response to climate change. *Current Climate Change Reports*, 4(3):287–300.
- Ye, H. (2018). Changes in duration of dry and wet spells associated with air temperatures in russia. *Environmental Research Letters*, 13(3):034036.
- Zampieri, M., D’Andrea, F., Vautard, R., Ciais, P., de Noblet-Ducoudré, N., and Yiou, P. (2009). Hot European Summers and the Role of Soil Moisture in the Propagation of Mediterranean Drought. *Journal of Climate*, 22(18):4747–4758.
- Zarch, M. A. A., Sivakumar, B., and Sharma, A. (2015). Droughts in a warming climate: A global assessment of standardized precipitation index (spi) and reconnaissance drought index (rdi). *Journal of Hydrology*, 526:183–195.
- Zhao, T. and Dai, A. (2015a). The magnitude and causes of global drought changes in the twenty-first century under a low–moderate emissions scenario. *Journal of climate*, 28(11):4490–4512.
- Zhao, T. and Dai, A. (2015b). The Magnitude and Causes of Global Drought Changes in the Twenty-First Century under a Low–Moderate Emissions Scenario. *Journal of Climate*, 28(11):4490–4512.

- Zhu, Z., Piao, S., Myneni, R. B., Huang, M., Zeng, Z., Canadell, J. G., Ciais, P., Sitch, S., Friedlingstein, P., Arneeth, A., et al. (2016). Greening of the earth and its drivers. *Nature climate change*, 6(8):791.
- Zolina, O., Simmer, C., Belyaev, K., Gulev, S. K., and Koltermann, P. (2013). Changes in the duration of european wet and dry spells during the last 60 years. *Journal of Climate*, 26(6):2022–2047.
- Zotarelli, L., Dukes, M. D., Romero, C. C., Migliaccio, K. W., and Morgan, K. T. (2010). Step by step calculation of the penman-monteith evapotranspiration (fao-56 method). *Institute of Food and Agricultural Sciences. University of Florida*.
- Zscheischler, J., Michalak, A. M., Schwalm, C., Mahecha, M. D., Huntzinger, D. N., Reichstein, M., Berthier, G., Ciais, P., Cook, R. B., El-Masri, B., Huang, M., Ito, A., Jain, A., King, A., Lei, H., Lu, C., Mao, J., Peng, S., Poulter, B., Ricciuto, D., Shi, X., Tao, B., Tian, H., Viovy, N., Wang, W., Wei, Y., Yang, J., and Zeng, N. (2014). Impact of large-scale climate extremes on biospheric carbon fluxes: An intercomparison based on MsTMIP data. *Global Biogeochemical Cycles*, 28(6):585–600.
- Zscheischler, J., Orth, R., and Seneviratne, S. I. (2017). Bivariate return periods of temperature and precipitation explain a large fraction of European crop yields. *Biogeosciences Discuss.*, 2017:1–18.
- Zscheischler, J. and Seneviratne, S. I. (2017). Dependence of drivers affects risks associated with compound events. *Science Advances*, 3(6):e1700263.
- Zscheischler, J., Westra, S., Hurk, B. J., Seneviratne, S. I., Ward, P. J., Pitman, A., AghaKouchak, A., Bresch, D. N., Leonard, M., Wahl, T., et al. (2018). Future climate risk from compound events. *Nature Climate Change*, 8:469–477.

Zurovec, O., Vedeld, P., and Sitaula, B. (2015). Agricultural sector of bosnia and herze-
govina and climate change—challenges and opportunities. *Agriculture*, 5(2):245–
266.

Chapter 6

Appendix: Published Article

Soil Moisture Drought in Europe: A Compound Event of Precipitation and Potential Evapotranspiration on Multiple Time Scales

COLIN MANNING AND MARTIN WIDMANN

School of Geography, Earth and Environmental Sciences, University of Birmingham, Birmingham, United Kingdom

EMANUELE BEVACQUA

Wegener Center for Climate and Global Change, University of Graz, Graz, Austria

ANNE F. VAN LOON

Department of Geography, Earth and Environmental Sciences, University of Birmingham, Birmingham, United Kingdom

DOUGLAS MARAUN

Wegener Center for Climate and Global Change, University of Graz, Graz, Austria

MATHIEU VRAC

Laboratoire des Sciences du Climat et de l'Environnement (LSCE-IPSL), Centre d'Etudes de Saclay, Gif-sur-Yvette, France


(Manuscript received 27 January 2018, in final form 26 April 2018)

ABSTRACT

Compound events are extreme impacts that depend on multiple variables that need not be extreme themselves. In this study, we analyze soil moisture drought as a compound event of precipitation and potential evapotranspiration (PET) on multiple time scales related to both meteorological drought and heat waves in wet, transitional, and dry climates in Europe during summer. Drought indices that incorporate PET to account for the effect of temperature on drought conditions are sensitive to global warming. However, as evapotranspiration (ET) is moisture limited in dry climates, the use of such drought indices has often been criticized. We therefore assess the relevance of the contributions of both precipitation and PET to the estimation of soil moisture drought. Applying a statistical model based on pair copula constructions to data from FluxNet sites in Europe, we find at all sites that precipitation exerts the main control over soil moisture drought. At wet sites PET is additionally required to explain the onset, severity, and persistence of drought events over different time scales. At dry sites, where ET is moisture limited in summer, PET does not improve the estimation of soil moisture. In dry climates, increases in drought severity measured by indices incorporating PET may therefore not indicate further drying of soil but the increased availability of energy that can contribute to other environmental hazards such as heat waves and wildfires. We therefore highlight that drought indices including PET should be interpreted within the context of the climate and season in which they are applied in order to maximize their value.

1. Introduction

Soil moisture plays a critical role in agriculture and the variability of temperature (Seneviratne et al. 2006).

 Denotes content that is immediately available upon publication as open access.

Corresponding author: Colin Manning, cjm317@bham.ac.uk

As soil moisture observations are sparse, soil moisture drought must be monitored and quantified using indirect methods. These include land surface models that provide physically based estimates of soil moisture (Mitchell et al. 2004; Sheffield et al. 2014) and drought indices that are used as a proxy of soil moisture (Dai et al. 2004; Vicente-Serrano et al. 2012). The simplicity of drought indices is advantageous, but it also leaves their output open to interpretation, which we assess in this article.

DOI: 10.1175/JHM-D-18-0017.1

© 2018 American Meteorological Society. For information regarding reuse of this content and general copyright information, consult the [AMS Copyright Policy](https://www.ametsoc.org/PUBSReuseLicenses) (www.ametsoc.org/PUBSReuseLicenses).

Many studies have highlighted the multivariate nature of soil moisture drought as well as the importance of incorporating temperature in drought analysis (Seneviratne et al. 2012b; Teuling et al. 2013; AghaKouchak et al. 2014). Through the inclusion of temperature via potential evapotranspiration (PET) in drought indices such as the standardized precipitation evapotranspiration index (SPEI; Vicente-Serrano et al. 2010), the Palmer drought severity index (PDSI; Palmer 1965), and the reconnaissance drought index (RDI; Tsakiris and Vangelis 2005), studies have been able to analyze how drought conditions may change in a warming climate at regional and global scales (Dai et al. 2004; Dai 2011; Sheffield et al. 2012; Dai 2013; Trenberth et al. 2014; Törnros and Menzel 2014; Vicente-Serrano et al. 2014; Zarch et al. 2015; Stagge et al. 2017).

With increasing temperatures, drought events are expected to set in quicker (Trenberth et al. 2014) and become more severe based on indices incorporating PET (Törnros and Menzel 2014; Zarch et al. 2015; Vicente-Serrano et al. 2014). However, the meaning of this increase in severity for soil moisture according to these indices can be quite unclear due to the differing contribution of PET to soil moisture drought in moisture-limited and energy-limited climates (Seneviratne et al. 2010). Understanding these differences can help in the interpretation of future changes depicted by drought indices and the potential implications they bring at a regional level where impacts of drought are felt.

Soil moisture drought refers to moisture deficits in the upper layer of soil known as the root zone. Soil moisture in the root zone is primarily controlled by antecedent precipitation while excesses in evapotranspiration (ET), related to high temperatures, are required to explain the severity of a negative soil moisture anomaly (Teuling et al. 2013; Seneviratne et al. 2012b). The contribution of ET to soil moisture drought depends on the availability of moisture in the soil for ET to take place (Seneviratne et al. 2010). PET measures the evaporative demand of the atmosphere and indicates the amount of ET that would occur given an unlimited water supply. Under moisture-limited conditions, values of PET and ET can diverge where ET may verge to zero while PET can continue to rise with an increase in temperature (Seneviratne et al. 2010). In such dry conditions, PET and temperature can therefore have little contribution to the estimation of soil moisture (Luo et al. 2017) and lead to drying biases in terms of moisture levels in soil when incorporated into drought indices (Sheffield et al. 2012; Seneviratne 2012).

Describing soil moisture with drought indices requires one to account for antecedent meteorological conditions that soil moisture holds memory of. This is done using integrations of a climatic water balance (precipitation minus PET) varying in length from 1 to 24 months

(e.g., SPEI), or through the use of recursive models (e.g., PDSI). The selection of this integration length for indices such as the SPEI is important; a length that is too short will not capture drought persistence while longer periods can include redundant information (Törnros and Menzel 2014). Studies using the SPEI or RDI to represent soil moisture generally use integration periods between 3 and 6 months (Hirschi et al. 2011; Törnros and Menzel 2014). The PDSI is calculated with monthly integrations and it can hold memory of the previous winter and spring in summer months (Dai et al. 2004).

The use of a climatic water balance implies that PET influences soil moisture over the same time scale as precipitation. However, drying of soil occurs on a daily time scale where excesses in ET can be driven by days of extreme temperature that are filtered out through the use of longer integration periods. Such a feature of long integrations of the climatic water balance can lead to an inability to capture both future changes in drying that may cause droughts to set in quicker in a warmer climate and the occurrence of flash droughts associated with short periods of warm temperature and rapidly decreasing soil moisture (Mo and Lettenmaier 2016).

High temperatures driving excesses in ET can be partly attributed to land–atmosphere interactions induced by deficits in precipitation. By leading to dry soil conditions, low antecedent precipitation is associated with an increased probability of hot days (Hirschi et al. 2011; Mueller and Seneviratne 2012; Whan et al. 2015; Ford and Quiring 2014), amplified extreme temperatures, and the persistence of heat waves (Miralles et al. 2014; Lorenz et al. 2010) that, in turn, can further deplete soil moisture where moisture is available.

The individual roles of precipitation and PET, and that of their dependence driven through land–atmosphere interactions, highlight the compound nature of soil moisture drought. Compound events are a class of events receiving an increased amount of attention in recent times. They encompass a broad range of impacts whose risk is influenced by the dependence between their drivers (Wahl et al. 2015; Hillier et al. 2015; Martius et al. 2016; Bevacqua et al. 2017). Understanding the dependence between hot and dry conditions and their impacts is of great importance. Overlooking nonlinear dependence between hot and dry conditions and crop yields leads to an underestimation of risk in reduced crop yields (Zscheischler et al. 2017), while the bivariate risk of hot and dry summers is underestimated when treating them independently (Zscheischler and Seneviratne 2017). Underlining this importance are findings of an increase in the concurrence of drought and heat wave events (Mazdiyasn and AghaKouchak 2015). Such an increase brings a potential rise in the risk of associated impacts, as the impact arising

TABLE 1. Summary of FluxNet sites used throughout this study.

Site	Site name	Lat	Lon	Site type
a	Dripsey, Ireland	51.99°N	8.75°W	Grassland
b	Hainich, Germany	51.08°N	10.45°E	Forest
c	Klingenberg, Germany	50.89°N	13.52°E	Grassland
d	Oensingen, Switzerland	47.28° N	7.73°E	Grassland
e	Pang/Lambourne, United Kingdom	51.45° N	1.27°W	Forest
f	Le Bray, France	44.72°N	0.77°W	Forest
g	Amplero, Italy	41.9°N	13.6°W	Grassland
h	Las Majadas del Tietar, Spain	39.94°N	5.77°W	Savanna/Grassland
i	Bugacpuszta, Hungary	46.69°N	19.6°E	Grassland
j	Mitra IV Tojal, Portugal	38.48°N	8.02°W	Grassland
k	Vall d'Alinya, Spain	42.15°N	1.45°E	Grassland

from the combination of drought and heat wave events can be greater than the sum of the impacts arising from individual events (Hegerl et al. 2011; Zscheischler et al. 2014).

In this study, we analyze soil moisture drought as a compound event of meteorological drought and heat waves in Europe. We use a conceptual framework developed in Bevacqua et al. (2017) and apply it to a system in which we describe soil moisture as a function of precipitation integrated over preceding months and PET integrated over recent days. This conceptual framework allows us to capture days of extreme temperature within the PET variable and its dependence on antecedent conditions. The framework is implemented via a multivariate statistical model based on pair copula constructions (PCCs; Aas et al. 2009). Copula-based methods, in particular PCCs, provide much flexibility in modeling multidimensional systems (Aas et al. 2009; Bevacqua et al. 2017), including the representation of nonlinear dependence associated with hot and dry conditions (Stage et al. 2015; Zscheischler and Seneviratne 2017). Their use has therefore become quite prominent in the analysis of compound events (Serinaldi et al. 2009; AghaKouchak et al. 2014; Bevacqua et al. 2017; Zscheischler et al. 2017; Zscheischler and Seneviratne 2017). More details on copula, PCCs, and the advantages of their use can be found in the following sections.

We assess the compound nature of soil moisture drought in Europe during the summer months June–August (JJA) at locations in wet, transitional, and dry climates. We aim to demonstrate the individual contributions of precipitation and PET to the estimation of soil moisture drought and highlight where, when, and over what integration period lengths PET and its dependence with precipitation are important for the estimation of soil moisture in a statistical setting. In doing so, we aim to characterize the compound nature of soil moisture drought in differing climates during summer to provide information that may aid with the interpretation

of drought indices incorporating PET and allow further insight to be gained from such indices.

The paper is organized as follows: the data employed in this study as well as the statistical methods involved are described in section 2, the main results are presented in section 3, and a summary and conclusions are provided in section 4.

2. Data and methods

a. Dataset

We employed the FluxNet dataset (Baldocchi et al. 2001) for this study using 11 stations situated across Europe. The selection of sites was based both on an initial review of data quality and length across many sites as well as the recommendations of Rebel et al. (2012). Table 1 provides a summary of the site characteristics. To aid the interpretation of the results, we classify the sites as wet or dry based on values of soil moisture. Locations are provided in Fig. 1. At each site, soil moisture measurements from the top 30 cm of soil are provided along with precipitation data as well as the variables required for the calculation of PET via the reference crop Penman–Monteith equation, as described in Zotarelli et al. (2010). These variables include incoming solar radiation, temperature, wind speed, and relative humidity. Among the selected sites, two general land cover types are available: grassland and forest. The data used here are at a daily resolution. We use soil moisture values for the summer months of JJA. For the contributing meteorological variables, we used observations that extend back into previous months in order to calculate integration periods prior to a given soil moisture observation.

b. Conceptual model

We design a conceptual model, based on a framework developed by Bevacqua et al. (2017), in which we describe soil moisture h as an impact of contributing

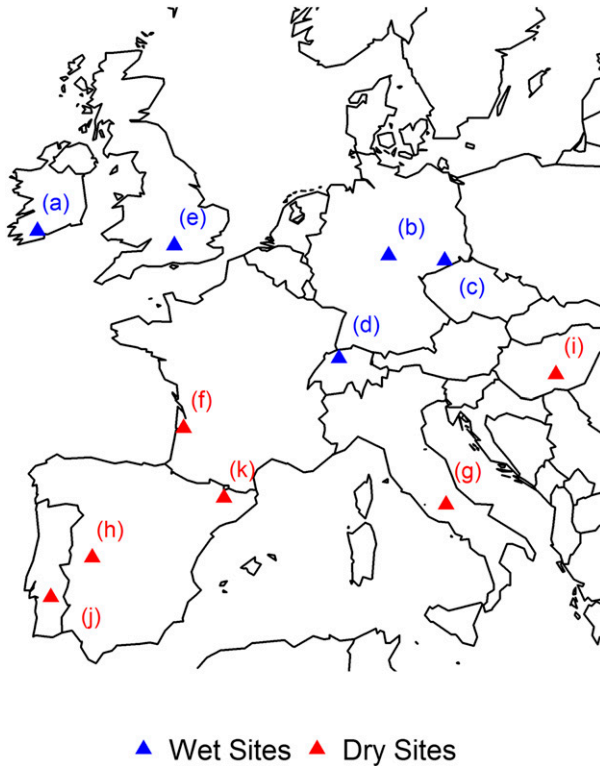


FIG. 1. Locations of FluxNet sites employed for this study.

meteorological variables Y . The contributing meteorological variables include a short-term precipitation variable (Y_{1ps}), a long-term precipitation variable (Y_{2pl}), and a PET variable (Y_{3PET}) that are integrated over periods L_1 , L_2 , and L_3 , respectively. A schematic representation of the variables modeled is given in Fig. 2.

The quantities Y_{1ps} and Y_{2pl} respectively represent the most recent and antecedent precipitation that influence the short- and long-term variability of soil moisture. Their respective integration periods L_1 and L_2 are nonoverlapping. Two precipitation variables are required to better capture the temporal distribution of precipitation that would otherwise be lost using one long-term integration only.

The quantity Y_{3PET} represents PET integrated over the period L_3 . PET is often employed as an estimate of ET in drought indices given the lack of ET data. We calculate PET using the reference crop Penman–Monteith equation as defined in Zotarelli et al. (2010), where it is derived from incoming solar radiation, temperature, wind, and the actual and saturation vapor pressures. The quantity Y_{3PET} includes temperature within its calculation and so can capture heat waves that influence the drying of soil moisture. Depending on the question at hand, the integration length L_3 is varied; more details of this are given in section 2e.

c. Copula

A copula is a multivariate distribution function that describes the dependence structure between random variables independent of their marginal behavior. The selection of structure of dependence, defined by the given copula family, is hence not constrained by the choice of the marginal distribution functions. This feature provides much flexibility in modeling multivariate distributions as it allows for the application of complex marginal distributions (Salvadori et al. 2007). According to Sklar's theorem (Sklar 1959), the joint cumulative distribution function (CDF) F of an n -dimensional random vector $\mathbf{Y} = (Y_1, \dots, Y_n)$ with marginal CDFs F_1, \dots, F_n can be written as

$$F(y_1, \dots, y_n) = C(u_1, \dots, u_n), \quad (1)$$

where C is an n -dimensional copula and $u_i = F_i(y_i)$ are uniformly distributed variables in the domain $[0, 1]$. Provided the marginal distributions F_i are continuous, the multivariate probability density function (PDF) may be decomposed as

$$f(y_1, \dots, y_n) = f_1(y_1) \times \dots \times f_n(y_n) \times c[F_1(y_1), \dots, F_n(y_n)], \quad (2)$$

where c is the copula density and f_i are marginal PDFs.

There exists a large number of bivariate copula families that each provide an explicit formulation for a given structure of dependence. However, the number of copula families applicable to a dimension of three or higher is quite limited (Aas et al. 2009) and in contrast to reality, where heterogeneous dependence structures often exist, each copula will usually assume the same structure of dependence between all marginals (Aas et al. 2009; Acar et al. 2012; Noh et al. 2013; Bevacqua et al. 2017). We therefore employ PCCs that provide higher flexibility than multivariate copulas and more simplicity in terms of the selection of dependence structure (Aas et al. 2009; Noh et al. 2013).

d. Pair copula constructions

PCCs, initially proposed by Joe (1997), allow us to mathematically decompose an n -dimensional copula density into a product of $n(n-1)/2$ bivariate copulas, of which some are conditional. They allow much flexibility in modeling multidimensional distributions (Aas et al. 2009; Bevacqua et al. 2017) and provide a means to easily calculate quantiles of the multivariate conditional distribution of an impact h given values of Y (Noh et al. 2013; Bernard and Czado 2015; Kraus and Czado 2017; Fischer et al. 2017).

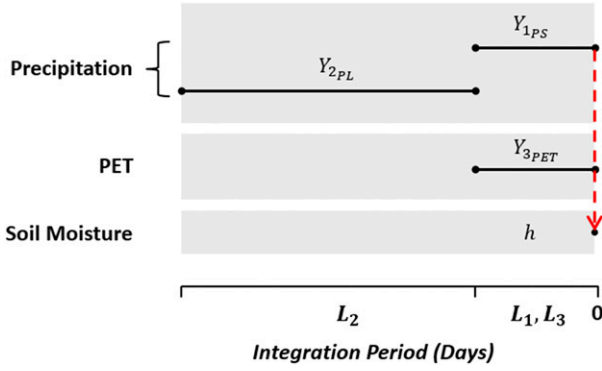


FIG. 2. Schematic of the variables used in this study to construct the soil moisture model.

For a high-dimensional distribution, there exists a significant number of decompositions of a multivariate PDF into a PCC that are each mathematically equivalent to one another (Aas et al. 2009). Two special types of decompositions called vines exist for PCCs, the canonical vine (C-vine) and the D-vine (Kurowicka and Cooke 2005). Throughout this study we employ a D-vine decomposition. For the four-dimensional distribution under study here, there are 12 possible D-vine decompositions. For convenience, we select one decomposition to be applied throughout the study at all sites; the procedure we follow for this selection is outlined in section 2e. The selected D-vine decomposition for the conditional model is given as

$$f_{3,2,1,h}(y_3, y_2, y_1, h) = f_3(y_3) \times f_2(y_2) \times f_1(y_1) \times f_h(h) \\ \times c_{32}(u_3, u_2) \times c_{21}(u_2, u_1) \times c_{1h}(u_1, u_h) \times c_{31|2}(u_{3|2}, u_{1|2}) \\ \times c_{2h|1}(u_{2|1}, u_{h|1}) \times c_{3h|21}(u_{3|21}, u_{h|21}). \quad (3)$$

The differences between each of the 12 possible decompositions are in the ordering of variables within the PCC, which determines the bivariate dependencies that are modeled. As can be seen in Eq. (3), the ordering of variables in the selected decomposition are (Y_3, Y_2, Y_1, h) . To sample h conditioning on the Y , we employ a sampling algorithm provided by the CDVineCopulaConditional R package (Bevacqua 2017), which uses a modified version of the algorithm presented in Aas et al. (2009). This algorithm requires that h is positioned last (or equivalently first) in the order of variables as shown above. This constraint reduces the number of possible decompositions to six. And although each of these possibilities are mathematically equivalent, the explanatory power of h from the resulting conditional

model varies depending on the order of the contributing variables Y within the decomposition, as each Y can have differing levels of influence over h (Kraus and Czado 2017).

1) ESTIMATION OF PCC

The estimation of the PCC given in Eq. (3) is obtained through a sequential approach. First, the unconditional bivariate copulas c_{32} , c_{21} , and c_{1h} are fitted to capture the respective pairwise dependencies of the variables u_3 , u_2 , u_1 , and u_h . Second, the conditional bivariate copulas $c_{31|2}$ and $c_{2h|1}$ are then fitted to the respective conditional probabilities $u_{3|2}$, $u_{1|2}$, $u_{2|1}$, and $u_{h|1}$. These variables are obtained from the conditional distributions given by the partial differentiation of the respective unconditional bivariate copula with respect to the conditioning variable:

$$u_{3|2} = F_{3|2}(u_3|u_2) = \frac{\partial}{\partial u_2} C_{32}(u_3, u_2), \\ u_{1|2} = F_{1|2}(u_1|u_2) = \frac{\partial}{\partial u_2} C_{21}(u_2, u_1), \\ u_{2|1} = F_{2|1}(u_2|u_1) = \frac{\partial}{\partial u_1} C_{21}(u_2, u_1), \quad \text{and} \\ u_{h|1} = F_{h|1}(u_h|u_1) = \frac{\partial}{\partial u_1} C_{1h}(u_1, u_h). \quad (4)$$

In the final step of the estimation procedure, a copula $c_{3h|21}$ is fitted to the conditional probabilities $u_{3|21}$ and $u_{h|21}$. These conditional probabilities are obtained from the conditional distributions given from the partial differentiation of the respective conditional bivariate copula with respect to the conditioning variable:

$$u_{3|21} = F_{3|21}(u_3|u_2, u_1) = \frac{\partial C_{31|2}[F_{3|2}(u_3|u_2), F_{1|2}(u_1|u_2)]}{\partial F_{1|2}(u_1|u_2)} \\ \text{and} \\ u_{h|21} = F_{h|21}(u_h|u_2, u_1) = \frac{\partial C_{2h|1}[F_{2|1}(u_2|u_1), F_{h|1}(u_h|u_1)]}{\partial F_{2|1}(u_2|u_1)}. \quad (5)$$

From the conditional copula $c_{3h|21}$, the conditional CDF $F_{h|321}$ can be obtained through partial differentiation of $C_{3h|21}$ with respect to $F_{3|21}$:

$$F_{h|321}(u_h|u_3, u_2, u_1) \\ = \frac{\partial C_{3h|21}[F_{3|21}(u_3|u_2, u_1), F_{h|21}(u_h|u_2, u_1)]}{\partial F_{3|21}(u_3|u_2, u_1)}. \quad (6)$$

As will be shown, all unconditional and conditional bivariate CDFs described above are required when sampling from the PCC.

2) SAMPLING FROM PCC

Sampling variables u_3 , u_2 , u_1 , and u_h from the four-dimensional D-vine PCC repeatedly results in four uniformly distributed variables that exhibit a dependence structure specified by the given PCC. Algorithms proposed by Aas et al. (2009) provide a convenient means of sampling variables u_3 , u_2 , u_1 , and u_h . Within these algorithms, variables w_3 , w_2 , w_1 , and w_h are first drawn independently from a random uniform distribution on $[0, 1]$. Then, u_3 , u_2 , u_1 , and u_h are determined as

$$\begin{aligned} u_3 &= w_3, \\ u_2 &= F_{2|3}^{-1}(w_2|u_3), \\ u_1 &= F_{1|2}^{-1}[F_{1|23}^{-1}(w_1|u_2, u_3)], \quad \text{and} \\ u_h &= F_{h|1}^{-1}[F_{h|21}^{-1}[F_{h|321}^{-1}(w_h|u_3, u_2, u_1)]]. \end{aligned} \quad (7)$$

Given specified values of Y , the model may be used to sample $h = F_h^{-1}(u_h)$ from a conditional distribution defined by the given Y values. In this case, the variables u_3 , u_2 , u_1 , and u_h are obtained as

$$\begin{aligned} u_3 &= F_3(y_3), \\ u_2 &= F_2(y_2), \\ u_1 &= F_1(y_1), \quad \text{and} \\ u_h &= F_{h|1}^{-1}[F_{h|21}^{-1}[F_{h|321}^{-1}(w_h|u_3, u_2, u_1)]]. \end{aligned} \quad (8)$$

Throughout this study, we use an algorithm proposed by Bevacqua et al. (2017) to sample from Eq. (8) and carry out all simulations using the CDVineCopulaConditional R package (Bevacqua 2017).

When sampling from Eq. (8) given an observed Y , we produce a stochastic time series of h . Repeated simulations conditioning on the observed Y will produce multiple time series with varying statistics and agreement with observed h values (Pham et al. 2016). Throughout this study, given an observed time series of Y , we produce an ensemble consisting of 1000 members of h time series and obtain a probabilistic forecast of h at each time step.

e. Model construction

In this section, we lay out the procedure taken for selecting integration period lengths L_i for the contributing meteorological variables Y_i (Fig. 2). We also provide details of the selection procedure for the D-vine decomposition of the PCC and the selection of copula families within the PCC.

1) METEOROLOGICAL PREDICTOR SELECTION

We describe soil moisture h as a function of two precipitation variables, $Y_{1\text{ps}}$ and $Y_{2\text{pl}}$, integrated over periods L_1 and L_2 , and a PET variable, $Y_{3\text{pet}}$ integrated over the period L_3 . By developing a statistical model with these variables and soil moisture, we look to answer the following three questions:

- 1) What are the individual contributions of the meteorological variables Y_i to the estimation of soil moisture h on time scales related to meteorological drought and heat waves?
- 2) What relevance does the dependence between antecedent precipitation ($Y_{2\text{pl}}$) and recent PET ($Y_{3\text{pet}}$) have for the estimation of low soil moisture values?
- 3) What relevance does PET have for the estimation of soil moisture over varying integration lengths L_3 ?

To answer these questions, we propose two sets of Y variables, S1 and S2. Questions 1 and 2 are then approached using variable set S1 while Question 3 is approached using variable set S2. The difference between S1 and S2 is the integration L_3 chosen at each site. A short integration period is considered for PET in S1, while a long integration period is considered for PET in S2. For each value of L_i used, the contributing meteorological variable Y_i may be defined as

$$\begin{aligned} Y_{1\text{ps}}(t) &= \sum_{t-L_1+1}^t p(t), \\ Y_{2\text{pl}}(t) &= \sum_{t-(L_1+L_2)+1}^{t-L_1} p(t), \quad \text{and} \\ Y_{3\text{pet}}(t) &= \sum_{t-L_3+1}^t \text{pet}(t), \end{aligned} \quad (9)$$

where $p(t)$ and $\text{pet}(t)$ are daily precipitation and PET, respectively.

We address the first two questions with variable set S1. The selected L_i for S1 must result in Y variables that provide satisfactory estimates of soil moisture h , hold physically meaningful dependencies, and capture time scales relevant for both meteorological drought and heat waves. Physically meaningful dependencies are obtained by constraining L_i such that $L_1 = L_3$ and through ensuring that there is no overlap between L_2 and the short-term integrations.

Based on the analysis described below, we find a difference between grassland sites and forest sites. Forest sites require a longer integration L_1 . This is possibly explained by the deeper root systems at forest sites, which filter the influence of short-term variability in rainfall on the integrated soil column. We therefore

choose two sets of L : LG and LF, for grassland and forest sites, respectively. At all grassland (forest) sites, the same LG (LF) are used.

We choose integrations of $LG_1 = LG_3 = 7$ and $LG_2 = 63$ for grassland sites. For forest sites, we choose integrations of $LF_1 = LF_3 = 30$ and $LF_2 = 60$. We thus use information of precipitation over the previous 70 and 90 days for each daily soil moisture observation at grassland and forest sites, respectively.

To select LG_i (LF_i) in S1, we first calculate the Spearman correlation between $Y_i(t)$ and $h(t)$ for multiple integrations within a window of 120 days prior to day t . We then choose the integration length that maximizes the Spearman correlation for each Y_i . Integration periods are then constrained such that $LG_1 = LG_3$ ($LF_1 = LF_3$). This ensures physically meaningful dependencies and avoids arbitrary dependencies that would otherwise arise between differing LG_1 (LF_1) and LG_3 (LF_3).

The sensitivity of the conditional model's performance, in representing h conditioning on Y , to changes in LF (LG) is tested by varying the short-term LG (LF) by ± 4 days while the long-term integration LG (LF) is varied by ± 10 days. Changes in performance are found to be minimal (not shown). Assuming the same LG (LF) at all grassland (forest sites) and constraining the integration periods is therefore expected to have little weight in the outcome of this analysis.

We acknowledge in S1 that the influence of most recent daily temperature extremes on soil moisture is potentially filtered out at forest sites by setting $LF_3 = 30$. This is addressed in variable set S2 where we assess the relevance of the selection of L_3 to the estimation of h (question 3). In S2, two models are constructed using a short- and long-term integration of L_3 . The same LG_1 , LF_1 , LG_2 , and LF_2 as S1 are used while LG_3 and LF_3 are set to 7 and 70 days and 7 and 90 days, respectively.

As the variables are all calculated on a daily resolution, from day t to day $t + 1$, there will be an overlap of $LG_i - 1$ or $LF_i - 1$ mutual days used in the integration periods associated with two consecutive days. We thus violate the assumption that data are independent and identically distributed, which the statistical methods used here are based upon. It should therefore be noted that the performance of the model as well as any estimated dependence between variables may be overestimated.

2) STATISTICAL INFERENCE OF THE MULTIVARIATE PDF

The parameters of each bivariate copula in Eq. (3) are estimated based on the marginal variables u_i drawn from the marginal CDFs F_i . We use a kernel density

estimate for all marginal distributions. All marginal densities are estimated using the *ks* R package (Duong 2017), which employs the bandwidth selector of Wand and Jones (1994).

The estimation of copula parameters requires that no equal ranks are present in u_i . We follow the approach used in Pham et al. (2016) to remove ties from the data. In this approach, a small random noise is drawn from a uniform distribution on $[-0.001, 0.001]$ and added to Y_{1ps} and Y_{2pl} values greater than zero. For values equal to zero, we add a random noise drawn from the uniform distribution on $[0, 0.001]$.

The use of kernel density estimates provides a convenient way of estimating the marginal distribution of h . Soil moisture has natural upper and lower bounds, according to its wilting and saturation points, respectively, and can also exhibit a bimodal distribution (Porporato and D'Odorico 2004; D'Andrea et al. 2006).

The selection of the D-vine decomposition in Eq. (3) is based on an initial test in which we assess the performance of each of the six possible decompositions in their ability to represent h when conditioning on the observed Y . At all sites we fit a PCC for each of the six decompositions and use the Akaike information criterion (AIC) when selecting the type of copulas to be used. The selection of copula families and the estimation of their parameters is carried out at each site separately. Each copula is chosen from a range of copulas provided by the VineCopula R package (Schepsmeier et al. 2017). To assess each of the six possible decompositions, a probabilistic forecast of h consisting of 1000 members is produced at all sites. These are compared with observed soil moisture using the root-mean-square error. We then select the decomposition that generally shows the highest explanatory power of h at all sites.

After selecting the decomposition to apply, the goodness of fit (GoF) of the selected copulas is tested. Copulas initially selected according to the AIC did not always provide a satisfactory fit. For this reason we use two criteria in the selection of a copula for each pair in the PCC. This procedure is carried out sequentially as outlined in section 2d(1), where unconditional copulas are first selected followed by the conditional copulas. For each pair, we first select the top three copulas according to the AIC and second test the GoF of each using K plots (Genest and Favre 2007; Bevacqua et al. 2017). We then select the highest ranked copula according to the AIC that shows satisfactory compliance in the K plots.

A K plot is a plot of the Kendall function $K(w) = P[C_{i,j}(U_i, U_j) \leq w]$ obtained from the fitted copula against $K(w)$ computed with the empirical copula obtained

using the observed data. Similarly to a Q–Q plot for univariate distributions, the K plot indicates good quality of fit when points follow the diagonal. These plots provide uncertainties around the empirical copula as well as a qualitative idea of the quality of fit of each copula (Bevacqua et al. 2017). Most selected copulas show good agreement according to the K plots (not shown) where parametric $K(w)$ values generally follow the mean of the empirical values and mostly remain within the uncertainty intervals calculated from 1000 simulations. Some small problems are found with the copulas at sites e and f, which may limit the strength of conclusions drawn from these sites.

f. Model evaluation metrics

The model simulations are evaluated overall and in their ability to represent low values of soil moisture h . Using the Brier score (BS), we evaluate the accuracy of probabilistic predictions of low h values defined as those below the 15th percentile of observed soil moisture. The closer BS is to zero, the better the predictions. The BS is defined as:

$$\text{BS} = \frac{1}{N} \sum_{t=1}^N (p_t - o_t)^2, \quad (10)$$

where p_t is the probability of getting a simulated value of h below the observed 15th percentile from the model at time t , while o_t is 1 if observed soil moisture $h^{\text{obs}}(t)$ is below the 15th percentile and 0 otherwise. Along with BS we calculate the associated Brier skill score (BSS) that evaluates the model relative to a reference model BS_{ref} :

$$\text{BSS} = 1 - \frac{\text{BS}}{\text{BS}_{\text{ref}}}, \quad (11)$$

We consider the climatology as the reference model in which the probability of a value occurring below the 15th percentile is always 0.15.

The model is also evaluated in its ability to capture the persistence of drought conditions by comparing the autocorrelation function (ACF) and using an empirical order 1 persistence probability (PP). Both are derived from the observed values and the mean of the simulated values. We choose an order 1 persistence after assessing partial autocorrelation function (PACF) at each site, which only showed significant correlations for order 1. The quantity PP is defined as

$$\text{PP} = \Pr[h_{t+1} < F_h^{-1}(0.15) | h_t < F_h^{-1}(0.15)]. \quad (12)$$

The PP may be interpreted as the probability that h_{t+1} will be below the 15th percentile given that h_t is below the 15th percentile.

3. Results

The set of variables S1, described in section 2e(1), are employed to evaluate the contributions of the individual Y variables and that of their dependence structure to soil moisture. To achieve this we perform a number of sensitivity simulations and compare them with a control simulation (CTRL). All simulations carried out are done through a K-fold cross validation to avoid overfitting. Parameter K here is the number of summers in a time series at a given site. In each simulation, we thus remove one summer at a time when fitting the copula parameters but use the same marginal PDFs for each period. In this way we only cross-validate the PCC rather than the entire multivariate statistical model. For each simulation, we then produce a probabilistic forecast of h consisting of 1000 members through conditioning on specified values of Y .

a. Model performance

The CTRL simulation is performed through sampling h conditioned on observed values of Y [Eq. (8)]. The performance of CTRL may be qualitatively gauged from Fig. 3. Plots shown in Figs. 3a–e are results from wet sites while those from Figs. 3f–k are results from dry sites. The mean value of h from CTRL at each time step can be seen to follow the temporal evolution of observed soil moisture (h^{obs}) quite well, while h^{obs} is generally found within the 95% confidence interval of CTRL. Also shown within each panel in Fig. 3 are the order 1 persistence probabilities of low h for observed (PP_{obs}) and mean simulated h (PP_{sim}). The quantities PP_{sim} and PP_{obs} are found to be very similar at all wet sites and most dry sites, although PP_{sim} is generally less than PP_{obs} at dry sites. A comparison of the observed ACF, estimated up to order 10, with the ACF derived from the mean of the simulation also showed close correspondence at each site (not shown). Such results indicate good agreement between the observed h and simulated mean h in terms of temporal evolution and the persistence of low values.

To provide information of the performance of the model in terms of the probabilistic forecast, we calculate BS and BSS for CTRL at each site (Table 2). In general we see good BS and positive BSS that range from 0.06 to 0.12 and 0.04 to 0.51, respectively, with medians of 0.09 and 0.25. These BSS indicate that the model is better than the climatology at predicting low soil moisture values. Low BSS values are seen at site c, where we also see poor correspondence between h^{obs} and the mean of CTRL. Optimizing the performance of the model at this site through changing integration periods does not bring a noticeable improvement,

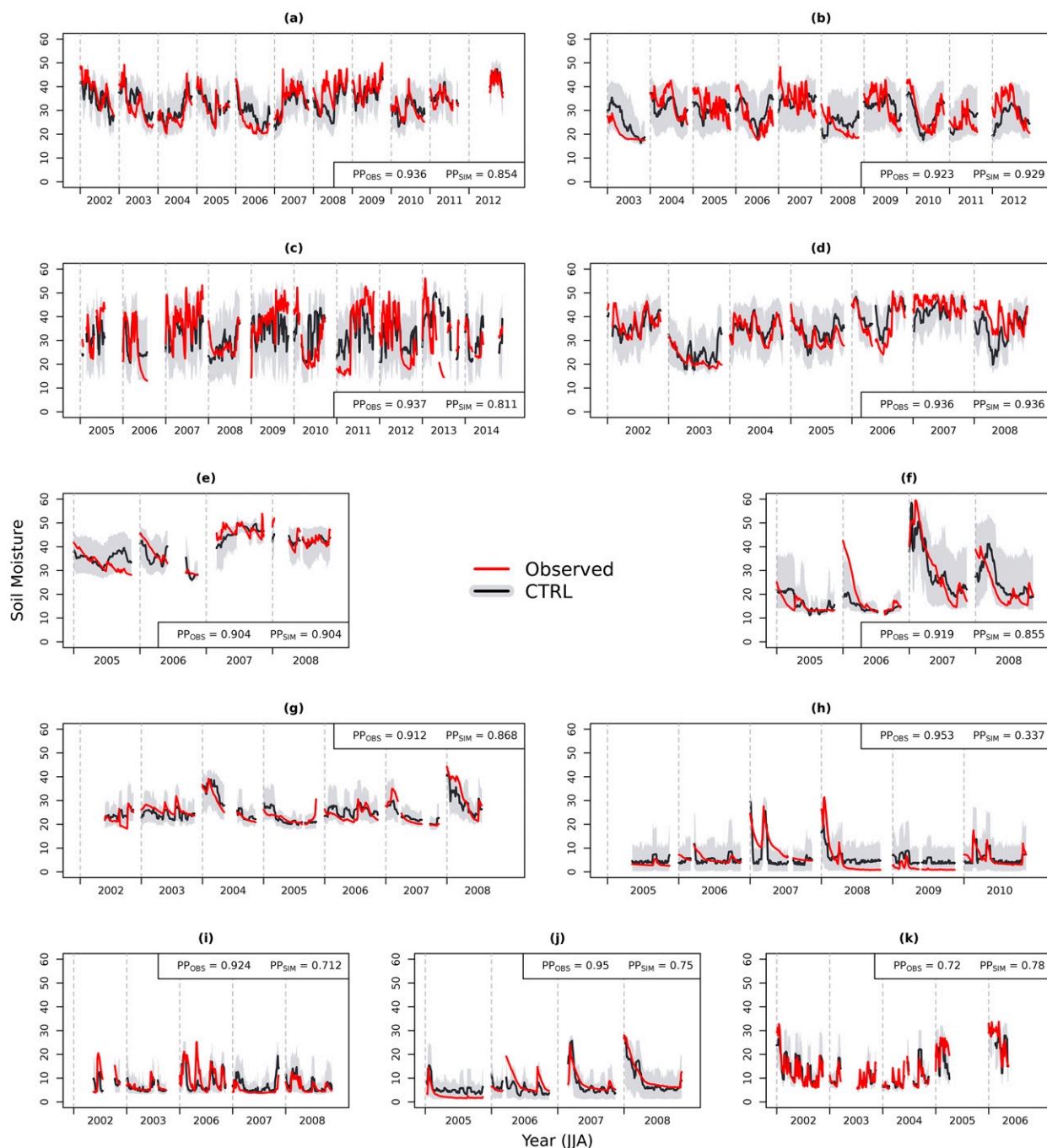


FIG. 3. Observed time series (red) alongside the cross-validation time series of the CTRL mean (black) and the 95% prediction interval (gray), obtained from 1000 simulations, at (a)–(e) wet sites and (f)–(k) dry sites. Also provided within each panel are the order 1 persistence probabilities calculated from the observed (PP_{obs}) and CTRL mean (PP_{sim}) time series.

indicating that the proposed model and variables included do not predict soil moisture correctly at all sites. However, with satisfactory results generally obtained at most sites, we employ the model for use in sensitivity analysis in a number of tests presented below.

b. Assessment of contributing variables to soil moisture

We test the contribution of Y_{1ps} (short-term precipitation), Y_{2pl} (long-term precipitation), and Y_{3pet} (PET) to the estimation of h in three sensitivity simulations

TABLE 2. BS, BSS, and mean bias for CTRL, SENS- Y_{1PS} , SENS- Y_{2PL} , and SENS- Y_{3PET} simulations calculated for soil moisture values below the observed 15th percentile. Bias values for SENS- Y_{1PS} , SENS- Y_{2PL} , and SENS- Y_{3PET} are given as percentage change relative to CTRL.

Site	Score	CTRL	SENS- Y_{1PS}	SENS- Y_{2PL}	SENS- Y_{3PET}
a	BS	0.09	0.10	0.12	0.10
	BSS	0.25	0.21	0.01	0.18
	Bias	3.89	+5%	+113%	+45%
b	BS	0.11	0.13	0.10	0.11
	BSS	0.15	-0.01	0.17	0.15
	Bias	4.33	+107%	-1%	+33%
c	BS	0.12	0.14	0.11	0.12
	BSS	0.04	-0.1	0.13	0.06
	Bias	10.66	+51%	-24%	+2%
d	BS	0.06	0.06	0.09	0.08
	BSS	0.51	0.49	0.26	0.39
	Bias	3.52	+45%	+149%	+83%
e	BS	0.09	0.10	0.09	0.12
	BSS	0.28	0.25	0.27	0.03
	Bias	3.62	-15%	+78%	+81%
f	BS	0.08	0.07	0.06	0.13
	BSS	0.36	0.43	0.53	-0.01
	Bias	0.37	-215%	+207%	+720%
g	BS	0.09	0.09	0.11	0.09
	BSS	0.31	0.24	0.15	0.30
	Bias	1.48	+43%	+86%	+6%
h	BS	0.12	0.13	0.12	0.13
	BSS	0.04	0.00	0.05	0.003
	Bias	3.28	+9%	-3%	+4%
i	BS	0.12	0.13	0.12	0.13
	BSS	0.07	0.002	0.04	-0.06
	Bias	1.24	-9%	+5%	+52%
j	BS	0.12	0.12	0.12	0.12
	BSS	0.09	0.10	0.05	0.06
	Bias	2.8	-8%	+10%	+16%
k	BS	0.08	0.13	0.12	0.08
	BSS	0.36	0.01	0.09	0.37
	Bias	1.05	+205%	+146%	+10%

SENS- Y_{1PS} , SENS- Y_{2PL} , and SENS- Y_{3PET} , respectively. For each sensitivity simulation, h is sampled conditioning on the median value of the respective variable to be tested and the observed values of the other two Y variables. To assess the contributions of all variables, we compare the mean of each simulation with the CTRL mean. We also compare the probabilistic forecasts from SENS- Y_i with CTRL using the BS, BSS, and the mean ensemble bias computed for values of h below the observed 15th percentile (Table 2).

At wet sites, precipitation is generally seen to have the most influence on low soil moisture values, while PET can act to amplify the low soil moisture anomaly during

drought periods. Comparing the means of the three sensitivity simulations with the mean of CTRL (Fig. 4), larger overestimations of low h values with respect to CTRL are generally seen in either of the simulations assessing the influence of a precipitation variable, SENS- Y_{1PS} or SENS- Y_{2PL} , than is, seen in SENS- Y_{3PET} . Underlining this are larger changes in positive bias of low soil moisture values seen from SENS- Y_{1PS} or SENS- Y_{2PL} than from SENS- Y_{3PET} (Table 2). A comparison of BSS for each simulation in Table 2 also shows a larger reduction in skill of forecasting values below 15th percentile in either SENS- Y_{1PS} or SENS- Y_{2PL} than in SENS- Y_{3PET} . Focusing on drought events at wet sites a, b, and d in 2003 and 2006, years in which heat waves have also occurred (Ciais et al. 2005; Rebetez et al. 2009), we see from the mean of the simulations (Fig. 5) that removing the influence of precipitation can lead to the misspecification of a drought event with the green line largely above the black line (CTRL). On the other hand, removing the influence of PET can result in the underestimation of the severity of the event, with the blue line only just higher than the black during a drought event.

At dry sites, we see that precipitation again holds the main influence over soil moisture while PET generally offers little added benefit to the estimation of soil moisture. The main differences of CTRL with SENS- Y_{1PS} and SENS- Y_{2PL} are found for high values of soil moisture (Fig. 4). Low values in these sensitivity simulations are generally equivalent with CTRL, as the medians of Y_{1PS} and Y_{2PL} are associated with relatively low values due to the positively skewed nature of the variables' distributions. Little or no difference is seen between SENS- Y_{3PET} and CTRL simulations for low values of soil moisture. Large percentage changes in bias for low soil moisture values are seen at sites f and i, though the actual changes in soil moisture are relatively low (Table 2). This would be expected at dry sites during summer where soil moisture normally reaches low levels such that ET is moisture-limited and will diverge from PET. Extremes of PET driven by extreme temperatures would then have little added effect to the severity of soil moisture drought in dry locations.

c. Assessing the relevance of Y dependence structure

The contribution of the dependence between Y_{2PL} and Y_{3PET} to the estimation of low h values is assessed using the sensitivity simulation IND- Y_{2PL} , which is used to highlight where interactions between drought and heat wave conditions, arising through land-atmosphere interactions, act to amplify drought conditions. To illustrate the dependence between Y_{2PL} and Y_{3PET} , we calculate Spearman's ρ and a measure of tail dependence λ_q , calculated as

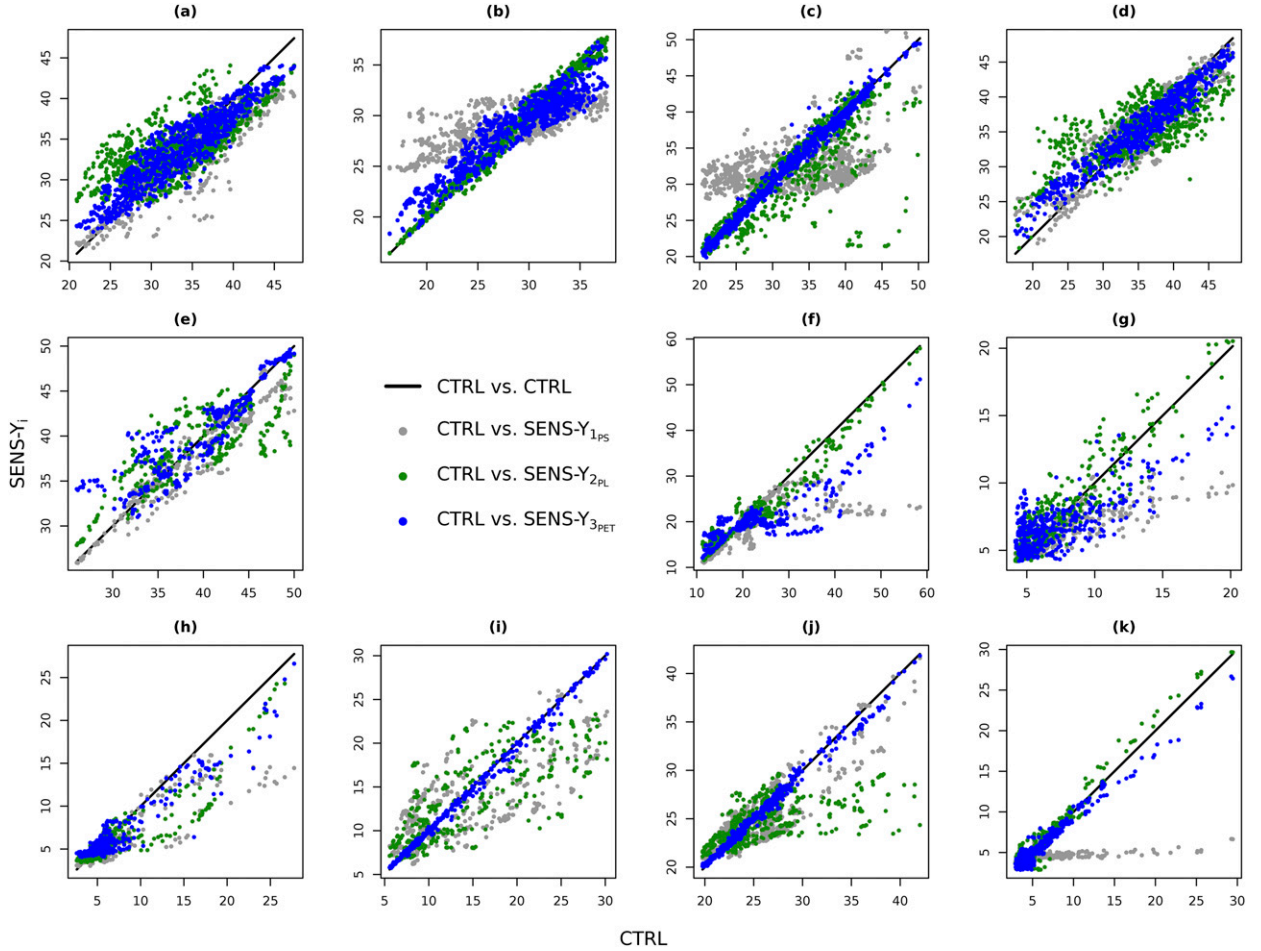


FIG. 4. Comparison of the mean of the cross-validation simulations of CTRL with SENS- Y_{1ps} (gray dots), SENS- Y_{2pl} (green dots), and SENS- Y_{3pet} (blue dots) at (a)–(e) wet sites and (f)–(k) dry sites. Values are ordered according to CTRL from low to high such that the closer the correspondence of points to the diagonal, the smaller the change in the estimation of soil moisture in the given sensitivity simulation.

$$\lambda_q = \Pr[Y_{3pet} > F_3^{-1}(q) | Y_{2pl} < F_2^{-1}(1-q)], \quad (13)$$

where $q = 0.9$ in this case. The quantity λ_{90} can be interpreted as the fraction of days when Y_{3pet} was greater than its observed 90th percentile when Y_{2pl} was less than its 10th percentile. For two independent variables, the expected value of λ_q is $1 - q$. Values of ρ and λ_q for each site are given in Fig. 6. At many sites we observe a negative dependence between Y_{2pl} and Y_{3pet} , as measured by ρ , and an increased probability of extreme PET (Y_{3pet}) when antecedent precipitation (Y_{2pl}) had been extremely low.

To test the relevance of such dependence in IND- Y_{2pl} , we break the dependence between Y_{2pl} and the short-term variables Y_{1ps} and Y_{3pet} . This is achieved by shuffling Y_{2pl} such that it is randomly associated with them. A probabilistic forecast of h , consisting of

1000 members, is then produced, sampling from the multivariate distribution where we condition on the observed values of Y_{1ps} and Y_{3pet} and the shuffled Y_{2pl} . To account for sampling variability of the shuffling process, we produce 1000 IND- Y_{2pl} probabilistic forecasts.

We obtain a kernel density estimate of the PDF produced from each of the 1000 IND- Y_{2pl} simulations. The mean density and the 95% confidence interval of IND- Y_{2pl} PDFs are calculated and presented alongside the PDFs of CTRL and h^{obs} (Fig. 6). The statistical significance of the difference between the CDFs of CTRL and IND- Y_{2pl} is assessed at the 5th, 10th, and 15th percentiles of observed soil moisture. CTRL is considered significantly different for a given percentile if the associated soil moisture value of CTRL is less than the lower bound of 95% confidence interval of that percentile from IND- Y_{2pl} . This would signify that the probability

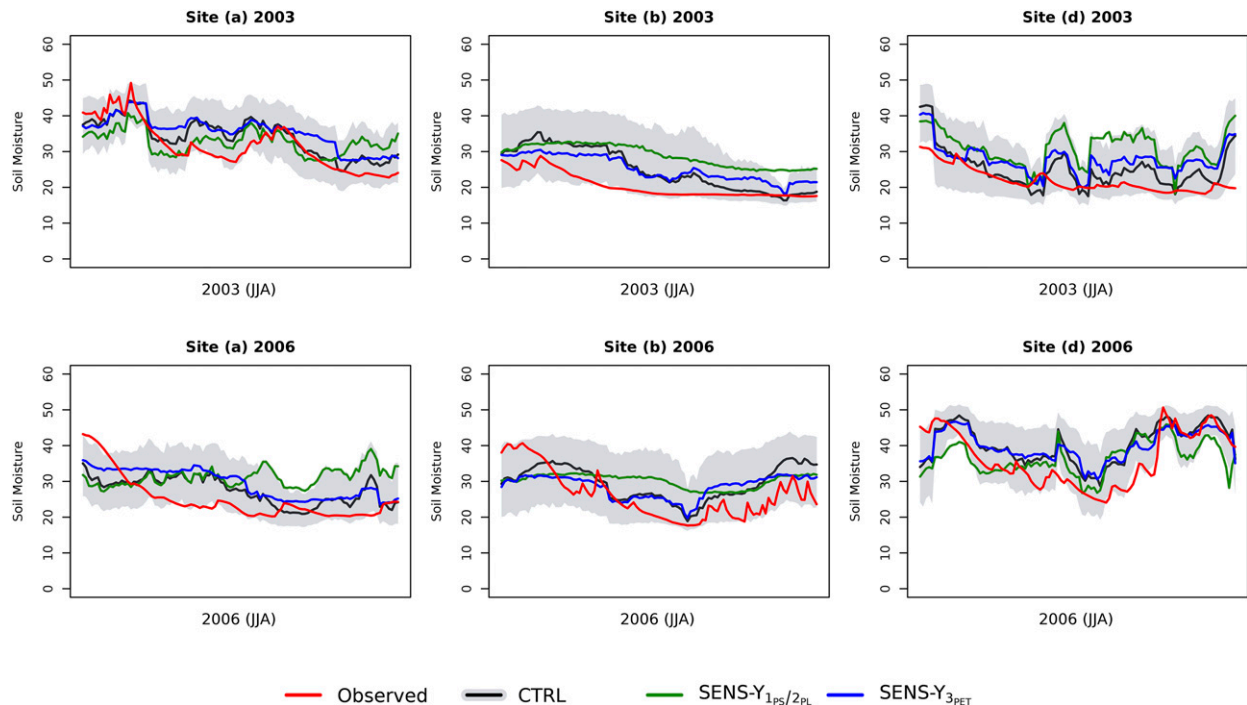


FIG. 5. Mean cross-validated time series of simulations assessing the contributions of precipitation and PET to the estimation of soil moisture and CTRL (black) for the summers (JJA) of (top) 2003 and (bottom) 2006 at wet sites a, b, and d. Time series of mean simulated values are presented for SENS- Y_{2pl} (green) and SENS- Y_{3pet} (blue) at wet sites a and d while time series of SENS- Y_{1ps} (green) and SENS- Y_{3pet} (blue) are presented for site b.

of values below that percentile are underestimated when the dependence between Y_{2pl} and Y_{3pet} is broken.

Statistically significant differences are found between all three percentiles at site d, where we also see a noticeable difference between PDFs (Fig. 6d). A negative dependence as well as a significant dependence in the tails is also observed here. Site d lies in a transitional region where land–atmosphere interactions can lead to the mutual reinforcement of drought and heat wave events (Seneviratne et al. 2010). This result highlights the importance of the interplay between drought and heat wave conditions, driven by land–atmosphere interactions, to the reinforcement of drought conditions in such locations.

Statistically significant differences between the percentiles tested are also found at wet sites a, b, and e and dry sites g and j, though relatively little difference is observed between CTRL and IND- Y_{2pl} PDFs at these sites for values below the tested percentiles (Fig. 6). We observe negative dependencies (ρ) and tail dependencies (λ_q) at these sites, which highlights that the concurrence of such conditions may be important for the estimation of low values of soil moisture. These dependencies are also observed at other dry sites, but no significant differences between assessed percentiles are found. Such dependencies at these sites are perhaps

of little relevance for soil moisture during summer, as extremes of PET may be energy limited in wet climates while soil in dry climates may have little available moisture for ET. In dry conditions then, extremes of PET in combination with extremely low antecedent precipitation will have little effect on moisture levels in soil.

d. Relevance of PET over short and long integration periods

The variable set S2, as described in section 2e(1), is used to demonstrate the relevance of PET, integrated over various durations LG_3 and LF_3 , to the estimation of soil moisture h . We fit two models at wet sites a, b, and d, where we see contributions of PET to the estimation of soil moisture drought in variable set S1 (Fig. 5). The integration periods used for precipitation variables Y_{1ps} and Y_{2pl} in S1 remain the same. For the simulation PET-INT_S, we set $LG_3 = LF_3 = 7$, and for the simulation PET-INT_L, we set $LG_3 = 70$ and $LF_3 = 90$.

Based on the mean of the simulations (Fig. 7), better representation of drought onset can be seen at sites a and d in the PET-INT_S simulations where the black line generally follows red (observed) at the beginning of an event when initial drying is taking place. On the other hand, drought persistence is generally captured better

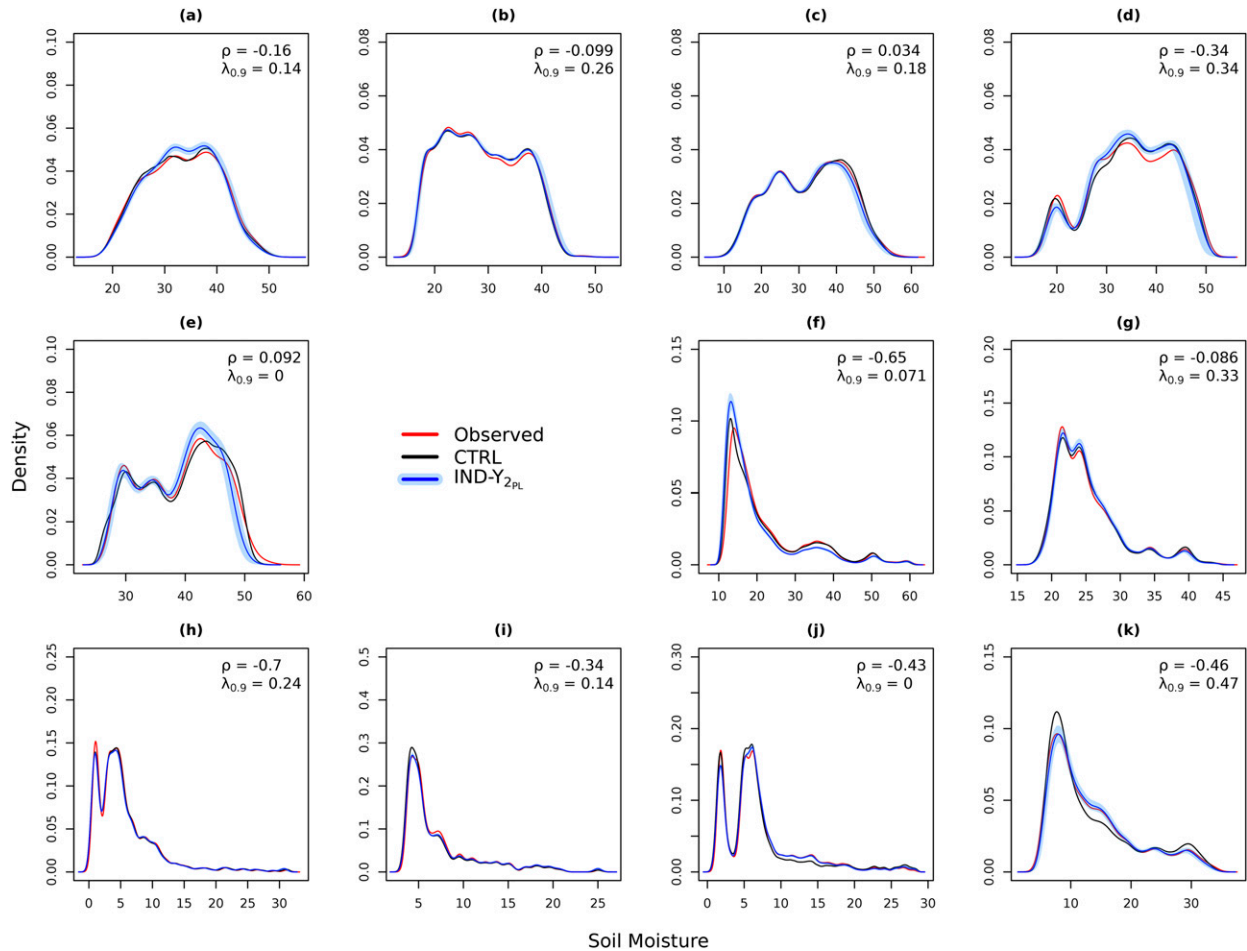


FIG. 6. Kernel density estimates of observed soil moisture (red) and soil moisture simulated via cross-validation from probabilistic forecasts CTRL (black) and $\text{IND-}Y_{2\text{PL}}$ (blue) simulations. The blue line and shading respectively represent the mean density and 95% confidence interval obtained from the 1000 $\text{IND-}Y_{2\text{PL}}$ simulations.

by the PET-INT_L simulation where the blue line remains low with the red line in comparison to the black. Better BSSs are found for simulations using a long-term integration of PET at sites a and b. Increases of BSS, from PET-INT_S to PET-INT_L , from 0.24 to 0.36 and from 0.18 to 0.25 are found at each site, respectively, while little difference is seen between simulations at site d with BSS equal to 0.51 and 0.52.

Although these results are somewhat qualitative, they highlight that both short- and long-term integrations of PET are important for the estimation of drought events in this framework. Longer integrations are generally better in capturing the persistence of drought conditions as they can account for the memory soil moisture holds of drying during the event. Short-term integrations, however, are better in capturing drought onset as they are able to account for short intense periods of drying that can accelerate the propagation of meteorological drought to soil moisture drought. With drought events expected to set in

quicker in a warming climate (Trenberth et al. 2014), it will be important to detect such changes in the intensity of drying over short periods in spring and summer that are filtered out in longer integrations of PET. This may be of particular relevance in Europe, where early onset of drought conditions can have large implications for extreme temperatures in summer (Vautard et al. 2007).

4. Summary and conclusions

Compound events are multivariate extreme events in which the contributing variables need not be extreme themselves, but their joint dependent concurrence produces an extreme impact (Leonard et al. 2014; Bevacqua et al. 2017). We have analyzed soil moisture drought over Europe as a compound event of variables employed in common drought indices, namely, precipitation and PET, and assessed the individual roles of these variables and that of their dependence structure to the estimation of soil

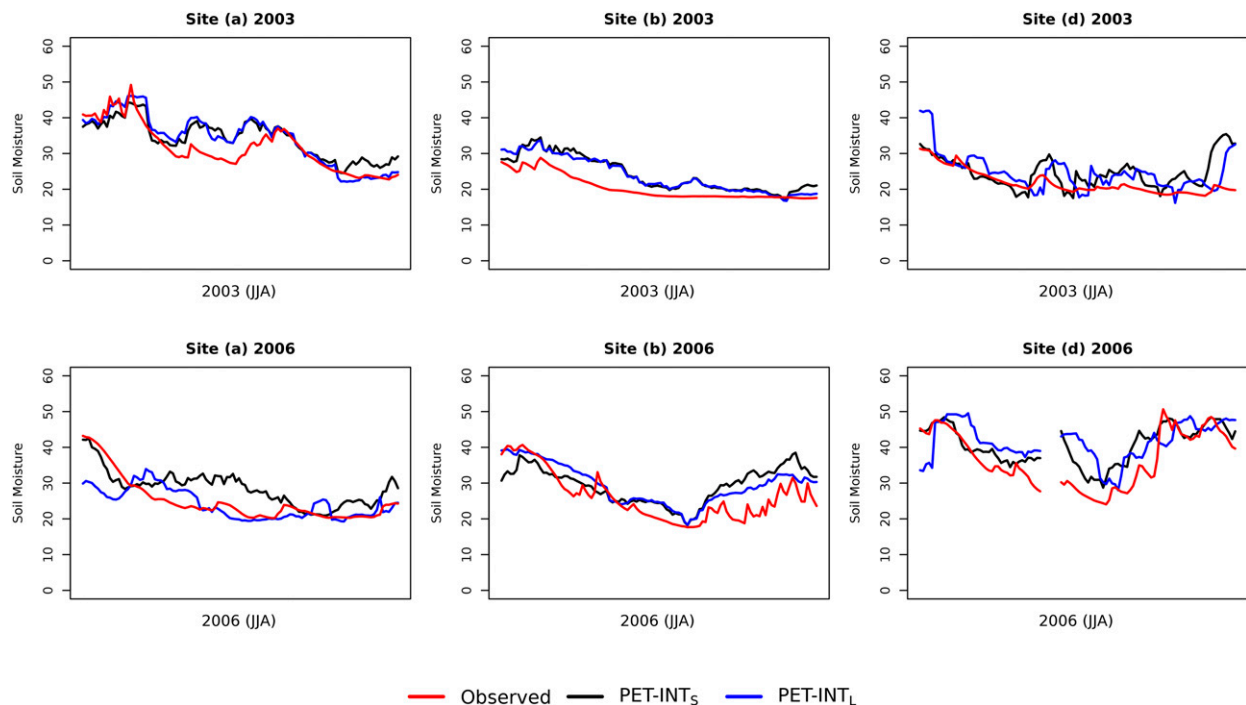


FIG. 7. Mean cross-validation time series of simulations from models PET-INT_S, in which PET is considered over a short integration period (black), and PET-INT_L, in which PET is considered over a long integration period (blue), along with the observed time series (red) for the (top) 2003 and (bottom) 2006 drought events at wet sites a, b, and d.

moisture. The overall aim was to explore the compound nature of soil moisture drought and the differences that exist between wet and dry climates.

To achieve our aim, we developed a statistical model based on pair copula constructions. Within the model we considered precipitation and PET over time scales related to meteorological drought and heat waves, respectively. These time scales were considered to assess the influence of heat wave conditions on soil moisture, as well as dependencies driven by land–atmosphere interactions that can cause a mutual reinforcement between drought and heat wave events in Europe. We applied the model to data from 11 FluxNet sites situated in wet, transitional, and dry climates in Europe and generally found satisfactory performance of the model. We thus employed it in a number of sensitivity experiments to assess the relevance of contributing variables and their dependence structure to the estimation of soil moisture drought.

Results obtained from sensitivity experiments were in line with previous studies. Precipitation was found to hold the main control over soil moisture drought. PET was required only when it departs from normal conditions (Vicente-Serrano et al. 2010) to partly explain the severity of drought conditions in wet climates (Seneviratne et al. 2012b; Teuling et al. 2013), while little or no contribution was found in dry climates (Luo et al. 2017)

during summer. The concurrence of extremely low antecedent precipitation with extremely high PET was found to be most relevant at a site situated in a transitional climate region between wet and dry climates where land–atmosphere interactions are most relevant for the development of soil moisture drought (Seneviratne et al. 2006, 2012a). The concurrence of these conditions was also seen at many dry sites, though they were found to have little relevance for soil moisture. This lack of relevance at dry sites is presumably related to the limited availability of moisture in soil for actual ET to occur, such that PET and extremes of PET could have little influence to a low soil moisture anomaly.

The aforementioned contribution of PET is based on a short-term integration period that was used to capture the influence of heat waves on soil moisture. At wet sites, this short integration period is found to be effective in describing the onset of drought events as it can capture initial drying that occurs on a daily basis. It can, however, be ineffective in capturing the persistence of drought conditions, which longer integrations can better account for, as it neglects the memory soil moisture may hold of PET and the intense drying that may have occurred throughout a drought event. The differences found between short and long integrations of PET may become relevant in the analysis of changes in the

onset of drought events using drought indices. A warmer climate may cause droughts to set in quicker (Trenberth et al. 2014) and lead to flash droughts (Mo and Lettenmaier 2016). Such drying may be hidden through the use of longer integration periods of PET in an index such as the SPEI or through a recursive model used for the PDSI that retains memory of PDSI values from previous time steps.

Advantages of using drought indices include the simplicity they offer and the widespread availability of meteorological datasets compared to those of soil moisture. Although they are not specifically designed to represent soil moisture (Seneviratne et al. 2010), indices such as the SPEI, PDSI, and RDI provide a convenient means of combining precipitation and PET into a kind of impact function that may be implicitly linked to soil moisture.

However, soil moisture drought is not a simple phenomenon to characterize with drought indices due to differing contributions and relevant integration periods of meteorological variables in wet and dry climates. The use of a climatic water balance (precipitation – PET) in the SPEI and PDSI assumes oversimplified relationships between precipitation, PET, and soil moisture (Seneviratne 2012) and implies that the statistical relevance of precipitation and PET to the estimation of soil moisture are the same over a given integration period. With such simplifications comes a loss of information, such as short intense periods of drying that may be filtered out through the inclusion of redundant information when using a long integration period for PET.

Through the inclusion of PET, these indices are expected to provide a better picture of changes in drought conditions in a warming climate than indices that use precipitation alone such as the standardized precipitation index (SPI). Ubiquitously applying indices that incorporate PET across different climates can provide a general overview of the response of drought conditions to global warming. It is, however, important to note that severe drought, as depicted by these indices, will have a different meaning for soil moisture drought in wet and dry climates. ET is limited by moisture availability and so will diverge from PET in dry conditions, leading to an overestimation of the actual drying taking place with respect to soil. In contrast, land surface models account for this moisture limitation by capturing the physical relationship between PET and soil moisture; they can therefore provide a more reliable estimate. Their use within coupled climate models to study changes in soil moisture drought is particularly advocated for by Berg et al. (2017), who also demonstrate the added complexity of diverging changes to soil moisture at different soil depths that cannot be disentangled using drought indices.

Despite discrepancies between PET and ET in dry conditions, extremes of PET will still be indicative of the

drying potential of the atmosphere, provided it is calculated using a reliable physically based method such as the Penman–Monteith equation. Such atmospheric drying potential may possibly have adverse effects on crop yields and contribute to other environmental hazards such as wildfires that are mediated by the availability of moisture in vegetation (Gudmundsson et al. 2014; Ruffault et al. 2016).

Much information of soil moisture and other drought impacts may be deduced from drought indices and their response to a warming climate. To do so requires careful interpretation and detailed knowledge of the involved variables' influence on soil moisture in a given climate. It is therefore important that drought indices incorporating PET are interpreted within the context of the climate in which they are applied, while also keeping in mind the applications they are designed for.

In our impact focused approach, we have made use of the little soil moisture data that are available across different locations and climate types in Europe to demonstrate the compound nature of soil moisture drought during summer. These results provide further insight into the relationship between soil moisture and drought indices that incorporate PET. It is hoped that this insight will aid with the interpretation of drought indices in a given climate and season so that as much information as possible may be gained from their application.

Acknowledgments. Colin Manning received funding from the Volkswagen Foundation's CE:LLO project (Az.: 88469), which also supported project meetings. The authors thank Prof. Arnaldo Frigessi and Prof. Ingrid Hobaek Haff for fruitful discussions and the hosting of a project meeting at the Norwegian Computing Center. The authors would also like to sincerely thank the anonymous reviewers for their constructive comments that have enhanced the quality of the manuscript.

REFERENCES

- Aas, K., C. Czado, A. Frigessi, and H. Bakken, 2009: Pair-copula constructions of multiple dependence. *Insur. Math. Econ.*, **44**, 182–198, <https://doi.org/10.1016/j.insmatheco.2007.02.001>.
- Acar, E. F., C. Genest, and J. Nelehov, 2012: Beyond simplified pair-copula constructions. *J. Multivariate Anal.*, **110**, 74–90, <https://doi.org/10.1016/j.jmva.2012.02.001>.
- AghaKouchak, A., L. Cheng, O. Mazdinyasni, and A. Farahmand, 2014: Global warming and changes in risk of concurrent climate extremes: Insights from the 2014 California drought. *Geophys. Res. Lett.*, **41**, 8847–8852, <https://doi.org/10.1002/2014GL062308>.
- Baldocchi, D., and Coauthors, 2001: FluxNet: A new tool to study the temporal and spatial variability of ecosystem-scale carbon dioxide, water vapor, and energy flux densities. *Bull. Amer. Meteor. Soc.*, **82**, 2415–2434, [https://doi.org/10.1175/1520-0477\(2001\)082<2415:FANTTS>2.3.CO;2](https://doi.org/10.1175/1520-0477(2001)082<2415:FANTTS>2.3.CO;2).

- Berg, A., J. Sheffield, and P. C. Milly, 2017: Divergent surface and total soil moisture projections under global warming. *Geophys. Res. Lett.*, **44**, 236–244, <https://doi.org/10.1002/2016GL071921>.
- Bernard, C., and C. Czado, 2015: Conditional quantiles and tail dependence. *J. Multivar. Anal.*, **138**, 104–126, <https://doi.org/10.1016/j.jmva.2015.01.011>.
- Bevacqua, E., 2017: CDVineCopulaConditional: Sampling from conditional C- and D-vine copulas. R package, version 0.1.0, <https://CRAN.R-project.org/package=CDVineCopulaConditional>.
- , D. Maraun, I. Hobk Haff, M. Widmann, and M. Vrac, 2017: Multivariate statistical modelling of compound events via pair-copula constructions: Analysis of floods in Ravenna (Italy). *Hydrol. Earth Syst. Sci.*, **21**, 2701–2723, <https://doi.org/10.5194/hess-21-2701-2017>.
- Ciais, P., and Coauthors, 2005: Europe-wide reduction in primary productivity caused by the heat and drought in 2003. *Nature*, **437**, 529–533, <https://doi.org/10.1038/nature03972>.
- Dai, A., 2011: Drought under global warming: A review. *Wiley Interdiscip. Rev.: Climate Change*, **2**, 45–65, <https://doi.org/10.1002/wcc.81>.
- , 2013: Increasing drought under global warming in observations and models. *Nat. Climate Change*, **3**, 52–58, <https://doi.org/10.1038/nclimate1633>.
- , K. E. Trenberth, and T. Qian, 2004: A global dataset of Palmer drought severity index for 1870–2002: Relationship with soil moisture and effects of surface warming. *J. Hydrometeor.*, **5**, 1117–1130, <https://doi.org/10.1175/JHM-386.1>.
- D'Andrea, F., A. Provenzale, R. Vautard, and N. De Noblet-Decoudr, 2006: Hot and cool summers: Multiple equilibria of the continental water cycle. *Geophys. Res. Lett.*, **33**, L24807, <https://doi.org/10.1029/2006GL027972>.
- Duong, T., 2017: ks: Kernel smoothing. R package, version 1.10.7, <https://CRAN.R-project.org/package=ks>.
- Fischer, M., D. Kraus, M. Pfeuffer, and C. Czado, 2017: Stress testing German industry sectors: Results from a vine copula based quantile regression. arXiv, 12 pp., <https://arxiv.org/abs/1704.00953>.
- Ford, T. W., and S. M. Quiring, 2014: In situ soil moisture coupled with extreme temperatures: A study based on the Oklahoma Mesonet. *Geophys. Res. Lett.*, **41**, 4727–4734, <https://doi.org/10.1002/2014GL060949>.
- Genest, C., and A.-C. Favre, 2007: Everything you always wanted to know about copula modeling but were afraid to ask. *J. Hydrol. Eng.*, **12**, 347–368, [https://doi.org/10.1061/\(ASCE\)1084-0699\(2007\)12:4\(347\)](https://doi.org/10.1061/(ASCE)1084-0699(2007)12:4(347)).
- Gudmundsson, L., F. Rego, M. Rocha, and S. I. Seneviratne, 2014: Predicting above normal wildfire activity in southern Europe as a function of meteorological drought. *Environ. Res. Lett.*, **9**, 084008, <https://doi.org/10.1088/1748-9326/9/8/084008>.
- Hegerl, G. C., H. Hanlon, and C. Beierkuhnlein, 2011: Climate science: Elusive extremes. *Nat. Geosci.*, **4**, 142–143, <https://doi.org/10.1038/ngeo1090>.
- Hillier, J. K., N. Macdonald, G. C. Leckebusch, and A. Stavrinides, 2015: Interactions between apparently primary weather-driven hazards and their cost. *Environ. Res. Lett.*, **10**, 104003, <https://doi.org/10.1088/1748-9326/10/10/104003>.
- Hirschi, M., and Coauthors, 2011: Observational evidence for soil-moisture impact on hot extremes in southeastern Europe. *Nat. Geosci.*, **4**, 17–21, <https://doi.org/10.1038/ngeo1032>.
- Joe, H., 1997: *Multivariate Models and Multivariate Dependence Concepts*. CRC Press, 424 pp.
- Kraus, D., and C. Czado, 2017: D-vine copula based quantile regression. *Comput. Stat. Data Anal.*, **110**, 1–18, <https://doi.org/10.1016/j.csda.2016.12.009>.
- Kurowicka, D., and R. M. Cooke, 2005: Distribution-free continuous Bayesian belief. *Modern Statistical and Mathematical Methods in Reliability*, Series on Quality, Reliability and Engineering Statistics, Vol. 10, World Scientific, 309–322, https://doi.org/10.1142/9789812703378_0022.
- Leonard, M., and Coauthors, 2014: A compound event framework for understanding extreme impacts. *Wiley Interdiscip. Rev.: Climate Change*, **5**, 113–128, <https://doi.org/10.1002/wcc.252>.
- Lorenz, R., E. B. Jaeger, and S. I. Seneviratne, 2010: Persistence of heat waves and its link to soil moisture memory. *Geophys. Res. Lett.*, **37**, L09703, <https://doi.org/10.1029/2010GL042764>.
- Luo, L., D. Apps, S. Arcand, H. Xu, M. Pan, and M. Hoerling, 2017: Contribution of temperature and precipitation anomalies to the California drought during 2012–2015. *Geophys. Res. Lett.*, **44**, 3184–3192, <https://doi.org/10.1002/2016GL072027>.
- Martius, O., S. Pfahl, and C. Chevalier, 2016: A global quantification of compound precipitation and wind extremes. *Geophys. Res. Lett.*, **43**, 7709–7717, <https://doi.org/10.1002/2016GL070017>.
- Mazdiyasi, O., and A. AghaKouchak, 2015: Substantial increase in concurrent droughts and heatwaves in the United States. *Proc. Natl. Acad. Sci. USA*, **112**, 11 484–11 489, <https://doi.org/10.1073/pnas.1422945112>.
- Miralles, D. G., A. J. Teuling, C. C. van Heerwaarden, and J. Vil-Guerau de Arellano, 2014: Mega-heatwave temperatures due to combined soil desiccation and atmospheric heat accumulation. *Nat. Geosci.*, **7**, 345–349, <https://doi.org/10.1038/ngeo2141>.
- Mitchell, K. E., and Coauthors, 2004: The multi-institution North American Land Data Assimilation System (NLDAS): Utilizing multiple GCIP products and partners in a continental distributed hydrological modeling system. *J. Geophys. Res.*, **109**, D07S90, <https://doi.org/10.1029/2003JD003823>.
- Mo, K. C., and D. P. Lettenmaier, 2016: Precipitation deficit flash droughts over the United States. *J. Hydrometeor.*, **17**, 1169–1184, <https://doi.org/10.1175/JHM-D-15-0158.1>.
- Mueller, B., and S. I. Seneviratne, 2012: Hot days induced by precipitation deficits at the global scale. *Proc. Natl. Acad. Sci. USA*, **109**, 12 398–12 403, <https://doi.org/10.1073/pnas.1204330109>.
- Noh, H., A. E. Ghouch, and T. Bouezmarni, 2013: Copula-based regression estimation and inference. *J. Amer. Stat. Assoc.*, **108**, 676–688, <https://doi.org/10.1080/01621459.2013.783842>.
- Palmer, W. C., 1965: Meteorological drought. U.S. Weather Bureau Research Paper 45, 58 pp., <http://www.ncdc.noaa.gov/temp-and-precip/drought/docs/palmer.pdf>.
- Pham, M. T., H. Vernieuwe, B. De Baets, P. Willems, and N. Verhoest, 2016: Stochastic simulation of precipitation-consistent daily reference evapotranspiration using vine copulas. *Stochastic Environ. Res. Risk Assess.*, **30**, 2197–2214, <https://doi.org/10.1007/s00477-015-1181-7>.
- Porporato, A., and P. D'Odorico, 2004: Phase transitions driven by state-dependent Poisson noise. *Phys. Rev. Lett.*, **92**, 110601, <https://doi.org/10.1103/PhysRevLett.92.110601>.
- Rebel, K. T., R. A. M. de Jeu, P. Ciais, N. Viovy, S. L. Piao, G. Kiely, and A. J. Dolman, 2012: A global analysis of soil moisture derived from satellite observations and a land surface model. *Hydrol. Earth Syst. Sci.*, **16**, 833–847, <https://doi.org/10.5194/hess-16-833-2012>.
- Rebetez, M., O. Dupont, and M. Giroud, 2009: An analysis of the July 2006 heatwave extent in Europe compared to the record year of 2003. *Theor. Appl. Climatol.*, **95**, 1–7, <https://doi.org/10.1007/s00704-007-0370-9>.
- Ruffault, J., V. Moron, R. Trigo, and T. Curt, 2016: Objective identification of multiple large fire climatologies: An application

- to a Mediterranean ecosystem. *Environ. Res. Lett.*, **11**, 075006, <https://doi.org/10.1088/1748-9326/11/7/075006>.
- Salvadori, G., C. De Michele, N. T. Kottegoda, and R. Rosso, 2007: *Extremes in Nature: An Approach Using Copulas*. Water Science and Technology Library, Vol. 56. Springer, 292 pp.
- Schepsmeier, U., J. Stoeber, E. C. Brechmann, B. Graeler, T. Nagler, and T. Erhardt, 2017: VineCopula: Statistical inference of vine copulas. R Package, version 2.1.1, <http://CRAN.R-project.org/package=VineCopula>.
- Seneviratne, S. I., 2012: Climate science: Historical drought trends revisited. *Nature*, **491**, 338–339, <https://doi.org/10.1038/491338a>.
- , D. Lthi, M. Litschi, and C. Schr, 2006: Land–atmosphere coupling and climate change in Europe. *Nature*, **443**, 205–209, <https://doi.org/10.1038/nature05095>.
- , T. Corti, E. L. Davin, M. Hirschi, E. B. Jaeger, I. Lehner, B. Orlowsky, and A. J. Teuling, 2010: Investigating soil moisture–climate interactions in a changing climate: A review. *Earth Sci. Rev.*, **99**, 125–161, <https://doi.org/10.1016/j.earscirev.2010.02.004>.
- , and Coauthors, 2012a: Changes in climate extremes and their impacts on the natural physical environment. *Managing the Risks of Extreme Events and Disasters to Advance Climate Change Adaptation*, C. B. Field et al., Eds., Cambridge University Press, 109–230.
- , and Coauthors, 2012b: Swiss prealpine Rietholzbach research catchment and lysimeter: 32 year time series and 2003 drought event. *Water Resour. Res.*, **48**, W06526, <https://doi.org/10.1029/2011WR011749>.
- Serinaldi, F., B. Bonaccorso, A. Cancelliere, and S. Grimaldi, 2009: Probabilistic characterization of drought properties through copulas. *Phys. Chem. Earth*, **34**, 596–605, <https://doi.org/10.1016/j.pce.2008.09.004>.
- Sheffield, J., E. F. Wood, and M. L. Roderick, 2012: Little change in global drought over the past 60 years. *Nature*, **491**, 435–438, <https://doi.org/10.1038/nature11575>.
- , and Coauthors, 2014: A drought monitoring and forecasting system for sub-Saharan African water resources and food security. *Bull. Amer. Meteor. Soc.*, **95**, 861–882, <https://doi.org/10.1175/BAMS-D-12-00124.1>.
- Sklar, M., 1959: Fonctions de repartition an dimensions et leurs marges. *Publ. Inst. Stat. Univ. Paris*, **8**, 229–231.
- Stagge, J. H., I. Kohn, L. M. Tallaksen, and K. Stahl, 2015: Modeling drought impact occurrence based on meteorological drought indices in Europe. *J. Hydrol.*, **530**, 37–50, <https://doi.org/10.1016/j.jhydrol.2015.09.039>.
- , D. G. Kingston, L. M. Tallaksen, and D. M. Hannah, 2017: Observed drought indices show increasing divergence across Europe. *Sci. Rep.*, **7**, 14045, <https://doi.org/10.1038/s41598-017-14283-2>.
- Teuling, A. J., and Coauthors, 2013: Evapotranspiration amplifies European summer drought. *Geophys. Res. Lett.*, **40**, 2071–2075, <https://doi.org/10.1002/grl.50495>.
- Törnros, T., and L. Menzel, 2014: Addressing drought conditions under current and future climates in the Jordan River region. *Hydrol. Earth Syst. Sci.*, **18**, 305–318, <https://doi.org/10.5194/hess-18-305-2014>.
- Trenberth, K. E., A. Dai, G. d. Schrier, P. D. Jones, J. Barichivich, K. R. Briffa, and J. Sheffield, 2014: Global warming and changes in drought. *Nat. Climate Change*, **4**, 17–22, <https://doi.org/10.1038/nclimate2067>.
- Tsakiris, G., and H. Vangelis, 2005: Establishing a drought index incorporating evapotranspiration. *Eur. Water*, **9**, 3–11, https://www.ewra.net/ew/pdf/EW_2005_9-10_01.pdf.
- Vautard, R., and Coauthors, 2007: Summertime European heat and drought waves induced by wintertime Mediterranean rainfall deficit. *Geophys. Res. Lett.*, **34**, L07711, <https://doi.org/10.1029/2006GL028001>.
- Vicente-Serrano, S. M., S. Beguera, and J. I. López-Moreno, 2010: A multiscale drought index sensitive to global warming: The standardized precipitation evapotranspiration index. *J. Climate*, **23**, 1696–1718, <https://doi.org/10.1175/2009JCLI2909.1>.
- , and Coauthors, 2012: Performance of drought indices for ecological, agricultural, and hydrological applications. *Earth Interact.*, **16**, 1–27, <https://doi.org/10.1175/2012EI000434.1>.
- , and Coauthors, 2014: Evidence of increasing drought severity caused by temperature rise in southern Europe. *Environ. Res. Lett.*, **9**, 044001, <https://doi.org/10.1088/1748-9326/9/4/044001>.
- Wahl, T., S. Jain, J. Bender, S. D. Meyers, and M. E. Luther, 2015: Increasing risk of compound flooding from storm surge and rainfall for major US cities. *Nat. Climate Change*, **5**, 1093–1097, <https://doi.org/10.1038/nclimate2736>.
- Wand, M. P., and M. C. Jones, 1994: Multivariate plug-in bandwidth selection. *Comput. Stat.*, **9** (2), 97–116.
- Whan, K., J. Zscheischler, R. Orth, M. Shongwe, M. Rahimi, E. O. Asare, and S. I. Seneviratne, 2015: Impact of soil moisture on extreme maximum temperatures in Europe. *Wea. Climate Extremes*, **9**, 57–67, <https://doi.org/10.1016/j.wace.2015.05.001>.
- Zarch, M. A. A., B. Sivakumar, and A. Sharma, 2015: Droughts in a warming climate: A global assessment of standardized precipitation index (SPI) and reconnaissance drought index (RDI). *J. Hydrol.*, **526**, 183–195, <https://doi.org/10.1016/j.jhydrol.2014.09.071>.
- Zotarelli, L., M. D. Dukes, C. C. Romero, K. W. Migliaccio, and K. T. Morgan, 2010: Step by step calculation of the Penman–Monteith evapotranspiration (FAO-56 method). IFAS Publ. AE459, 10 pp., <http://edis.ifas.ufl.edu/ae459>.
- Zscheischler, J., and S. I. Seneviratne, 2017: Dependence of drivers affects risks associated with compound events. *Sci. Adv.*, **3**, e1700263, <https://doi.org/10.1126/sciadv.1700263>.
- , and Coauthors, 2014: Impact of large-scale climate extremes on biospheric carbon fluxes: An intercomparison based on MsTMIP data. *Global Biogeochem. Cycles*, **28**, 585–600, <https://doi.org/10.1002/2014GB004826>.
- , R. Orth, and S. I. Seneviratne, 2017: Bivariate return periods of temperature and precipitation explain a large fraction of European crop yields. *Biogeosciences*, **14**, 3309–3320, <https://doi.org/10.5194/bg-2017-21>.